Received: 12 April 2022 | Revised: 4 August 2022 | Accepted: 10 August 2022

DOI: 10.1111/bre.12713

Basin Research | IAS EAGE | WILEY

RESEARCH ARTICLE

Salt tectonics vs. inversion tectonics: The anticlines of the western Maestrazgo revisited (eastern Iberian Chain, Spain)

Carlos L. Liesa | **Antonio M. Casas-Sainz** | **Marcos Aurell** | **José L. Simón** | **Ana R. Soria**

Departamento de Ciencias de la Tierra-Instituto de Ciencias Ambientales (IUCA), Facultad de Ciencias, Universidad de Zaragoza, Zaragoza, Spain

Correspondence
Carlos L. Liesa, Departamento de Ciencias de la Tierra-Instituto de Ciencias Ambientales (IUCA), Facultad de Ciencias, Universidad de Zaragoza, Pedro Cerbuna 12, Zaragoza 50009, Spain.
Email: carluis@unizar.es

Funding information
Agencia Estatal de Investigación, Grant/Award Number: AEI/10.13039/501100011033; Gobierno de Aragón, Grant/Award Number: LMP127_18 and E32_20R; Ministerio de Ciencia e Innovación, Grant/Award Number: PID2019-108705-GB-I00, PID2019-108753GB-C22 and CGL2017-85038-P

Abstract

Many works in the last decades underline the role of evaporites, not just as a conditioning factor but as the engine for subsidence and eventually basin inversion. The western Mediterranean alpine ranges are being investigated in this regard because of the presence of discontinuous units of Permian to Triassic evaporites, deposited in the western Tethys basins. This work presents a thorough analysis of two particular structures (Cañada Vellida and Miravete anticlines) in the intraplate Maestrazgo basin (eastern Iberian Chain, Spain) in which evidence to support their reinterpretation as salt-driven structures have been recently reported. Our analysis includes (i) a comprehensive stratigraphic and structural study of the folds along their entire trace, (ii) the compilation of thickness and distribution of evaporite–bearing and supraevaporite units, paying special attention to changes in the thickness of units in relation to anticlines, and (iii) the study of fault patterns, sometimes in relation to the mechanical stratigraphy. All three aspects are also documented and discussed on a regional scale. The new data and interpretations reported here reinforce the extensional origin of the Late Jurassic–Early Cretaceous basins, and the role of regional extensional tectonics as the responsible for the development of first-order syn-sedimentary normal fault zones driving the formation and evolution of sub-basins. These basins were subsequently inverted and deformed, including the formation of complex, box-geometry anticlines that, in their turn, controlled deposition in Cenozoic basins. The review of the arguments that support the alternative of salt tectonics for the origin of such anticlines has allowed us to delve into the sedimentary and tectonic evolution of the inverted extensional basins and to propose a specific model for the development of these faulted anticlines. The role of salt levels and other interlayered detachments in the structuring of sedimentary basins and their inversion is also pondered. The observations in the eastern Iberian Chain reported here

have implications to assess ongoing reinterpretations in terms of salt tectonics in other alpine basins and ranges of the western Mediterranean.

KEYWORDS

basin evolution, driving mechanism, extensional tectonics, Iberia, salt tectonics, tectono–sedimentary relationships

1 | INTRODUCTION

There is a general consensus that the western Mediterranean alpine chains formed primarily in response to the compression generated by the collision between the European and African plates in the Cenozoic and were the result of inversion and deformation of Mesozoic rift basins that developed in relation to the fragmentation of Pangea (Ziegler, 1987). These inverted basins were developed at plate margins (Pyrenean and Betic basins) or within the plates (Atlasic and Maestrazgo basins). The importance of the Triassic evaporites as the principal detachment layer for the Mesozoic extensional rifting processes and the Cenozoic thrusts has since long been recognized for these chains (e.g. Álvaro et al., 1979; Cámara & Klimowitz, 1985; Guimerà, 1984; Salas & Casas, 1993; Séguret, 1972). These evaporitic units were responsible for the development of local diapirs and salt walls, especially in the western Pyrenees, in its junction with the Basque-Cantabrian basin (Quintà et al., 2012), and in the Atlas (Saura et al., 2014; Teixell et al., 2017), and forming salt sheets and nappes in the Betics (Flinch & Soto, 2017).

These western Mediterranean alpine chains are being investigated revisiting the role of salt tectonics (e.g. Granado et al., 2018; Labaume & Teixell, 2020; López-Mir et al., 2015; Saura et al., 2014, 2016; Vergés et al., 2017, 2020) because evaporite deposition, though discontinuous, took place in the western Tethys basins from the Permian to the Early Jurassic, especially during the Triassic (Soto et al., 2017; Ziegler, 1990). As in other regions, these new studies have revealed details about the mechanical control that the depositional configuration of salt exerts on extensional and contractional deformation, especially in the evolution of individual thrust systems (e.g. Burrel & Teixell, 2021; Hudec et al., 2021; Jackson et al., 1994, and references therein). In some works, salt tectonics sometimes challenges crustal tectonism associated with extension and inversion/contraction stages as the main driving mechanism of sedimentary basin formation and inversion, thus substituting horizontal tectonics with vertical mass movements. Salt tectonics phenomena have been interpreted to explain the formation of thrusts, unconformities and growth strata that had been previously attributed to extensional and subsequent compressional tectonics. As a result, some sedimentary basins traditionally regarded as formed by normal faulting are being alternatively explained as minibasins controlled by salt migration (Jackson & Hudec, 2017). It is true that both end-member evolutionary models are not completely opposite to each other and can interact indeed; for example activation of extensional faults is able to trigger gravitational instability leading to diapirism (Jackson & Vendeville, 1994; Koyi, 1996; Koyi et al., 1993; Nalpas & Brun, 1993).

To which extent are salt tectonics and extensional tectonics exclusive of one another or rather co-existing mechanisms able to explain basin evolution? The eastern Iberian Chain is one of many examples in the western Mediterranean in which salt tectonics has been applied to explain the origin of pre-compressional sedimentary basins and their subsequent evolution (Vergés et al., 2020). This mountain belt contains certain structural features that at first glance fit with the definition of a 'diapiric province': (i) numerous outcrops of Triassic rocks containing evaporites (mainly gypsum, Ortí et al., 2017, 2020) and sub-surface data documenting salt (Lanaja, 1987), (ii) complex folding directions interfering with the regional contractive trends

Highlights

- Mesozoic normal faults nucleated NW-SE to N-S trending anticlines during the Cenozoic contraction.
- Thickness changes of Lower Cretaceous units are related to the activity of NNW-SSE normal faults.
- Regional information and geometry of drag folds suggest fold kinematics not compatible with salt extrusion.
- We question the diapiric origin of anticlines and the role of salt in the formation of the Maestrazgo basin.

(Simón, 2004, 2005), (iii) box-fold geometries (Liesa et al., 2018; Simón, Arenas, et al., 1998), (iv) 'welding' of stratigraphical units (Vergés et al., 2020), (v) varying thickness of units associated with faulted anticlines (Liesa et al., 2004, 2018; Vergés et al., 2020), (vi) interruptions in sedimentation during successive basin stages reflected by either paraconformities or angular unconformities (Álvaro et al., 1979; Aurell et al., 2003; Capote et al., 2002; Liesa, Soria, Casas, et al., 2019), among others.

Recently, Vergés et al. (2020) provided an alternative explanation for relatively well-known anticlines in the eastern Iberian Chain with complex box geometries, stating that they were almost controlled by salt tectonics, especially during their Jurassic and Cretaceous evolution. Conversely, previous works provided arguments supporting the interpretation of these and similar structures in the region as originated during Mesozoic extensional rifting, being subsequently inverted during the Alpine compression (e.g. Álvaro et al., 1979; Aurell et al., 2016, 2019; Casas et al., 2000; Cortés et al., 1999; Guimerà, 1988, 2018; Liesa et al., 2004, 2018; Liesa & Simón, 2004; Simón, Arenas, et al., 1998; Simón & Liesa, 2011; Simón-Porcar et al., 2019).

The aim of this work is to review the inversion model proposed for the eastern Iberian Chain, in particular for the Maestrazgo Mesozoic basin, and confront it with the salt model. In order to focus the discussion as much as possible, the two anticlines proposed by Vergés et al. (2020) as keystones for their interpretation, the NW-SE to NNW–SSE striking Cañada Vellida and Miravete box-folds are studied in detail. Special attention is put on key features invoked for supporting diapirism, such as (1) thickness and facies variations and unconformities shown by the Jurassic and Lower Cretaceous sequences in relation to anticlines, (2) flaps and related onlaps and hook geometries, (3) thickness and facies of the Triassic evaporite succession and (4) welding structures. Compilation of previous observations, together with new data and interpretations, have been the way to propose a specific tectono-sedimentary evolutionary model for these structures, which clearly exemplifies and refines the previously well-established model of inversion tectonics in the Iberian Chain. Analysing the same structures (and outcrops) under two different viewpoints allows offering a critical review of the arguments supporting the salt vs inversion tectonic hypotheses. Other regional information, such as the varying thickness of the salt-bearing and overlying sedimentary sequences has been included to enrich the discussion about the role played by salt tectonics in both the basinal and contractional stages in the eastern Iberian Chain.

2 | GEOLOGICAL SETTING

2.1 | The Mesozoic and Cenozoic tectono-sedimentary evolution of the Iberian Chain

The NW-SE-trending Iberian Chain is an intraplate alpine mountain range, oblique to the northern (Pyrenean) and southern (Betic) active margins of the Iberian Plate (Figure 1a). It is a double-vergence, fold-and-thrust belt that resulted from positive inversion of the Mesozoic Iberian Basin mainly from late Eocene to early Miocene times (Álvaro et al., 1979; Capote et al., 2002; Guimerà, 2018; Liesa et al., 2018; Salas & Casas, 1993; among others). It shows a moderate total deformation, with scarce magmatism, metamorphism and alpine foliation (Álvaro et al., 1979; Julivert, 1978).

After the episode of late-Variscan strike-slip fracturing postdating the Variscan orogeny (e.g. Aldega et al., 2019; Álvaro et al., 1979; Arthaud & Matte, 1977), the Mesozoic evolution of eastern Iberian has been linked with the breakup of Pangea, the opening of the Central and North Atlantic and the westward expansion of the Tethys (Capote et al., 2002; Liesa, Soria, Casas, et al., 2019; Peace et al., 2019; Salas & Casas, 1993; Salas et al., 2001; Soto et al., 2019). As indicated by subsidence analysis (e.g. Salas & Casas, 1993), Mesozoic subsidence was governed by two stages of rifting (Late Permian–Hettangian and Kimmeridgian–middle Albian), each followed by post-rifting stages of relative tectonic quiescence (Sinemurian–Oxfordian and late Albian–Campanian, respectively).

The Triassic of the Iberian Chain shows germanic-type Triassic facies (i.e. Buntsandstein, Muschelkalk and Keuper facies). During the Early Triassic rifting stage, sedimentation was mostly terrestrial, and the Buntsandstein synrift succession shows abrupt changes in thickness, from 0 to more than 1000 m (De Vicente et al., 2009; García-Lasanta et al., 2015 and references therein). This stage is characterized by thick-skin extensional tectonics associated with the reactivation of previous Variscan contractional structures. Geometries associated with rifting are relatively simple: half-grabens dominating in some areas, probably associated with deep detachments in the Silurian shales (Marcén et al., 2018), and full grabens in others, constrained by planar marginal faults on their conjugate structures (Arche et al., 2007; García-Lasanta et al., 2015; López-Gómez et al., 2019; Sopeña et al., 1988).

During the Middle and Late Triassic, rifting slowed down and changes in the thickness of the Muschelkalk and Keuper facies were less significant. Sedimentation took place in coastal to shallow platform environments, recording successive transgressive–regressive cycles, with alternation of shallow marine carbonates and

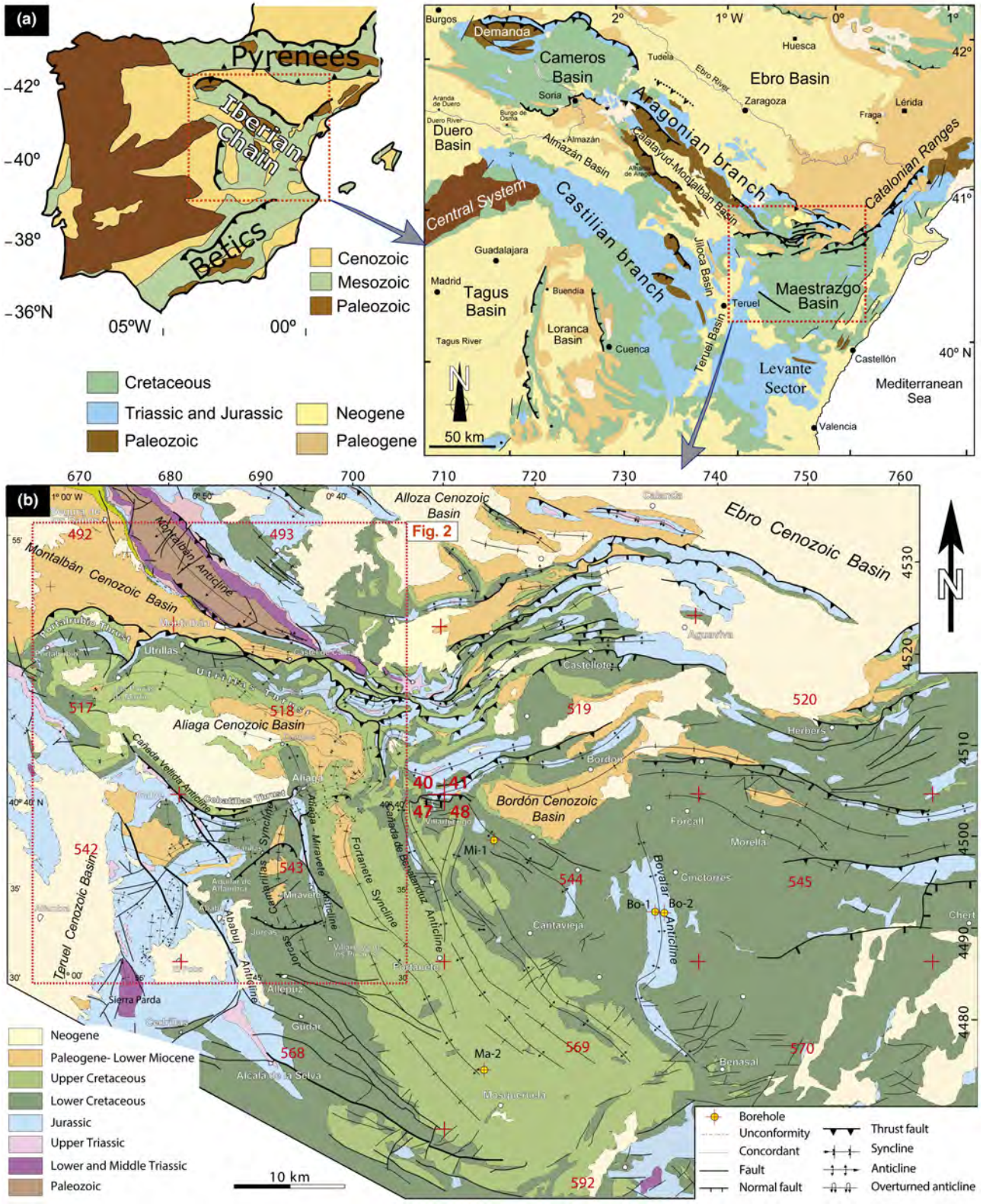

FIGURE 1 Geological map of the Iberian Chain (a) and detail of the northwestern Mesozoic Maestrazgo basin (b). The three-digit numbers and crosses in figure b in red indicate the number of sheet 1:50,000 of the National Geological Map and its limits, respectively. Two-digit numbers indicate the 1:200,000 Geological Map sheet.

mudstone-dominate successions (e.g. López Gómez et al., 1998, 2002; Meléndez et al., 1995). The successions include sandstones, representing sedimentation in fluvial and alluvial environments, and dolostones and evaporites deposited in coastal plains (Ortí et al., 2017). The evaporites are mainly gypsum/anhydrite and, to a lesser extent,

halite (Lanaja, 1987). In most of the central Iberian Chain, the two main muddy-evaporitic successions (i.e. Middle Muschelkalk and Keuper facies) are up to 200 m thick each. The Middle and Upper Triassic successions thin towards the western and southern margins of the Iberian basin, progressively lapping onto the Palaeozoic Iberian Massif (López Gómez et al., 2002; Meléndez et al., 1995).

Around the Triassic–Jurassic transition, intensification of extensional tectonics favoured the localized deposition (up to 200 m) of alternating peritidal limestones and evaporites (Aurell et al., 2007; Ortí et al., 2017, 2020; San Román & Aurell, 1992) or evaporite-dominated units, especially in the area situated close to the boundary with the Cenozoic Ebro basin (Lecera Fm; Bordonaba & Aurell, 2002). Diagenetic dissolution of evaporites contributed to the development of carbonate breccia in most parts of the region (San Román & Aurell, 1992).

During most of the Jurassic, the post-rifting thermal cooling stage resulted in the formation of a large, shallow marine gulf located in the tropical fringe (20–25°N). An up to a 900-m-thick succession of shallow carbonate platform limestones and marls was deposited, progressively diminishing in thickness with the eventual onlap onto the Iberian basement in the westernmost parts of the basin (e.g. Aurell et al., 2003). The Jurassic sequence recorded successive long-term transgressive–regressive stages that nearly fit the Early, Middle and Late Jurassic epochs. The Lower Jurassic sequence forms a relatively thick and homogeneous succession with the open marine areas located to the north. The Middle Jurassic involved a major restructuring of the platform, with the formation of local uplifted and subsident areas in the central part of the basin. The Upper Jurassic platforms were open to the south and received significant, but local, siliciclastic inputs (e.g. Aurell, Bádenas, et al., 2019; Aurell et al., 2003; Aurell, Fregenal-Martínez, et al., 2019; Gómez & Fernández-López, 2006; Gómez & Goy, 2005).

The sedimentary sequence deposited during the first rifting–post-rifting stages provided a particular mechanical stratigraphy, with a relatively thick weak-level (Middle Muschelkalk and/or Keuper) overlain by a cover of competent Jurassic rocks whose thickness can be more than twice that of the detachment. This rheological frame interacted with a complex pattern of basement normal faulting during the latest Jurassic–Early Cretaceous rifting stage. During this second rifting stage, two extension directions, NE–SW (Iberian) and NW-SE (Tethysian, García-Lasanta et al., 2016; Liesa, 2011a), acted on the already existing fault pattern (NW-SE to N-S and NE–SW to E-W, Antolín-Tomás et al., 2007; Liesa, 2000, 2011a; Liesa et al., 2004; Liesa, Soria, Casas, et al., 2019) in different parts of the basin, thus conforming a complex pattern of horsts, grabens and halfgrabens. Two opposed factors combined to finally produce a variety of extensional basin geometries: (i) the existence of a detachment (<10 km deep in most of the basinal domain) within the basement favoured the formation of large listric faults, whereas (ii) the existence of the Triassic shallow detachment level contributed to the development of smaller-scale fault systems (see, e.g. Rodríguez-López et al., 2007; Soto et al., 2007).

The latest Jurassic–Early Cretaceous rifting stage involved the breakup of the Jurassic platforms and the formation of an ensemble of basins (Cameros, Maestrazgo, Valencia) and subbasins in the compartmentalized Iberian Basin (Capote et al., 2002; Salas & Casas, 1993). Two sets of nearly perpendicular main faults (trending NW-SE to NNW–SSE and NE–SW to ENE–WSW, respectively), reactivated or newly formed, and affecting the basement rocks, determined a complex extensional structure with up to seven subbasins in the Maestrazgo area (Antolín-Tomás et al., 2007; Liesa et al., 2004, 2006; Liesa, Soria, Casas, et al., 2019; Salas et al., 2001; Soria, 1997). Differential subsidence driven by normal faults was encompassed by general uplift related to doming processes in eastern Iberia, especially during the Berriasian–Hauterivian (Antolín-Tomás et al., 2007; Liesa, Soria, Casas, et al., 2019). As a result, sedimentation was firstly restricted to depocentral areas of sub-basins, dominated by shallow marine to coastal environments during the latest Jurassic (Aurell, Bádenas, et al., 2019; Aurell et al., 2016; Liesa, Soria, Casas, et al., 2019) and mostly terrestrial ones during the earliest Cretaceous (Aurell, Bádenas, et al., 2019; Aurell et al., 2016; Meléndez et al., 2009; Soria, 1997). Conversely, the areas between basins and sub-basins experienced fault block tilting and differential erosion. During the Early Cretaceous, tectonic subsidence together with high sea level gave rise to a progressive connection between sub-basins, and the development of local and regional synrift (and intrarift) angular unconformities (Liesa, Soria, Casas, et al., 2019). Sedimentation took place firstly in transitional settings (Navarrete, 2015; Navarrete, et al., 2013a, 2013b; Soria, 1997) and, then, in shallow marine environments (Bover-Arnal, 2010; Peropadre, 2012). The Early Cretaceous synrift stage ended with an increase in extensional activity and sedimentation of coastal mudstones and sandstones with coal (Salas et al., 2001). The thickness of the synrift series is highly variable between sub-basins and within each sub-basin (Liesa et al., 2004, 2006; Navarrete, et al., 2013b; Peropadre, 2012; Soria, 1997).

During the Albian and the Late Cretaceous, extensional tectonics practically stopped and eastern Iberia became dominated by post-rift thermal subsidence. Sedimentation was extensive on both basin margins and intrabasin highs, and a regional post-rift unconformity developed along the Iberian Basin (Álvaro et al., 1979; Capote et al., 2002; Salas & Casas, 1993). The post-rift sequence starts with a

succession (typically <300 m) of sands and shales from a desert system and coastal plains (Rodríguez-López et al., 2009) and continues with a thick marine carbonate succession (~400 m), mainly consisting of dolostones, limestones and marls (Canérot et al., 1982). This sequence, very uniform in thickness and facies in the central-eastern Iberian Chain, recorded two transgressive–regressive cycles.

The scenario of convergence between the Eurasian, Iberian and African plates mostly during the Paleogene to Early Miocene resulted in a compressional stage, producing the inversion of the extensional fault systems (e.g. Cameros and Maestrazgo), giving rise to the complex fold and thrust pattern that conforms the intraplate Iberian Chain (Figure 1a) (Álvaro et al., 1979; Capote et al., 2002; Guimerà, 2018; Liesa et al., 2018; Salas & Casas, 1993). Numerous intramountain basins developed within the chain, bounded by major compressional structures (e.g. Casas et al., 2000; González & Guimerà, 1993) (Figure 1). Terrestrial Cenozoic sedimentation includes alluvial fan conglomerates and clays, and palustrine and lacustrine carbonates. Several tectono-sedimentary units within the Paleogene-Neogene series (T1 to T6) have been distinguished based on regional angular unconformities and their sequential evolution (Figure 2), allowing to establish tectono-sedimentary relationships and characterize the evolution of compressional structures (González & Guimerà, 1993; Simón, Arenas, et al., 1998).

The alpine deformation was dominated by the main NE–SW to NNE–SSW compression during the Paleogene, related to the oblique convergence between Iberia and Europe (development of the Pyrenees), and by an NNW–SSE to N–S compression during the Early Miocene, related to the Iberia-Africa convergence and the collision forming the Betics in southern Iberia (Capote et al., 2002; Liesa, 2000). From the dynamic analysis of brittle structures, a more complex picture has been drawn for the Iberian Chain, with three successive, partially overlapping regional stress fields (*Pyrenean-Iberian*, *Betic*, and *Late Pyrenean*), partially superposing over space and time (Liesa, 2000; Liesa & Simón, 2007, 2009).

The main Middle Eocene to Late Oligocene NE–SW compressional stage was responsible for the principal, NW-SE trending system of folds and thrusts of the Iberian Chain (Figure 1a). Structures turn to nearly E-W direction in the northwestern and southeastern parts of the chain (Cameros and eastern Maestrazgo, respectively) and to NNW–SSE direction in specific areas of the eastern Iberian Chain (northwestern Maestrazgo) (Figures 1 and 2). Particularly, in the eastern part of the chain, the second set of buckle folds (and thrusts) trending WSW–ENE overprints the previous Alpine structures (Liesa, 2000; Simón, 1980, 2004, 2005; Simón, Arenas, et al., 1998). This second set of folds and thrusts, developed during the early Miocene, has an irregular spatial distribution and is mostly concentrated within narrow bands. Fault propagation fold geometry dominates, related to the positive inversion of inherited normal faults (Cortés et al., 1999; Guimerà & Salas, 1996; Liesa et al., 2004, 2018; Simón, Arenas, et al., 1998). Their detachment level is either in the Middle–Upper Triassic or, locally, in the incompetent Lower Cretaceous levels (Simón, 2004). The mechanical stratigraphy favoured the formation of thin-skinned structures that involved the basement, with thrusts with displacements of up to 6–11 km (Capote et al., 2002; Casas et al., 2000; Guimerà, 2018; Guimerà & Alvaro, 1990; Izquierdo-Llavall et al., 2019; Liesa et al., 2000, 2018; Nebot & Guimerà, 2016b, 2018; Simón & Liesa, 2011).

2.2 | A review of the Mesozoic stratigraphy around the study area

The study area, located around the Cañada Vellida and Miravete anticlines, exposes an almost-complete Mesozoic series. The thickness of the successive Mesozoic sedimentary sequences is generally homogeneous in the studied region and around the central-eastern Iberian Chain for the post-rift Jurassic and Upper Cretaceous sequences, at least when compared with the Triassic and latest Jurassic–Lower Cretaceous synrift sequences (Table 1). However, the individual thickness of the different formations may change laterally much more than the total sedimentary sequence due to lateral facies changes.

The Triassic succession crops out in the Montalbán anticline and in Peña Parda, 30 km north and south, respectively, of the studied area (see location in Figures 1b and 2). There, the Buntsandstein facies shows variable thickness (50–230 m) and mainly consists of continental sandstones and lutites (Godoy, Ramírez, Moissenet, et al., 1983; Ferreiro et al., 1991; Soria et al., 2011). The Muschelkalk facies crops out 2 km southeast of Cañada Vellida (Corral del Zancado section of A. Meléndez; in Ferreiro et al., 1991; see location in Figure 3 and a field view in Figure 4). This sequence rests on c. 20 m of red clays and green marls with cm-scale intercalations of dolostones (Röt facies) and consists of 20 m of laminated dolostones and marls, 10–15 m of mudstones with thin intercalations of dolostones, silts and sandstones, gypsum appearing as isolated crystals or nodules (Middle Muschelkalk) and 80–100 m of tabular dolostones. The Keuper facies crops out in the core of the Cañada Vellida and Miravete anticlines (Figures 2 and 3) and consist of a c. 100-m-thick succession of red and green mudstones

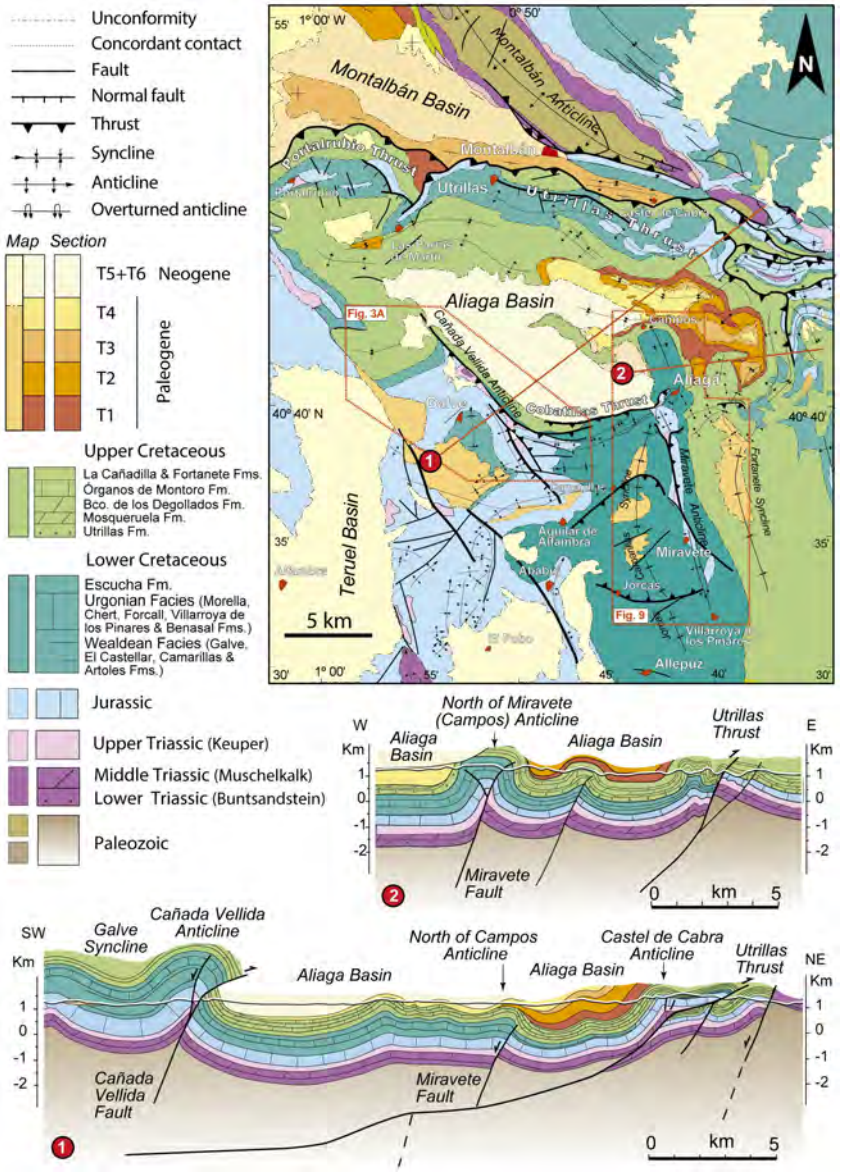

FIGURE 2 Geological map of the western Maestrazgo basin with the location of the Cañada-Vellida and Miravete anticlines (see location in Figure 1). The two geological cross-sections cut key structures associated with the NE–SW regional shortening responsible for the main Cenozoic structuring of the Iberian Chain (modified from Simón & Liesa, 2011).

with interbedded levels of white, green and black gypsum, brown dolostones and red sandstones. Similar facies with equivalent thicknesses crop out along the limbs of the Montalbán anticline, which includes c. 50 m of the Middle Muschelkalk with the local presence of gypsum levels, and up to 100–120 m of clays interbedded with gypsum of the Keuper facies (Marin, 1974). The uppermost Triassic peritidal dolostones of the Imón Fm (up to 30 m) crop out discontinuously. It should be noted that the Triassic evaporite-bearing units may form thick successions in the region to the east of the study area, with up to 600 m for the Keuper in the SE of the chain (Valencia area; Figure 1a; Ortí, 1973, 1974; Ortí et al., 2017). In the Bovalar-2 well (central Maestrazgo basin; Figure 1b; Table 1), 1200 m of the Middle Muschelkalk were drilled (Lanaja, 1987), although, as discussed later, the structural location of the borehole does not ensure that this represents its true stratigraphical thickness.

The eastern limb of the Galve syncline offers a complete exposure to the Jurassic marine succession (Martín Fernández et al., 1979) (Figures 3 and 4, and Table 1). The Lower Jurassic is formed by a ca. 360 m thick succession of peritidal to shallow marine carbonates, the Middle Jurassic consists of a 30–70 m succession dominated by oolitic limestones, whereas the Upper Jurassic marine carbonate sequence is ca. 160 m thick (Simón, Arenas, et al., 1998). In the core of the investigated anticlines, these Jurassic carbonates are cut by numerous extensional faults, which explains why it is tectonically thinned and even omitted in most of the region.

The three units deposited around the Jurassic–Cretaceous transition (latest Kimmeridgian-lower Valanginian) consist of mixed carbonate-siliciclastic successions with strong changes in thickness (Figure 4), controlled by extensional tectonics, and bounded by regional unconformities (Aurell et al., 2016; Aurell,

TABLE 1 Thickness (in metres) of the Mesozoic sedimentary sequences in and around the studied area from stratigraphic and borehole information

	Sheets of the National Geological Map						Studied area				Sheets of the National Geological Map										
	1:50,000 scale						Cañada Vellida		Miravete		1:50,000 scale								1:200,000 scale		
Sedimentary sequence (units)	*590* SSW	*567* SW	*542* W	*517* NW	*518* N	*543*	*SW GSb*	*NE LPSb*	*WSW GSb*	*ENE Mhigh*	*568* S	*569* SE		*544* E			*519* NE		*40* NW	*47* SW	*48* E
Upper Cretaceous (Mo, Bd, Om, LC and F Fms)	>250	No	No	440	>265	449	No	390	No	≈450	>400	≈450	*180*	460			420		360–430	330–590	400
Albian (utrillas Fm)	40	No	No	35–100	80–250	150–180	No	200	No	200–250	100–200	60–110	*125*	125–150			50–150		10–250	120	150
SRS-2b, Aptian (Mo, Ch, Fo, Vp, Be and E Fms. or equivalents)	Hiatus	No	No	170	230–350	450–700	>350–450	280–380	550–850	350–400	370–460	220–260	0	*35*	280–300		310–405		0–350	550–630	100–550
SRS-2a, Hauterivian-Barremian (Cas, Ca and Ar Fms. or equivalents)	Hiatus	325	520	30–70	50–175	390–425	400–520	65–150	650–1400	400–700	390–440	195–220	*0*	*162*	180–190		301		0–300	590–640	250–900
SRS-1, Upperm. Jurassic-lowerm. Cretac. (Ce, Ag and Ga Fms, or eq.)	=300	300	>120	0 - >50	Hiatus	265	200–300	0–100	0–150	0–100	260–300	100–150	*658*	*369*	*629*	*616*	280	105	0–100	350	600–1000
Upper Jurassic (Y, So, Lo and Hi Fms.)	245	305	285	230	>220	270	230	220	110–130	100–170	>120	>70		*112*			200	150	160–220	265	450
Middle Jurassic (Ch Fm)	145–160	115	165	70	16	30–50	50	50	30	30	50	No		*52*	*89*	*91*	No	25	15–160	60–150	
Lower Jurassic (CL, RP, C, B and Tu Fms.)	215	232	165	95	75	160	270	230	125–200	105	120	No	*292*	*490*	*286*	*263*	No	55	160–290	120–230	?
Lowermost Jurassic (Cortes de Tajuña Fm)	30–40	80	70–90	100	150	100	80	80	90	80	50	No	*158*	*156*			No	150	73–150	<145	100
Uppermost Triassic (Imon Fm)	30–35	20–25	20	?	25	20	20	20	?	?	?	No					No	?	25–35	35–40	40
Upper Triassic (Keuper facies)	≈150	0–100	>100	50–150	112	>100	≈200	No	No	No	>100	No	*212*	*261*	*246*	*230*	No	≈150	100–200	20–230	50–100
Upper Muschelkalk (M3)	100–110	100	100	100	60–70	No	100	No	No	No	>40	No	*128*	*137*	*163*	*178*	No	No	60–95	120	100–150
Middle Muschelkalk (M2)	No	0	0	15	15–20	No	15	No	No	No	No	No	*828*	*624*	*447*	*1213*	No	No	10–50	50	30

TABLE 1 (Continued)

	Sheets of the National Geological Map						Studied area				Sheets of the National Geological Map								
	1:50,000 scale						Cañada Vellida		Miravete		1:50,000 scale						1:200,000 scale		
Sedimentary sequence (units)	*590* SSW	*567* SW	*542* W	*517* NW	*518* N	*543*	*SW GSb*	*NE LPSb*	*WSW GSb*	*ENE Mhigh*	*568* S	*569* SE	*544* E			*519* NE	*40* NW	*47* SW	*48* E
Lower Muschelkalk (M1)	No	0	0	20	55	No	20	No	No	No	No	No	*222*	*92*		No	No	0–50	75	65
Röt facies	No			≈20	10	No	≈20	No	No	No	No	No	*>56*	*20*		No	No	10–20	40	10–20
Lower Triassic (Buntsandstein Fm)	No	>230	>230	No	50–150	No	No	No	No	No	No	No		*144*		No	No	20–250	550–670	380
													Ma-2	*Mi-1*	*Bo-1* *Bo-2*					
													Borehole information							

Note: Abbreviations of sedimentary units (first column) as in Figure 5. Triassic detachment levels highlighted with purple background. Stratigraphic data compiled from sheets of the National Geological Map at scales 1:200,000 (Anadón et al., 1985; Ferreiro et al., 1991; Hernández et al., 1985) and 1:50,000 (Canérot, Fernández-Luanco, et al., 1979; Canérot, Pignatelli, et al., 1979; Crespo-Zamorano et al., 1979; Gautier & Barnolas, 1980, 1981; Godoy, Moissenet, Ramírez, et al., 1983; Godoy, Ramírez, Moissenet, et al., 1983; Godoy, Ramírez, Olivé, et al., 1983; Martín-Fernández et al., 1979; Navarro-Vázquez et al., 1981), as well as from Soria (1997), Vennin and Aurell (2001), Peropadre (2012) and Navarrete (2015). The geographic initials (N, S...) indicate the location of the sheet with respect to the studied area. Borehole information (vertical thickness), shown with salmon background and italic number, is based on Lanaja (1987). Wells: Bo-1–Bovalar 1; Bo-2–Bovalar 2; Ma-2–Maestrazgo 2; Mi-1–Mirambel 1. The location of the geological sheets and wells is shown in Figure 1b. Key: (SRU) Syn-rift unit; (no) unit that does not crop out or has been eroded at present; (>) incomplete stratigraphic series normally due to erosion of its upper part; (?) unidentified unit; (GSb) Galve sub-basin; (LPSb) Las Parras sub-basin; (Mhigh) Maestrazgo high.

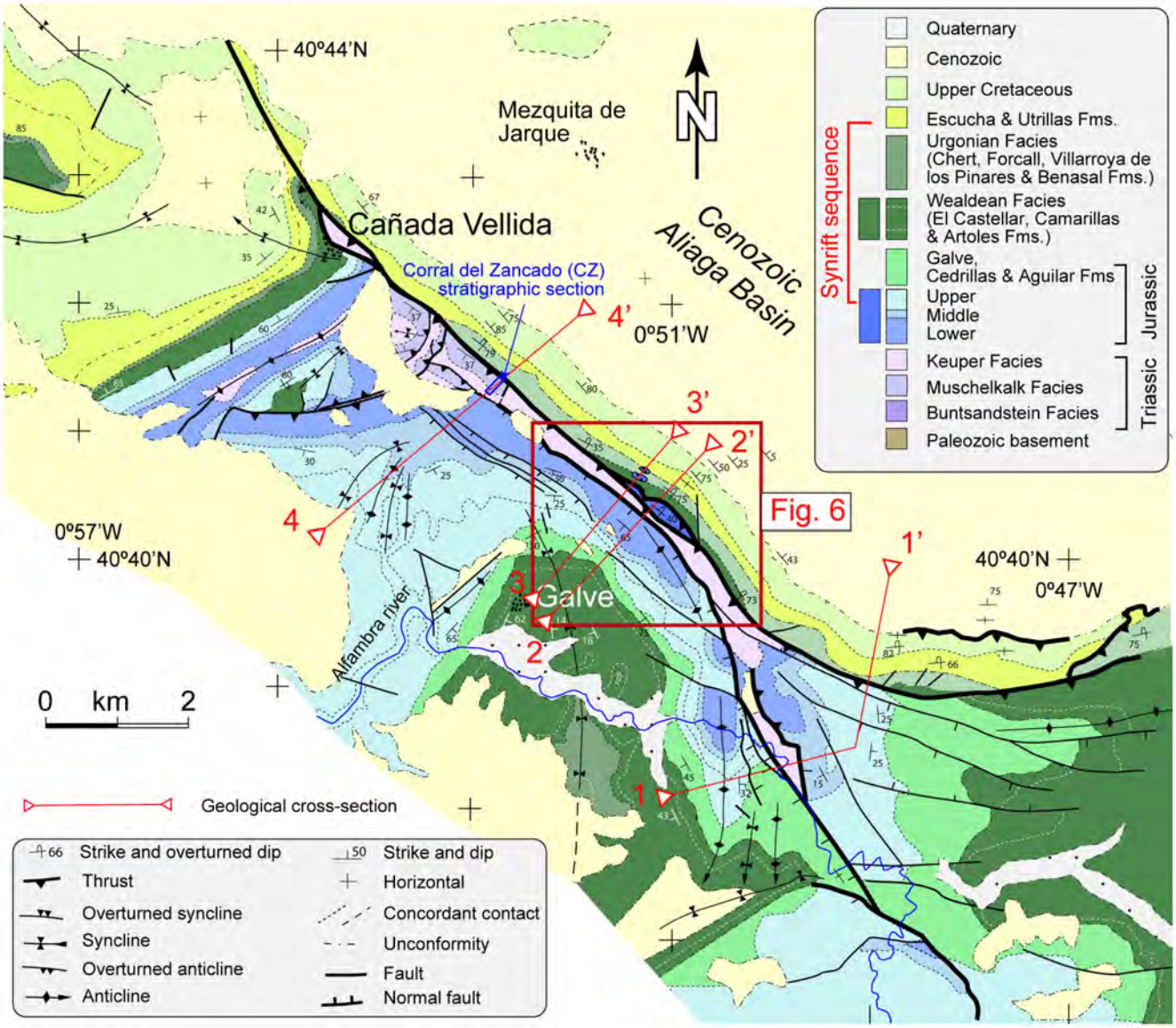

FIGURE 3 Cañada Vellida anticline (see Figure 2 for location). Geological map of the normal fault, anticline and thrust of Cañada Vellida, which separated two paleogeographical domains during the Late Jurassic–Early Cretaceous rifting stage, the Las Parras and Galve sub-basins (Liesa et al., 2004, 2006; Liesa, Soria, Casas, et al., 2019; Soria, 1997). Numbered lines are cross-sections shown in Figure 5.

Fregenal-Martínez, et al., 2019). The first unit consists of a well-bedded mixed succession of limestones, sandstones and claystones (Cedrillas Fm). Around Miravete, its thickness is 20–30 m, but it reaches 150 m west of Cañada Vellida, in the Galve syncline (Val et al., 2019). The second unit is made up of limestones, red lutites and cross-bedded sandstones (Aguilar del Alfambra Fm) and can reach more than 300 m around its type locality (Bádenas et al., 2018) and up to 150 m close to the Miravete village. The third unit is 0–100 m thick and consists of red lutites with cross-bedded and tabular-burrowed sandstones (Galve Fm). These three units are very reduced in thickness or even absent at the NE limbs of the Cañada Vellida and Miravete anticlines (Figures 3 and 4).

As shown by regional stratigraphic–structural works (Navarrete, 2015; Peropadre, 2012; Soria, 1997 among others), the Lower Cretaceous lies on a well-defined regional synrift angular unconformity, locally resting on Middle Jurassic rocks, and shows high variability in thickness in relation to normal faults. This sequence is totally exposed in the Cañada Vellida and Miravete fold limbs, having a lower thickness in the NE (Las Parras subbasin and Maestrazgo high, respectively) than in the SW limb/block (Galve subbasin). Thickness changes are more pronounced in the Hauterivian-Barremian sequence than in the Aptian sequence (Figure 4 and Table 1). The Hauterivian-Barremian sequence in the SW (Galve subbasin) is 400–1400 m thick and consists of 50–160 m of red lutites, brown sandstones and grey lacustrine limestones and marlstones (El Castellar

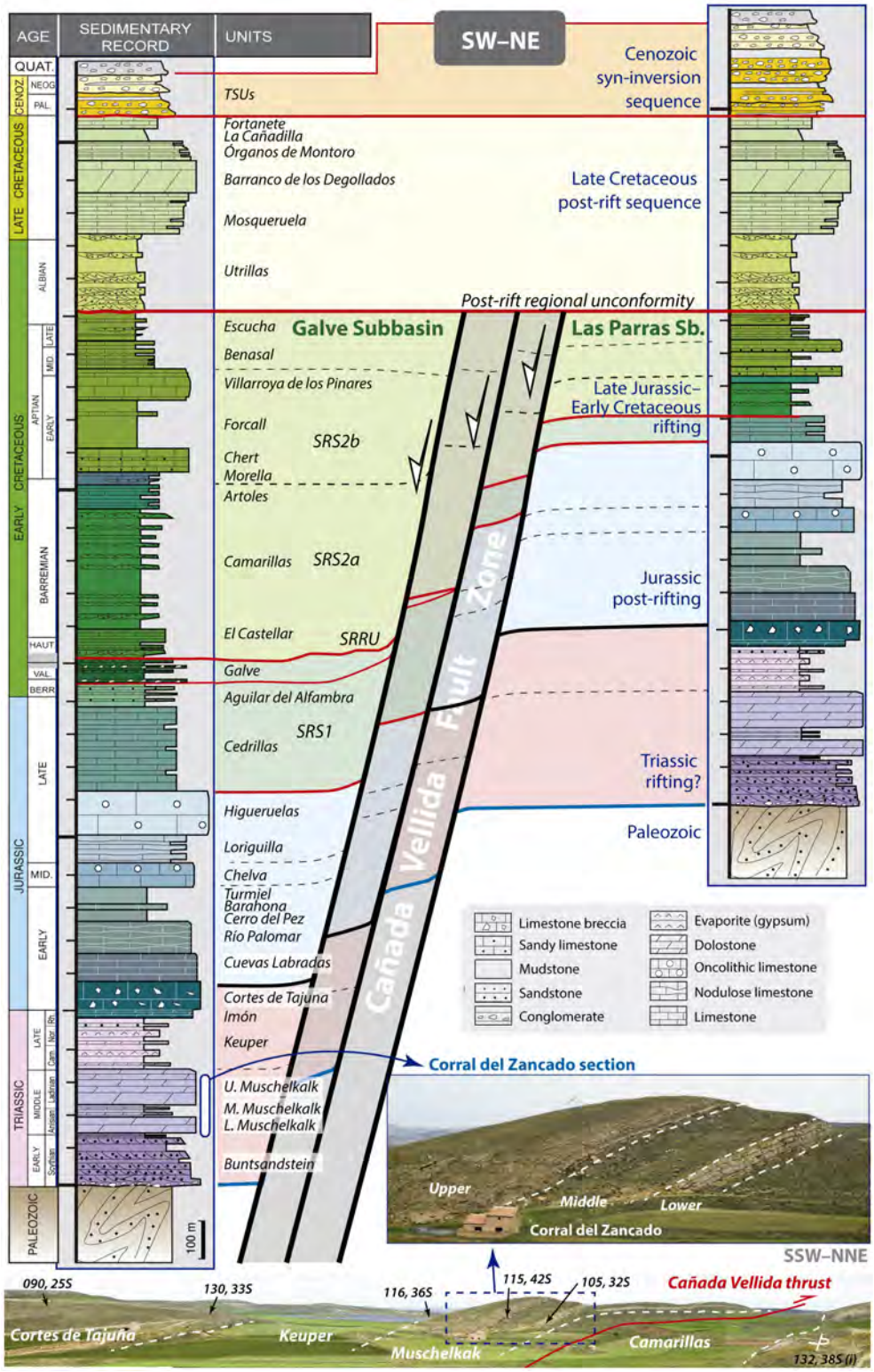

FIGURE 4 Local stratigraphy in Cañada Vellida area showing the differences in the Upper Jurassic-Lower Cretaceous units of the Las Parras and Galve sub-basins as a result of the synsedimentary activity of the Cañada Vellida normal fault zone. The thickness of the sedimentary units is based on stratigraphical sections logged in this area, except for the Buntsandstein facies, which are represented by their cited in Se average regional thickness. Data from regional works are cited in Section 4.1 and Table 1. Insets show a field view of the Middle-Upper Triassic at the Corral del Zancado section (see location in Figure 3 and in cross-sections 4–4′ of Figure 5). SRS1, SRS2a and SRS2b: Synrift sequences 1, 2a and 2b, respectively (as in Table 1).

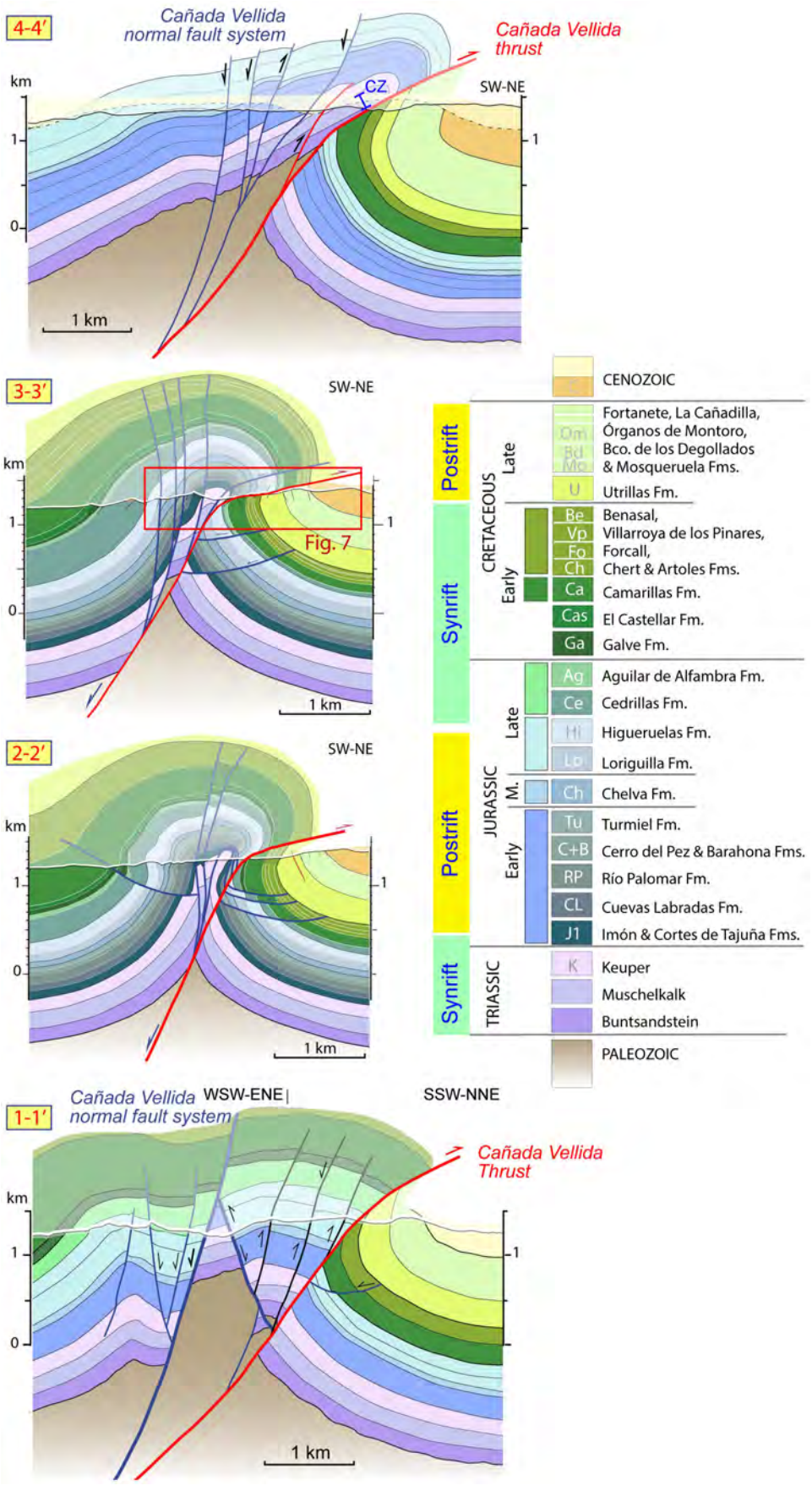

FIGURE 5 Geological cross-sections of the NW-SE Cañada Vellida structure (see location in Figure 3). CZ, Corral del Zancado stratigraphic section.

Fm; Liesa et al., 2006; Meléndez et al., 2009; Soria, 1997), 300–900 m of red clays and white sandstones (Camarillas Fm; Navarrete, 2015; Soria, 1997) and 100–200 m of oyster-bearing limestones and marls (Artoles Fm; Ibañez, 2014, 2015; Ibañez et al., 2015; Soria, 1997). In the NE limb of the Miravete anticline, the El Castellar Fm is recorded only locally (40–50 m, east of Peña de la Higuera), and the Camarillas and Artoles formations are 170–400 and 60–110 m thick, respectively (Navarrete, 2015; own data). In the NE block of Cañada Vellida, the sedimentary gap is more important (the El Castellar Fm was not deposited), and the recorded sequence is much thinner (30–65 and 20–40 m for the Camarillas and Artoles formations, respectively; Soria, 1997).

The Aptian sequence at the SW block of Cañada Vellida (Galve subbasin) is 550–850 m thick (Peropadre, 2012; Table 1) and consists of 100–110 m of red lutites, white sandstones and grey limestones (Morella Fm), 100–115 m of calcareous sandstones and bioclastic limestones (Chert Fm), 130–250 m of marlstones and an intercalated limestone bar (Forcall Fm), 55–75 m of rudist and coral limestones (Villarroya de los Pinares Fm) and 200–310 m of calcarenites, marlstones and limestones (Benasal Fm). No information is available for the Escucha Fm due to its subsequent erosion. Similarly, the Aptian sequence in the NE blocks is much thinner, totalizing up to 280–400 m (Peropadre, 2012; Vennin & Aurell, 2001).

The post-rift Albian-Upper Cretaceous sequences only crop out in the NE limbs of the Cañada Vellida and Miravete anticlines (Figures 2–4). The Albian sequence unconformably rests on the previous sequence and is made up of 200–250 m of white sandstones and pale-red and ochre mudstones (Utrillas Fm). The Upper Cretaceous sequence consists of peritidal to shallow marine carbonates totalizing a 390–450-m-thick succession (Table 1).

3 | METHODS

The review and argumentation supporting salt tectonics or inversion tectonics in the eastern Iberian Chain have involved a detailed reconstruction of the evolutionary stages of the Miravete and Cañada de Vellida anticlines as well as the analysis and discussion of some other key outcrops studied by Vergés et al. (2020). The folding model proposed here is based on stratigraphic and structural data acquired after extensive fieldwork and geological mapping, complemented by a comprehensive review of published information. The research workflow consisted of (1) stratigraphic characterization of the involved sedimentary sequence; (2) structural analysis and geological mapping with combined fieldwork and analysis of high-resolution aerial imagery (1:5000 scale orthoimages from Instituto Geográfico Nacional, Iberpix-IGN, and GoogleEarth) along the entire trace of the studied structures; (3) construction of detailed cross-sections and 3D outlines of folds and related faults from field data (unfortunately, seismic data are not available in the region); (4) measurement and analysis with Stereonet 8 software (Allmendinger et al., 2012) of fault planes and kinematic indicators in selected outcrops in order to understand timing, kinematics and evolution of faults; (5) analysis of the tectono-sedimentary relationships of faults and folds with the Mesozoic and Cenozoic stratigraphic sequences and (6) review and integration of data sets, that resulted in delineation of updated regional information to reconstruct the evolutionary model for the anticlines. The data, interpretations and tectono-sedimentary models proposed here are confronted with the observations, data set and interpretations exposed by Vergés et al. (2020) incorporating salt-tectonic concepts. Likewise, the discussion is enriched by incorporating analysis of other relevant regional information, such as (i) regional thickness variations of the salt-bearing sedimentary sequences and of the overlying carbonate units, (ii) mechanical behaviour of the stratigraphic sequence during the Mesozoic and Cenozoic tectonic stages and (iii) kinematics and timing of fold interference structures.

4 | RESULTS

4.1 | The Cañada Vellida anticline

4.1.1 | Description

The NW-SE to NNW-SSE trending Cañada Vellida anticline is more than 14 km long and represents the western boundary of the Cenozoic Aliaga basin (Figures 3 and 5). In the central part of its trace, the contractive structure is mainly defined by a tight box anticline that in detail shows an NE-directed, west-dipping thrust with overturned anticline and syncline in its hanging-wall and footwall blocks, respectively (cross-sections 2–2′ and 3–3′; Figure 5). The present-day topography allows recognizing the thrust, especially by the occurrence of two hectometre-scale klippes in which overturned Middle and Upper Jurassic strata lie onto overturned Barremian-Aptian units (Figures 6a and 7). In detail, the thrust is defined by a 1–2 m wide fault zone consisting of brown mudstones with embedded boulders of Aptian sandstones and Jurassic brecciated limestones, some of them showing striated facets (Figure 7b). In the core of the anticline, the Jurassic overturned beds are cut by hectometre-to kilometre-scale fault planes, mostly parallel to the fold trend, shallowly dipping (15–20°) to the west and showing reverse decametric displacements (cross-section 2–2′, Figure 5).

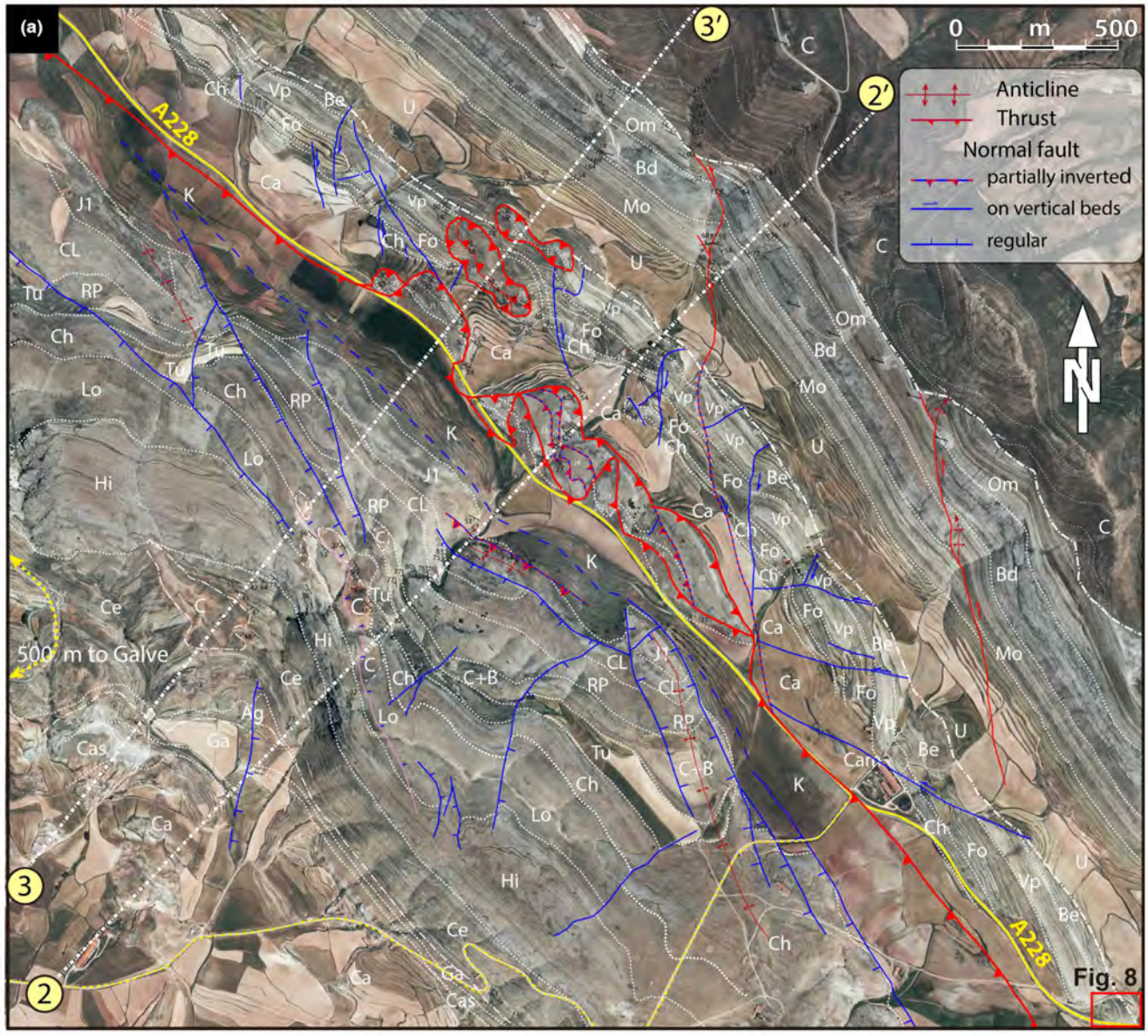

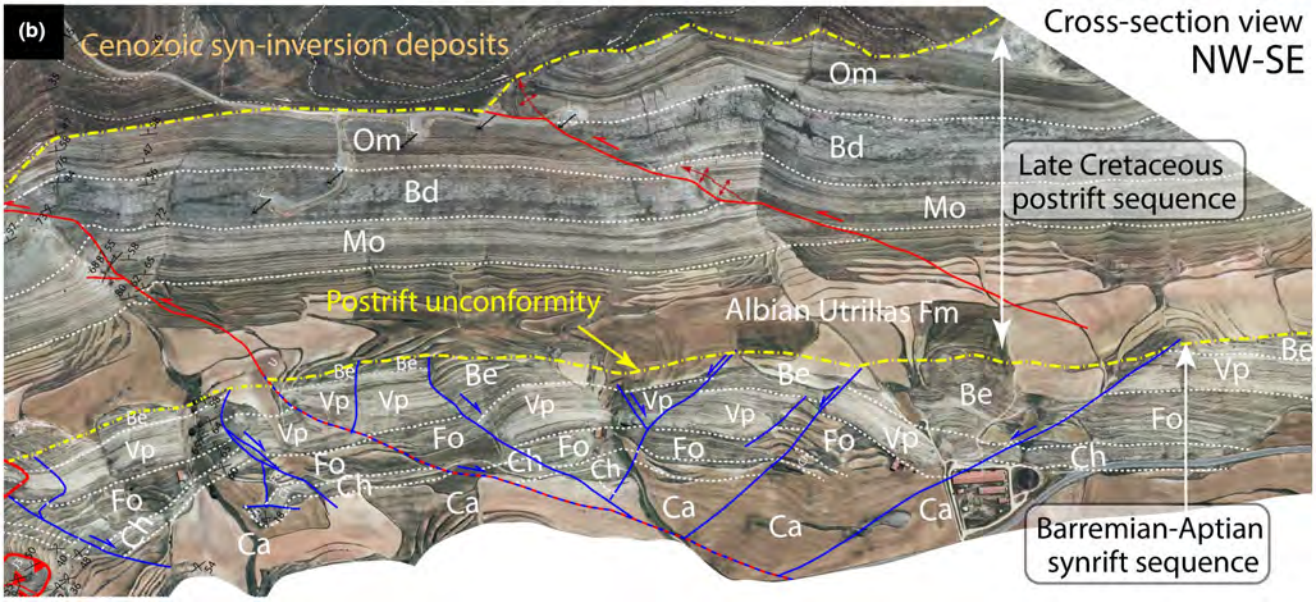

FIGURE 6 Detail of the Cañada Vellida structure in its central sector (see Figure 3 for location). (a) Geological map of the NW-SE trending anticline and thrust of Cañada Vellida on high-resolution (0.5 m/pixel), colour aerial orthoimage (available on the SITAR web page of the Aragón government; https://idearagon.aragon.es/descargas). Note the two hectometre-scale klippes of overturned Jurassic rocks surrounded by overturned Barremian-Aptian formations. Sections 2–2′ and 3–3′ are shown in Figure 5. (b) Detail of the eastern fold limb showing hectometre- to kilometre-scale graben and half-graben structures affecting the Barremian-Aptian sequence, which are sealed by the Albian Utrillas Formation (post-rift unconformity). The nearly vertical attitude of the beds allows the map to be viewed as a cross-section of the Early Cretaceous extensional structure.

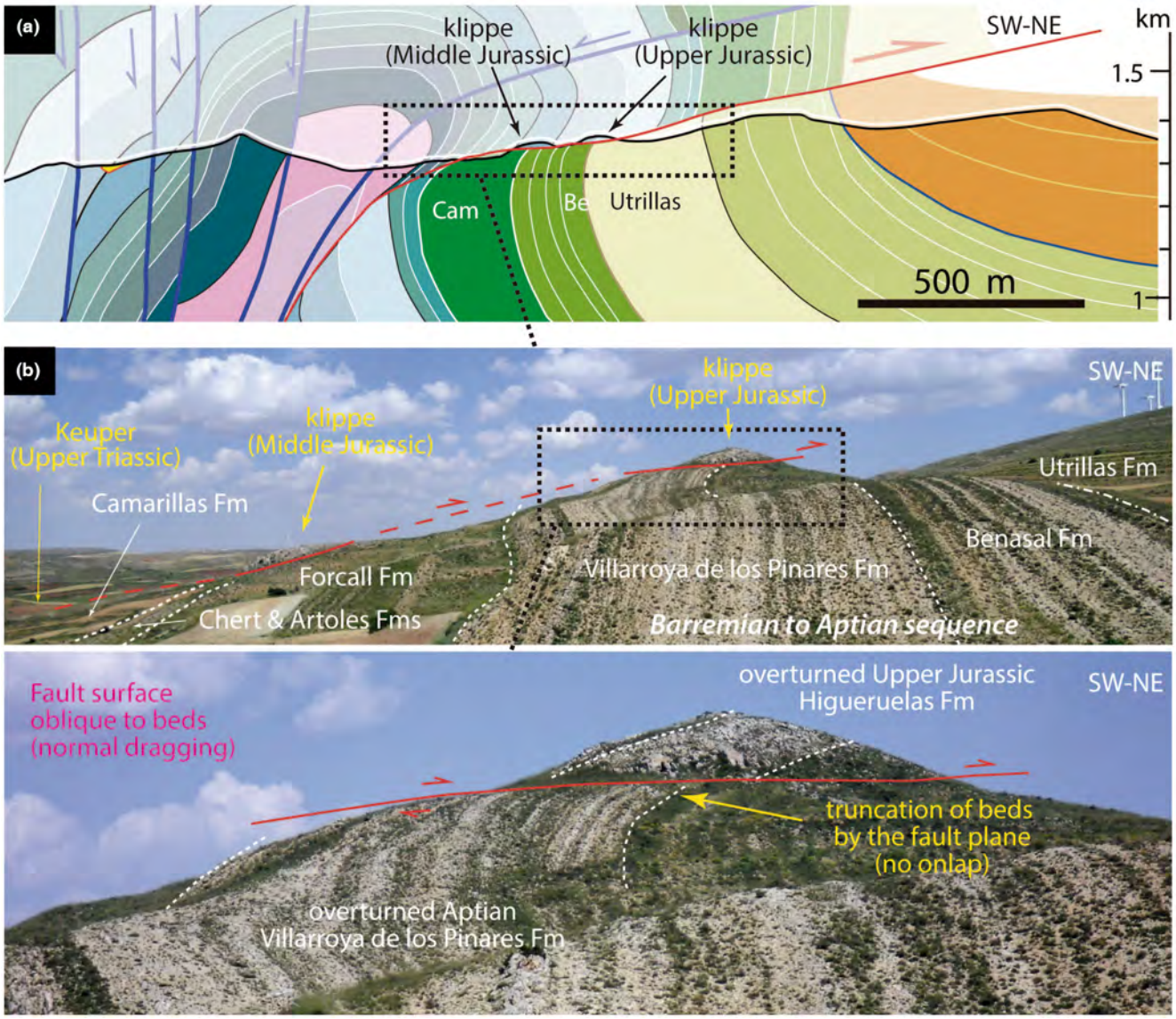

FIGURE 7 (a) Enlarged view of the klippes shown in cross-section 3–3′ of Figure 5. (b) Above, field photograph showing the two klippes of overturned Jurassic rocks associated with the main thrust and the geometrical relationships with the overturned Barremian-Aptian formations of the footwall block. Below, detail of the northeastern klippe showing the relationships of the hanging-wall and footwall beds with the fault plane, and the drag fold developed in the footwall block. Vergés et al. (2020) interpreted the truncation of beds by the fault plane as an onlap of the Aptian sediments on the diapiric flap structure of the Jurassic sequences.

Regarding the main thrust running along the anticline core, its horizontal displacement increases from southeast to northwest, from c. 300 m in section 2–2′, c. 600 m in section 3–3′, up to >1100 m in section 4–4′ (Figure 5). In turn, the anticline shape changes from box-fold geometry to an NE-verging overturned fold. More to the northwest, the thrust displacement decreases again, so that north of the Cañada Vellida locality the structure represents a narrow, tight, faulted anticline (Figure 3).

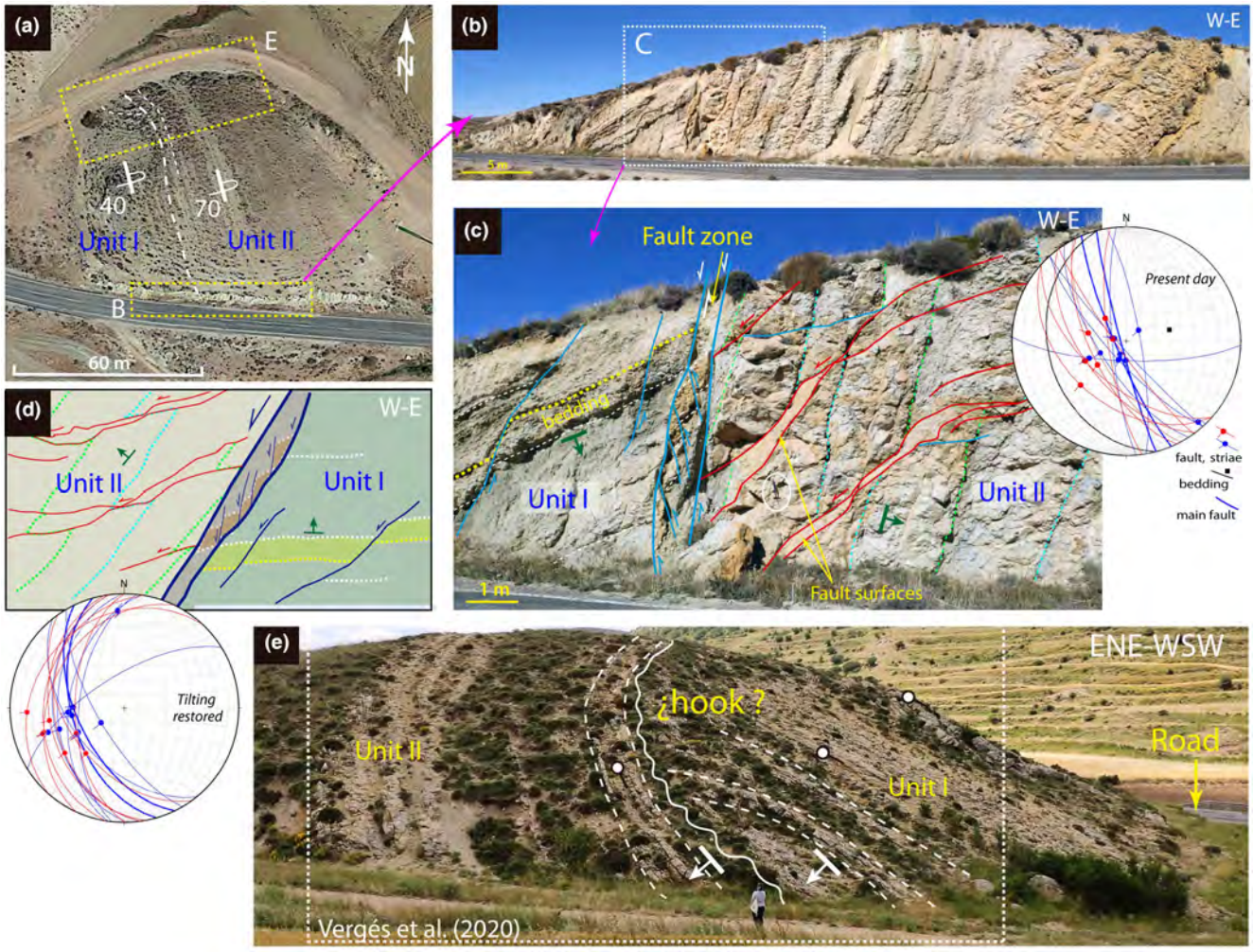

FIGURE 8 Fault zone vs. hook structure at the Cañada Vellida anticline (see Figure 6a for location). (a) The controversial structure as seen in the high-resolution (0.5 m/pixel) colour aerial orthoimage (available at SITAR web page of the Aragón government; https://idearagon.aragon.es/descargas), showing its southward continuity (60 m) to the fresh outcrop at the slope of the main road studied here. (b) Field view of the road cut locating the structure under discussion. (c) Detail of the structure, which actually represents a narrow fault zone separating two blocks with different bed attitudes (marked with green/yellow lines). Note that beds are overturned and that two different fault sets (blue and red colour lines) occur within the fault zone and its vicinity. (d) Line drawing of the structure after the restoration to the pre-compressional stage, showing the attitude of beds and fault zone, and the normal drag on the hanging-wall block. Insets in c and d show stereoplots (lower hemisphere, Schmidt net) of fault planes (colours as in photograph) and bedding at the present day and after tilting restoring, respectively. (e) Field view of the outcrop (dashed white line area) interpreted as a hook by Vergés et al. (2020) in the dirt road (see a for location); lines and symbols in white colour show their interpretation.

The Upper Jurassic–Lower Cretaceous sedimentary sequence is different in the two limbs of the anticline (Figure 4). The recorded sequence is thicker, about 3.5 times, in the western block than in the eastern one. It is also more complete so that the Tithonian-lowermost Barremian units (Aguilar del Alfambra, Galve and El Castellar formations) are only present in the western block. In the eastern block, the Barremian series (Camarillas Fm) rests on the Upper Jurassic sequence (Cedrillas Fm) through a low-angle unconformity, which truncates strata at an outcrop scale.

In the southern part, the incision of the Alfambra River allows a closer examination of the core of the Cañada Vellida anticline (Figure 3). There, the folding structure is not so tight and allows to recognize a set of faults (Cañada Vellida fault system) that run parallel to the anticline (Figure 3, and cross-sections 1–1′ in Figure 5). The main fault also strikes NNW–SSE and dips westwards, and juxtaposes the Upper Triassic (Keuper) in the footwall and the Upper Jurassic (Higueruelas Fm) strata in the hanging wall. It exhibits a normal displacement of c. 1 km in the Triassic–Lower Jurassic sequence, with a conspicuous normal drag in the footwall block. A set of synthetic normal faults, but also antithetic ones, completes the extensional structure. Only the northeasternmost fault shows a c. 500 m net reverse dip-slip, using the Triassic to Lower Jurassic strata as a reference.

In the eastern limb of the Cañada Vellida anticline, the vertical to overturned beds are crossed by numerous map-scale faults with several orientations (N-S, E-W, WNW-ESE, faults in blue in Figure 6a). These faults produce changes in the thickness of the Barremian-Aptian units and are responsible for the contrasting tilting between fault blocks, as shown by map relationships. Most of the faults are sealed by the unconformity of the post-rift Albian sandstones (Utrillas Fm). In the image obtained by rotating to the horizontal, this unconformity virtually represents a cross-section view of the pre-folding structure (Figure 6b). It shows the presence of graben and half-graben structures, probably with a roughly NE–SW trend, that is, perpendicular or very oblique to the section view. This normal fault system is therefore roughly orthogonal to the NW-SE to NNW-SSE Cañada Vellida master system. The faults are rooted in the red clays of the Barremian Camarillas Formation. Some of these faults show normal separation in the Lower Cretaceous units but reverse in the Upper Cretaceous-Cenozoic units (a fault with discontinuous blue and red trace in Figure 6b).

A road exposure allows a more detailed analysis of the deformation that occurs at the core of the main fold (Figure 8a–c). Two overturned sedimentary sequences (I and II; Forcall and upper part of the Villarroya de los Pinares to Benasal formations, respectively) are separated by an NNW–SSE-trending (N160°E) narrow fault zone (blue traces in Figure 8c) with a steep dip (82–86°) to the west, and a normal slip component (pitch 77° to 83°S) (thick blue great circles in stereoplots of Figure 8c). Within the fault zone, minor east-dipping faults currently show reverse slip components (pitch 84°N), while west-dipping ones show normal slip components (pitch 80–83°N). All of them are consistent with normal slip on the whole fault zone: according to the usual nomenclature in semi-brittle shear zones, west-dipping and east-dipping faults can be interpreted as C planes and R (Riedel) planes, respectively. A second striation with a dextral slip component (pitch 6° S) overprints the normal-slip striation on a west-dipping fault plane. Other synthetic, shallower dipping faults with decimetre-scale normal displacements also occur in the eastern block (red traces in Figure 8c). Some of the layers show apparent thickness changes associated with these faults. This outcrop can be correlated with the one investigated by Vergés et al. (2020) on the unpaved road that runs just 50 m to the north (Figure 8a) and interpreted as a hook geometry involving the same two Aptian sequences (Figure 8e).

4.1.2 | Remarks on the tectono-sedimentary evolution

We interpret that the Cañada Vellida anticline resulted from inversion during the Cenozoic of an NNW–SSE trending, west-dipping major normal fault, the Cañada Vellida fault, which runs through its core (see map and cross-section 1 in Figures 2 and 3). In detail, this extensional structure consists of several, nearly parallel faults, now folded together with the involved layers (Figures 3 and 5). This normal fault system was active from the latest Kimmeridgian to the middle Albian, as suggested by conspicuous thickness variations of the stratigraphic series between different fault blocks (see Figures 4 and 6), the latter corresponding to the Galve (southwest) and Las Parras (northeast) sub-basins (Aurell et al., 2016; Casas, Cortés, Liesa, et al., 1998; Guimerà & Salas, 1996; Liesa et al., 2004, 2006; Liesa, Soria, Casas, et al., 2019; Navarrete, 2015; Peropadre, 2012; Soria, 1997). The thickness of the Middle and Upper Triassic units in the western, downthrown fault block is comparable to that expected from regional information (Table 1), and the Lower–Middle Jurassic units have a similar thickness in both blocks, so the structure was probably not active during these periods. There is no information regarding the Lower Triassic.

The present-day structure (in an NE–SW cross-sectional view) is certainly complicated due to the deformation pattern of the Mesozoic Cañada Vellida fault zone during shortening. Geometric reconstruction of the Cañada Vellida anticline suggests that the main thrust, forming the two klippes, represents the inversion of a previous segment of the normal fault zone, while the upward decrease in the dip of the thrust surface can be probably due to a continuous folding after thrusting. The geometric relationship between the Jurassic limestones that overlie the Aptian sequence in these outcrops was interpreted by Vergés et al. (2020) as representing a diapir-related overturned flap, lapped onto by the Aptian beds. Inversion tectonics took place mainly during the Cenozoic, since the lower Miocene conglomerates of the Aliaga Cenozoic basin are also folded. In addition to the structural inversion, individual faults are interpreted to have undergone differential tilting and folding depending on their position in the fold (Figure 5). In the SW, back limb, the beds rotated towards the SW, so that (i) synthetic (southwest-dipping) normal faults have increased their dip, some of them changing their dip sense, while (ii) antithetic faults have decreased their dip (section 2–2′ in Figure 5). In the NE forelimb, limb rotations result in an opposite effect, and synthetic normal faults have decreased their dip favouring their slip during inversion.

Regarding the complex fault zone described in the road exposure in Cañada Vellida, several arguments also point to the development of normal faults during the Early Cretaceous and their subsequent deformation by compressional folding: (i) the general attitude

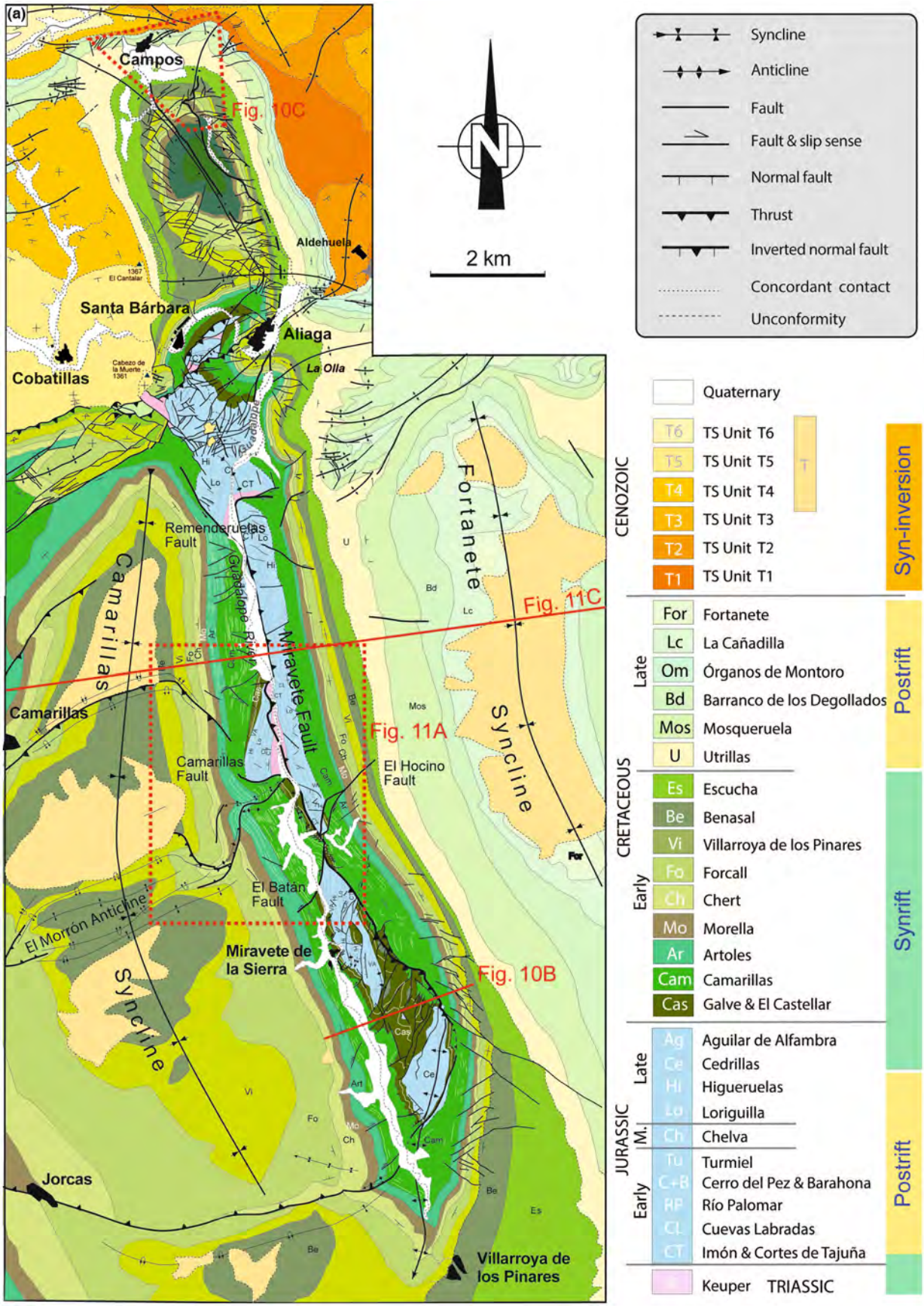

FIGURE 9 Detailed geological map of the Miravete (Campos–Aliaga–Miravete–Villarroya de Los Pinares) anticline cut at its core by the Miravete fault (see location in Figure 2).

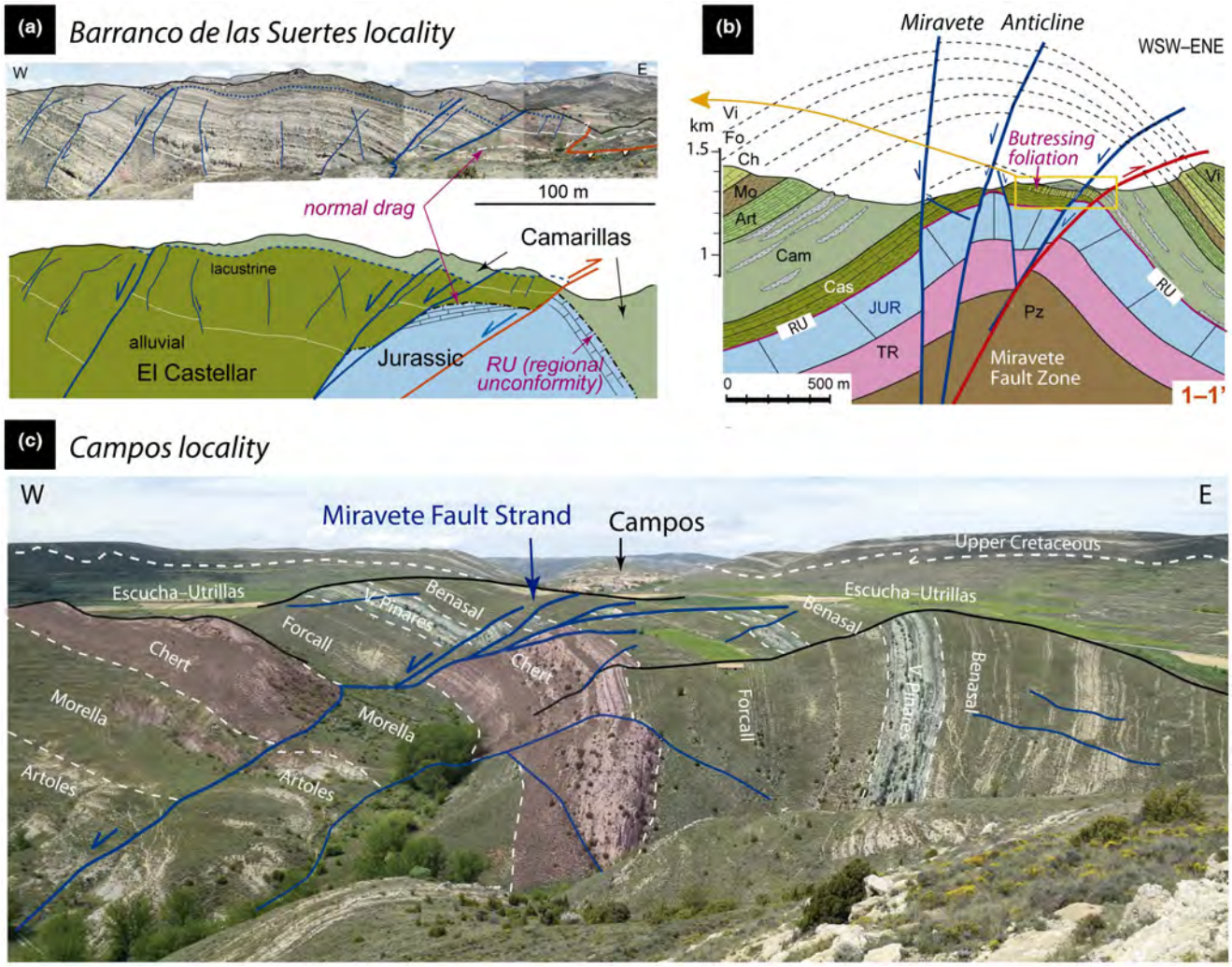

FIGURE 10 Views of the Miravete normal fault zone cropping out in the core of the Miravete anticline (see Figure 9 for location). (a) Detail of the structure at Barranco de las Suertes, where the upper Hauterivian-lower Barremian El Castellar Fm progressively decreases in thickness from one fault block to another and finally disappears in the eastern block. (b) Detailed geological cross-section of the Miravete anticline south of Miravete locality, showing its relationship with partial inversion of a near vertical, west-dipping normal fault zone (Miravete fault). The latter controlled sedimentation and thickness variations during the Late Jurassic-Early Cretaceous rifting stage, representing the eastern boundary of the Early Cretaceous Galve sub-basin. (c) Field view of the eastern limb of the periclinal domain of the Campos anticline (located in Figure 9), where two NW-SE to NNW–SSE striking normal ruptures belonging to the Mesozoic Miravete fault zone offset Barremian to Aptian units.

of overturned strata, showing different dips at each side of a near vertical fault zone; (ii) the occurrence of the high-dip, normal-slip fault zone; (iii) the superposition of a strike-slip (dextral) striation on the normal-slip striation; (iv) the apparent change in thickness in some of the layers displaced by these faults and (v) the numerous synsedimentary extensional faults widely recognized in this area and elsewhere (Figure 6b). After restoring the folding (by backtilting the bedding of Unit I, Figure 8d), the faults cluster in an N-S to NNW-SSE direction with an intermediate westwards dip, and all of them show a normal slip component. This suggests a prevailing E-W to ENE-WSW extension direction during their formation. It is also interpreted that normal drag occurred in the hanging wall of the fault (unit II). A similar scenario can be envisaged for the hectometre-to-kilometre scale faults cropping out in the core of the anticline near the klippes involving Jurassic units.

Faults in the eastern limb/block are interpreted to represent a second-order normal fault system trending ENE-WSW, nearly perpendicular to the Cañada Vellida structure, as suggested by the differential subsidence and erosion of the Barremian-Aptian sequence and the sealing of the faults by the Albian unconformity (Utrillas Fm, Figure 6b). Fault rooting in the Barremian Camarillas Fm suggests that this unit was probably the detachment

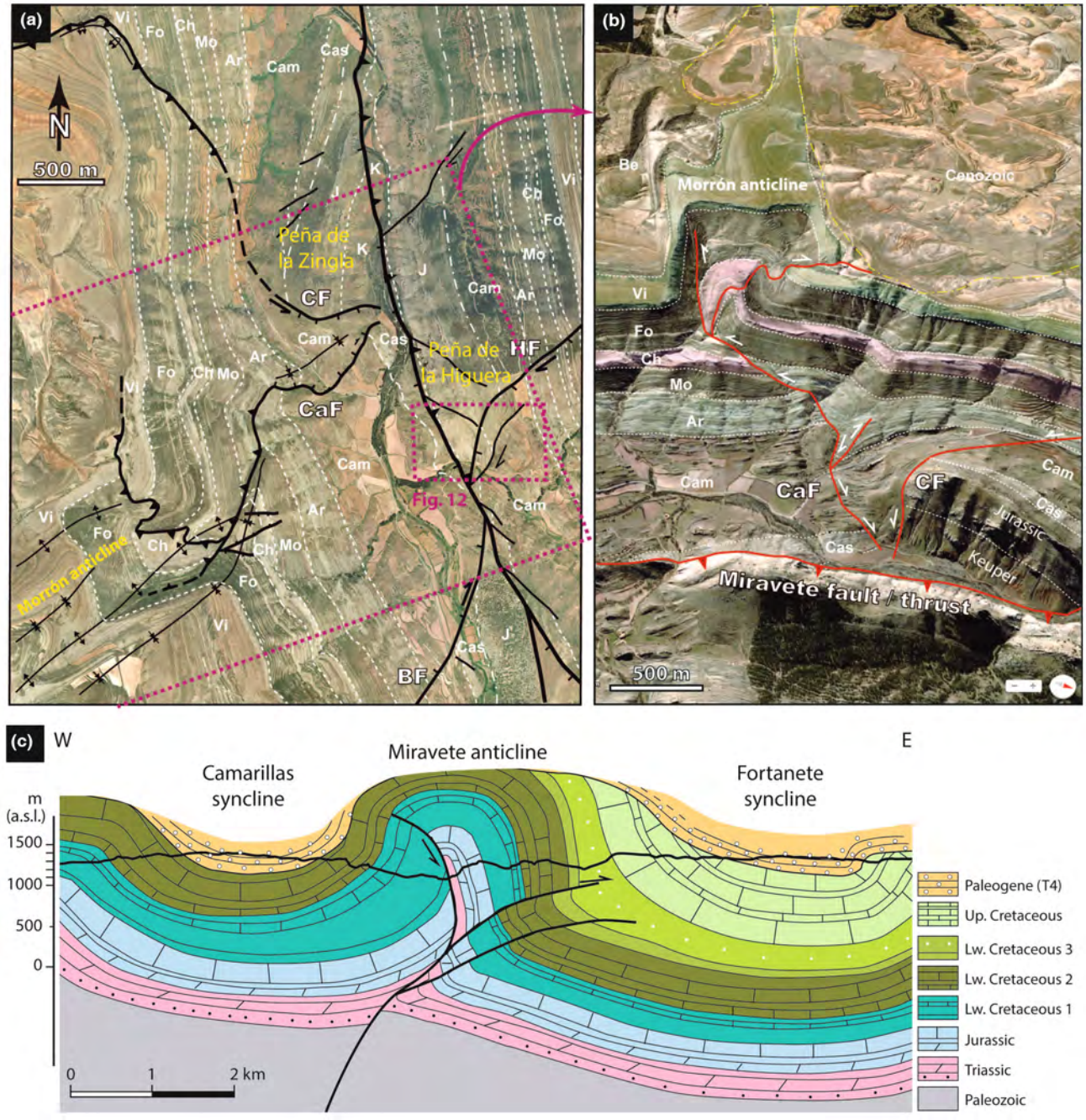

FIGURE 11 The Miravete normal fault zone and its inversion structure obliterate the anticline hinge north of the Miravete locality (see the location in Figure 9). (a) High-resolution (0.5 m/pixel), colour aerial orthoimage (available at SITAR web page of the Aragón government; https://idearagon.aragon.es/descargas) with detailed mapping of the fold and other related structures north of Miravete locality, as well as the location of Peña de la Higuera and Peña de la Zingla localities. Modified from Liesa et al. (2004, 2006, 2018), Liesa, Soria, Casas, et al. (2019, Liesa, Soria, and Simón (2019). (b) Oblique view of the El Morrón box-fold anticline and its relation with the inversion of a Mesozoic normal fault. (c) Geological cross-section of the Miravete anticline where the west-dipping Miravete fault has been folded to an eastwards dip and inverted during the Cenozoic shortening (modified from Simón et al., 1998).

level for this fault system. Partial inversion of some faults is indicated by the reverse slip of the Upper Cretaceous markers and Cenozoic growth strata, while the pre-Albian synrift sequence markers show normal slip. These reactivations likely accommodated posterior shortening parallel to the fold trend.

4.2 | The Miravete anticline

4.2.1 | Description

The Miravete anticline is a 20 km long complex fold showing an NNW-SSE to N-S direction (Figures 2 and 9). In

most of its traces, it has a fairly tight box geometry (2–2.5 km fold width at the Lower–Upper Cretaceous contact), which contrasts with the smoother geometry of the two flanking synclines, the Camarillas and Fortanete synclines, at least twice the width of the anticline. In detail, the anticline runs parallel and obliterates a first-order fault (the Miravete fault zone; MFZ), which crops out discontinuously along the fold core (Figure 9). The Jurassic units cropping out in its limbs are cut by a dense network of decametre-to-hectometre scale faults.

The hinge of the Miravete anticline is observed mainly in the southern and northern parts of the fold trace. Near the southern termination, at the Barranco de las Suertes outcrop (c. 2 km south of Miravete), the anticline shows a gentle hinge defined by the upper Hauterivian-lower Barremian El Castellar Fm and the Barremian Camarillas Fm (basal part). There, the fold hinge is cut by a pervasive set of mainly west-dipping, NNW–SSE to NNE–SSW trending normal faults of different lengths. The main faults have at present normal offsets of tens of metres, taking as a reference a characteristic limestone bed in the middle of El Catellar Fm (Figure 10a). All in all, this layout defines a stepped normal fault array in cross-section for the Miravete fault zone. In this outcrop, as already described by Liesa et al. (2004, 2006, 2018), the El Castellar Fm shows abrupt changes in thickness due to normal faulting, systematically decreasing towards the east. This unit disappears in the footwall of the easternmost fault in which only a centimetre-thick clay level with ferruginous pisolites is found between the Jurassic strata (mid-Tithonian-lower Berriasian Aguilar del Alfambra Fm) and the lower Barremian Camarillas Fm. In that fault, the El Castellar Fm overthrusts the sandstones of the Camarillas Fm, but the regional unconformity on top of the Jurassic shows a normal offset (Figure 10a,b). The upper Barremian-Aptian sequence (Camarillas to Benasal formations) shows a similar change in thickness from west to east, being twofold or threefold thicker in the western limb of the Miravete faulted anticline (Figure 10b, Table 1). Jurassic and Lower Cretaceous strata and synrift and intrarift unconformities usually display drag folds in the hanging-wall and footwall blocks of Mesozoic normal faults.

At its northern termination (Aliaga-Campos segment), the Miravete anticline has a typical box–fold geometry (cross-section 2 in Figures 2 and 9). Two kilometre-scale faults running parallel to the fold axis crop out in the anticline core and show a normal offset, with the Escucha and the Benasal formations appearing in the hanging-wall and footwall, respectively, at their northern tip, near the locality of Campos (Figure 9). The faults have an NW-SE to NNW–SSE strike and a westwards dip (25 to 70°W), depending on their position after folding (Figure 10c). At both fold limbs, minor normal faults affecting the Aptian units (Chert, Forcall, Villarroya de los Pinares and Benasal formations) stand out. This system of conjugate, E-W to NE-SW striking normal faults is associated with changes in thickness and lithology of Lower Cretaceous units, and an unconformity located within the Escucha Fm clearly seals them, as was described in detail by Simón, Arenas, et al. (1998), Simón, Liesa, et al., (1998). The fault system cropping out in the western and eastern limbs of the anticline shows a different asymmetry, with predominant dips to the north and south, respectively.

Regarding the central part of the Miravete anticline, the hinge is not observable in most cases because a major fault runs through its core and juxtaposes different sedimentary units from the two limbs of the fold (Figures 9 and 11). In this segment, the Miravete fault/thrust crops out with a steep eastwards dip, and the almost continuous Upper Triassic–Jurassic sequence of its eastern limb is locally superposed on younger strata of the western limb. This is the case in the Peña de la Higuera outcrop, also studied by Vergés et al. (2020), and the Peña de la Zingla outcrop, 2 km northwards (Figure 11a). The Early Cretaceous sequence of the western block is also 2.5 times thicker than that of the eastern one (Figure 11c).

The sedimentary units cropping out at the core of the anticline change along the trend, especially for the western limb or fault block (Figures 9 and 11a), because a number of kilometre-scale normal faults (Remenderuelas, Camarillas and El Batán faults), with hectometre-scale displacements, juxtapose the Triassic–Jurassic sequence on a thicker Lower Cretaceous series (mainly the Camarillas Fm). The near vertical attitude of the layers (75–90°W dips) in this segment of the western limb enables using the geological map as a cross-section view of the pre-folding structure. These main faults form a system of conjugate normal faults, trending ENE-WSW (near perpendicular to the Miravete fault and anticline trend), which define a structure of halfgraben and graben (Figure 9), namely the Remenderuelas halfgraben and Camarillas graben (e.g. Liesa et al. 2004, 2006, 2018; Navarrete, et al., 2013a, 2013b, 2014). Abrupt thickness changes of the Hauterivian-lower Aptian units (El Castellar, Camarillas and Artoles formations) are associated with these faults. The sedimentary sequence shows fan-shaped geometries and thickening towards the fault planes (Remenderuelas and El Batán faults) and local unconformities, such as the one of the Camarillas Fm recognized in the footwall block of the Camarillas fault (Figure 11a). On the contrary, the upper Aptian units (Morella to, at least, Villarroya de los Pinares formations) show a progressive southward increase in thickness, more pronounced in the vicinity of the Camarillas fault (Peropadre, 2012). Furthermore, the ENE-WSW striking, south-dipping Camarillas fault (CF) and the

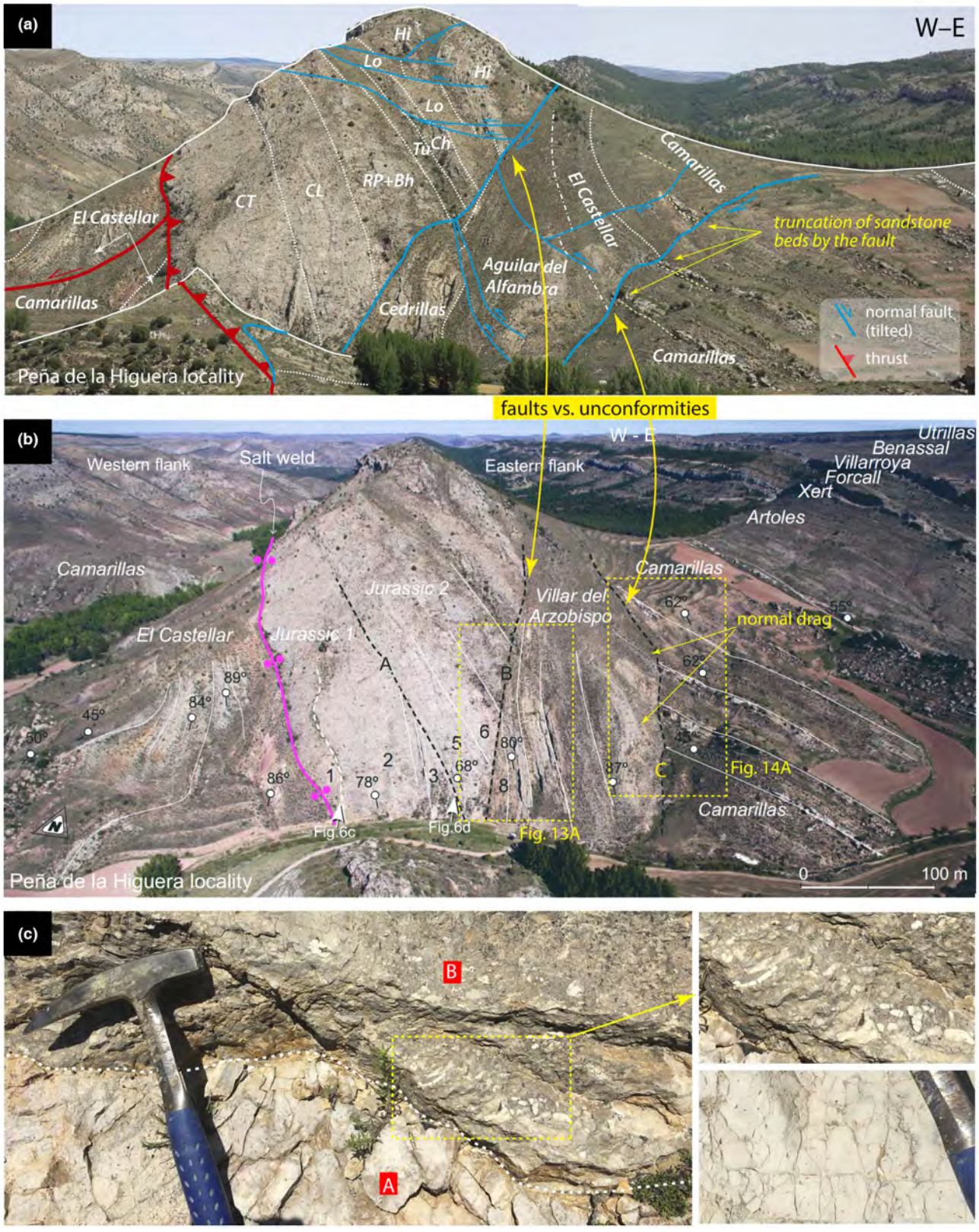

ENE-WSW striking, north-dipping Camarillas antithetic fault (CaF) have normal offsets in the lower part of their trace but reverse in the upper part, where they affect the upper Aptian carbonate or the Cenozoic conglomerate (Figures 9 and 11a). The ENE-WSW trending Morrón anticline, showing a box–fold geometry, follows the overall strike of the CaF and CF faults and is located above them (Figure 11a,b).

In the eastern limb of the Miravete anticline, there is a similar fault arrangement, although less

FIGURE 12 Faults vs. unconformities in the eastern limb of the Miravete anticline at the Peña de la Higuera locality (see location in Figure 11a). (a) Field photograph showing our interpretation of the supposed 'unconformities' B and C by Vergés et al. (2020, see b), which actually are tilted normal fault surfaces. These and other minor fault planes define an extensional fault system (El Hocino) that has been tilted during folding and locally reactivated as thrusts. The salt weld actually represents a fault slip lock between the Upper Triassic–Jurassic and the Lower Cretaceous units, each of them belonging to one of the fold limbs (Jurassic: CT–Cortes de Tajuña, CL–Cuevas Labradas, RP + Bh–Río Palomar and Barahona, Tu–Turmiel, Ch–Chelva, Lo–Loriguilla, Hi–Higueruelas). (b) Drone image with the Jurassic and Lower Cretaceous unconformities (surfaces A, B and C) and salt weld interpreted by Vergés et al. (2020) (letters and lines in yellow were included by us). Note that the interpretation proposed in this work for surfaces A, B and C overrides the progressive restitution carried out by Vergés et al. (2020) in this locality because the orientation of beds is affected by faults and associated dragging. (c) The 'erosional unconformity A' (contact between units 3 and 5) of Vergés et al. (2020) is interpreted here as a boundary of a shallowing upward sequence (sensu James, 1984); A– inter- to supratidal-laminated micritic limestone, B–flat pebble breccia (i.e. transgressive lag of the overlying sequence).

compartmentalized (Figures 9 and 11a). At this segment, a single major south-dipping normal fault (El Hocino fault; Liesa, Soria, & Simón, 2019; HF in Figure 11a) cuts the Jurassic-Lower Cretaceous sequence of the nearly vertical limb (75–85°E). Its displacement decreases upwards in the sequence, the fault plane being practically sealed by the unconformity of the Albian Utrillas Fm. The map shows that there is a change in thickness of the Lower Cretaceous associated with the fault, especially significant in the Barremian Camarillas and Artoles formations (Ibáñez, 2015; Navarrete, 2015; Figure 11a). The Jurassic sequence crops out almost in its entirety in the footwall (Peña de la Higuera outcrop), where it is strongly affected by faults having various orientations and scales (Figures 11a and 12a). The sequence is strongly tectonically thinned, and the Barremian Camarillas Fm unconformably rests on different tilted blocks of the upper Kimmeridgian–lower Tithonian Higueruelas and Cedrillas formations (Figure 9).

At the eastern side of the Peña de la Higuera outcrop, the El Hocino system includes two main fault planes (Figure 11a). Both show clear bed truncation in the hanging-wall and footwall blocks, with angles between strata and discontinuity surfaces relatively high (15°–40° in most cases) (Figures 12–14). The lower fault plane (boundary B of Vergés et al., 2020, in Figure 12b) juxtaposes the lower to upper Jurassic sequence with the uppermost Jurassic Cedrillas Fm (Figure 13a,b). It shows at present an NNE–SSW direction and a steep dip (60–70°) to the east and cuts at a high angle (>40°) practically all the Jurassic sequence, which strikes N145-155° E and dips 75°E (Figure 13a,d). The N-S striking, east-dipping (75°) strata of the Cedrillas and the Aguilar de Alfambra formations in the hanging wall block are also truncated by the fault but at a smaller angle (25°–30°), since these units are affected by normal drag and become more parallel to the fault plane. Minor metre- to decametre-scale antithetic faults cutting these layers converge into the main fault plane. Striation indicates a (present-day) dextral kinematics (pitch 12°S) of the main fault plane (F1 in Figure 13b,d), which also shows tectonic brecciation and decimetre-scale shearing features affecting calcareous rocks (Figure 13c).

The upper fault plane (boundary C of Vergés et al., 2020, in Figure 12b) has an attitude similar to the lower one, and juxtaposes the Barremian Camarillas Fm in the hangingwall block and the Aguilar de Alfambra and El Castellar formations in its footwall (Figures 12 and 14a). The angle between the affected layers and the fault plane is high (40°–60°). There are normal drag folds associated with the fault, one of them showing an erosive truncation and an angular unconformity between the Aguilar de Alfambra and El Castellar formations (Figure 14a). Along the fault surface, widespread metre-scale striated fault planes associated with truncation of the white sandstone layers of the Camarillas Fm can be recognized (Figures 12 and 14). The striae observed at different sites show low pitch and dextral slip componentS (Figure 14b–d).

4.2.2 | Remarks on the tectono-sedimentary evolution

Numerous evidences support the role of positive inversion of the NNW–SSE Miravete Fault Zone (MFZ) in the architecture of the Cenozoic Miravete anticline. At the Barranco de la Suertes outcrop, changes in the thickness of the El Castellar Fm associated with the stepped normal fault array indicate that the Miravete fault zone was active during its deposition, as remarked by Liesa and Simón (2004) and Liesa et al. (2004, 2006, 2018). The thickness change in the upper Barremian-Aptian sequence between the two limbs of the anticline are interpreted to occur progressively, in a similar way to that described for the El Castellar Formation. The difference in thickness thus probably represents the accumulated throw in the MFZ during the Barremian-Aptian. Normal drag in Jurassic rocks and synrift and intrarift unconformities in Lower Cretaceous strata is interpreted to be associated with the kinematics of these Mesozoic normal faults. At Barranco de las Suertes only partial inversion

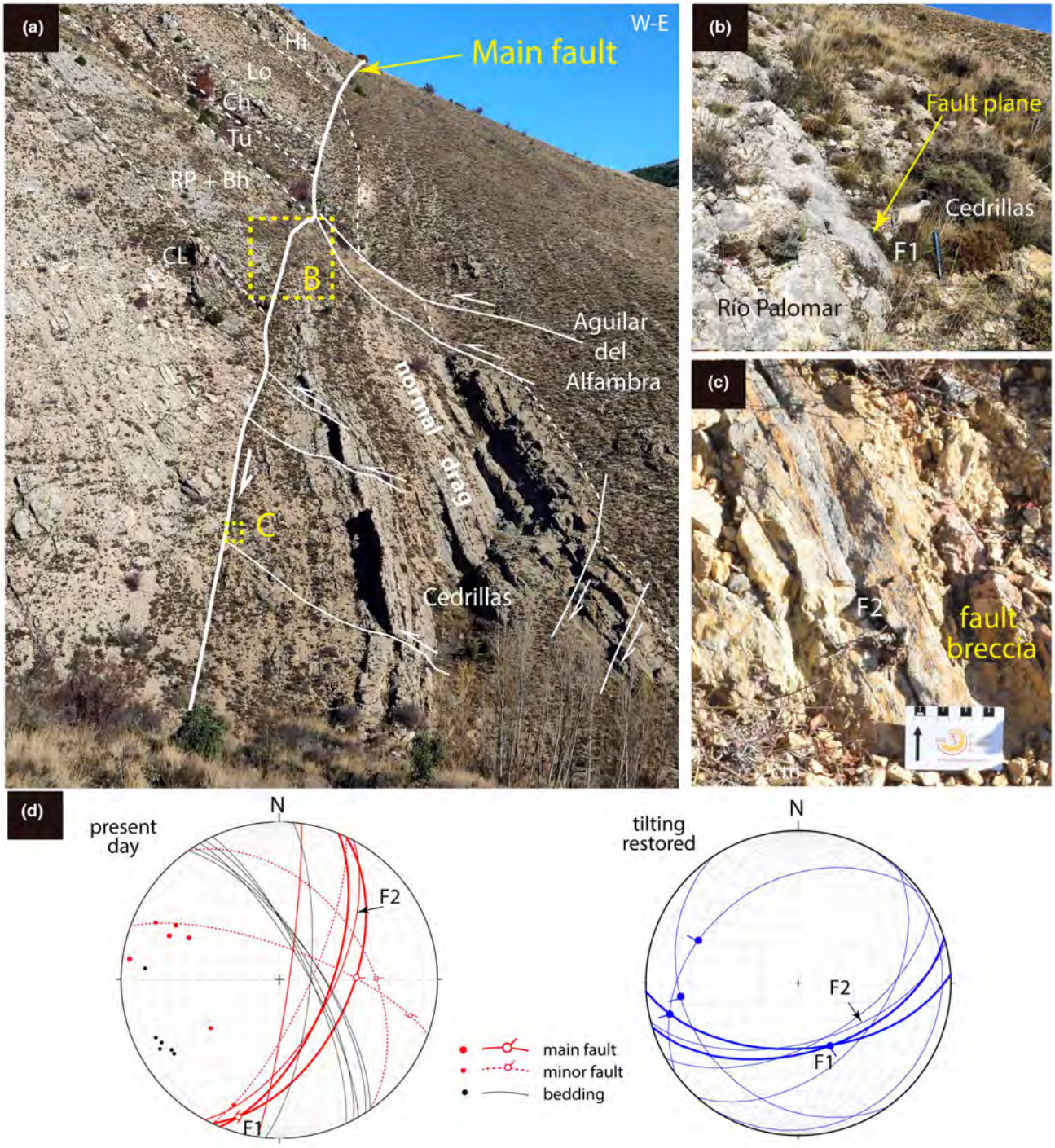

FIGURE 13 Main fault vs. unconformity B of Vergés et al. (2020) in Peña de la Higuera locality (see Figure 12b for location). (a) Main normal fault juxtaposing Lower-Upper Jurassic with uppermost Jurassic-lowermost Cretaceous rocks. Minor synthetic and antithetic faults affecting the Cedrillas Fm and the basal beds of the Aguilar del Alfambra Fm and probably rooted at the main fault (see also Figure 5a,b). Note that the beds of the eastern block (hanging-wall block) tend to be arranged at a low angle to the main fault, suggesting extensional drag folding. (b) Detail of the main fault plane (see location in A) here juxtaposing Lower Jurassic limestones (Río Palomar Fm) and uppermost Jurassic limestones (Cedrillas Fm). (c) Detail of fault breccia (see A for location). (d) Stereoplot (lower hemisphere, Schmidt net) showing the orientation of faults and bedding at present and after restoring the dip of the eastern limb of the Miravete anticline (150, 70 E).

occurred in the easternmost fault, where the El Castellar Fm overthrusts the Camarillas Fm, while the Jurassic-Early Cretaceous regional unconformity still has a normal offset (Figure 10a,b).

At the Aliaga-Campos segment, the typical box-fold geometry of the Miravete anticline has been related to the inversion of the MFZ (Simón, Arenas, et al., 1998; Simón, Liesa, et al., 1998; Simón & Liesa, 2011). Two

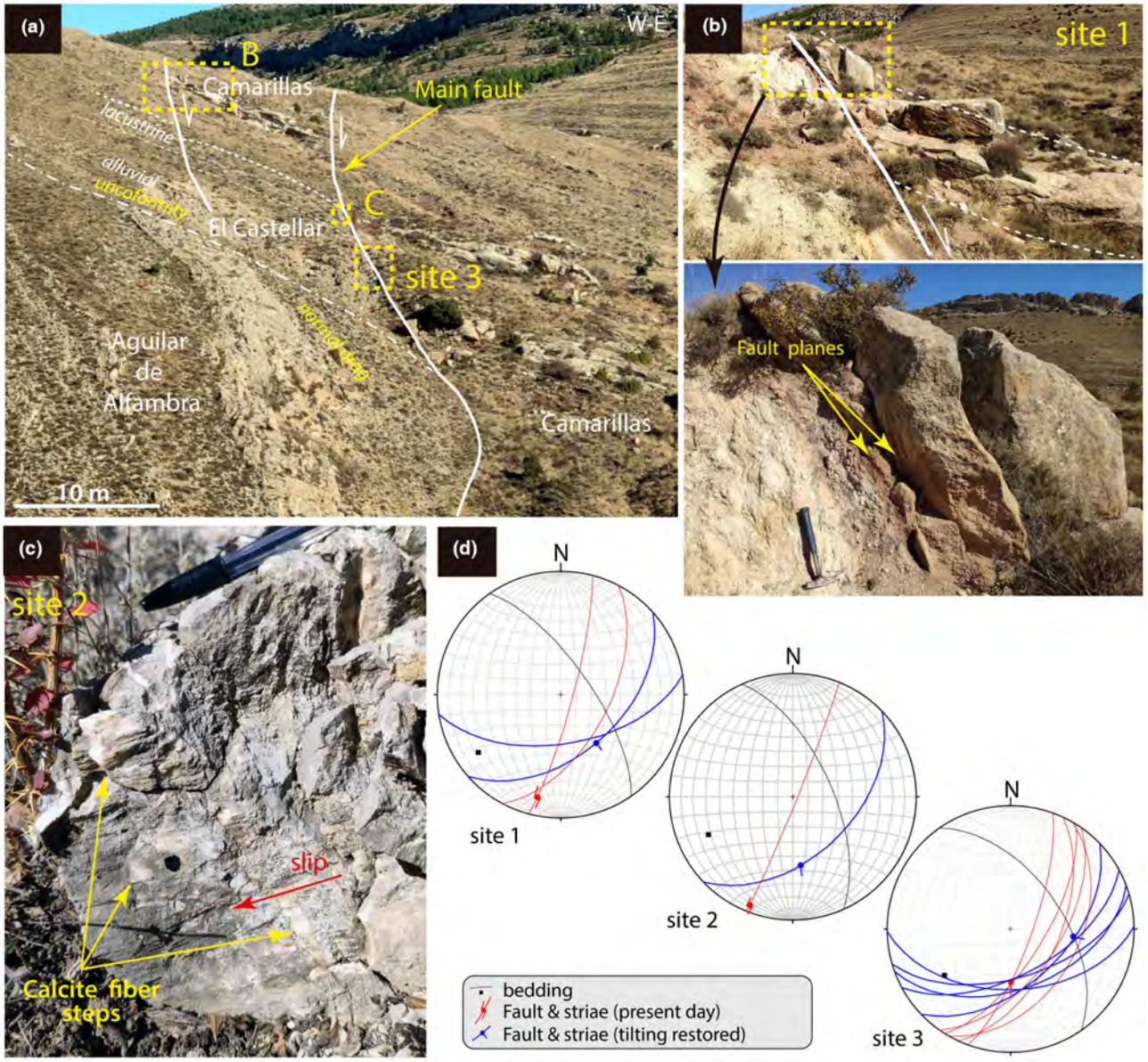

FIGURE 14 Main fault vs. unconformity C of Vergés et al. (2020) in Peña de la Higuera locality (see Figure 12b for location). (a) General outcrop view, indicating the location of the close images shown in B and C. Note the normal drag fold on the footwall block and the associated angular unconformity subsequently developed between the Aguilar de Alfambra and El Castellar formations indicating the Mesozoic activity of this normal fault. (b) Outcrop view and detail of the minor synthetic fault plane showing smeared red clay. (c) Minor fault plane with striae and calcite fibre steps, indicating a dextral-normal slip (the red arrow represents the movement of the removed block). (d) Stereoplots (lower hemisphere, Schmidt net) of faults and bedding planes, at present (in red) and restored to their original orientation after bedding backtilting (in blue), in sites 1, 2 and 3. Note the original ENE-WSW trend, southeast dip and normal slip (high pitch) of the fault planes during the synrift stage.

west-dipping normal faults, which are responsible for changes in thickness and block tilting of the Lower Cretaceous sequence, run along the anticline core (Figure 9). The different asymmetry of the nearly perpendicular fault system affecting the Aptian sequence in the western and eastern limbs of the anticline (predominant dips to the north and south, respectively) also points to the coeval activity of the MFZ. Geometric reconstruction of the perpendicular fault system suggests that it detached in the red clays of the Barremian Camarillas Fm (Simón, Liesa, et al., 1998). Sealing of this fault system by an intra-Escucha Fm unconformity and of major faults by the Albian unconformity (Utrillas Fm) clearly demonstrate the Mesozoic extensional activity of the MFZ.

The areal distribution and angular unconformities in syn-inversion deposits filling the Cenozoic Aliaga basin at both fold limbs of the Miravete anticline indicate a positive

inversion of the Miravete fault system in two stages to form the box anticline, as interpreted by González and Guimerà (1993) and Simón, Arenas, et al. (1998). Firstly, the eastern limb developed, probably associated with the upward propagation of the Miravete normal fault itself and the coeval deposition of tectonosedimentary units (TSU) T2 and T3 (Eocene-Early Oligocene) in the eastern part of the Cenozoic Aliaga basin (Figures 2 and 9). The western limb was formed during a second, short stage lasting until the Oligocene-Miocene transition, the sedimentation being then mostly transferred to the western Aliaga basin (unit T4).

The onset of the western limb has been related to the inversion of the upper segment of the Miravete normal fault (Simón, Arenas, et al., 1998). This initially west-dipping surface underwent passive rotation during the first inversion episode, changing the dip sense from west to east (Figure 11c). At the Peña de la Higuera section, the west-verging Miravete thrust is interpreted to primarily represent such an upper segment. After rotation, a net reverse slip could also have occurred on it, as suggested by the thrust of the Keuper facies of the eastern limb over the Jurassic series of the western one occurring north of Peña de la Zingla (Figure 11a). In this way, such reactivation does not represent a true structural inversion because the relative slip of fault blocks is the same during the Mesozoic extension and the Cenozoic shortening (Liesa et al., 2018).

The difference in rock units that crop out along the western and eastern fault blocks of the MFZ in the anticlinal core is interpreted to be associated with the action of a system of conjugate, ENE-WSW striking normal faults (Remenderuelas, Camarillas, El Batán and El Hocino faults). These faults formed half-graben and graben structures that were also responsible for differential tectonic subsidence, fan-shaped geometries and thickness changes in the Lower Cretaceous sequence, especially during the Hauterivian–early Aptian, as also stated by Soria (1997), Capote et al. (2002) and Liesa et al. (2004, 2006, 2018). The progressive southward increase in thickness of the upper Aptian units (more evident in the neighbourhood of the Camarillas fault; Figure 9) has been interpreted as a result of the activity as blind structures during deposition (Peropadre, 2012). Tectono-sedimentary relationships show that extensional tectonics was accompanied by block tilting, erosional truncation of layers and development of angular unconformities, such as those described between the El Castellar and Aguilar de Alfambra formations associated with the normal drag fold in the El Hocino fault. Based on its synsedimentary activity, back tilting of structures measured in the El Hocino fault shows how this structure had an ENE-WSW trend, a southwards dip (50°–60°), and a normal slip during the latest Jurassic-early Cretaceous rifting stage (Figures 13d and 14d).

The Camarillas fault and the Camarillas antithetic fault (CF and CaF, respectively) underwent partial inversion during the Cenozoic, as indicated by the folds associated with them, and the deformation of Paleogene conglomerates in the footwall of the upper thrust (Figures 9 and 11a,b). Such inversion was probably associated with the NNW–SSE or NNE–SSW compressions that affected the region during the early Miocene time (*Late Betic* and *Late Pyrenean* stress fields, respectively; Liesa, 2000; Liesa & Simón, 2007, 2009; Simón, 2006). The box-fold geometry of the ENE-WSW Morrón anticline and the thrust planes related to it are interpreted as the result of the two-stage CaF reactivation (Figure 11b): Firstly, the normal fault was partially inverted, nucleating an SSE-directed thrust in the Aptian sequence and developing its southern limb. Subsequently, an NNW-directed thrust was formed, developing the northern limb of the fold. The geometry and kinematics of this box fold also reveal the different behaviour during the shortening of differentially stretched sedimentary packages. In the most stretched pre- and synrift sequences, shortening appears to be responsible only for recovery of the previous extension and for partial inversion of faults. In the less stretched upper sequence, the shortening is however capable of producing important contractive structures without continuity at depth.

5 | INVERSION TECTONICS EVOLUTIONARY MODEL FOR THE INVESTIGATED ANTICLINES

The stratigraphic study, geological mapping and structural analysis and synthesis carried out in the Cañada Vellida and Miravete anticlines have revealed that (i) these complex folds run parallel to major faults or fault zones (the Cañada Vellida and Miravete fault zones; Figures 3 and 9, respectively), (ii) these fault zones represented major west-dipping extensional structures during the latest Jurassic-Early Cretaceous rifting stage, as indicated by their kinematics and the change in thickness of the involved sedimentary units (Figure 4) and (iii) the fault zones nucleated and controlled the evolution of the narrow and complex box-geometry anticlines during the Cenozoic shortening stage in which folding and partial inversion of fault planes controlled the present-day structure (Figures 5, 10b, and 11b).

The arguments summarized above support the evolutionary model depicted in Figure 15a. Major fault zones in this model are mainly defined by several associated fault planes showing a stepped arrangement in cross-section.

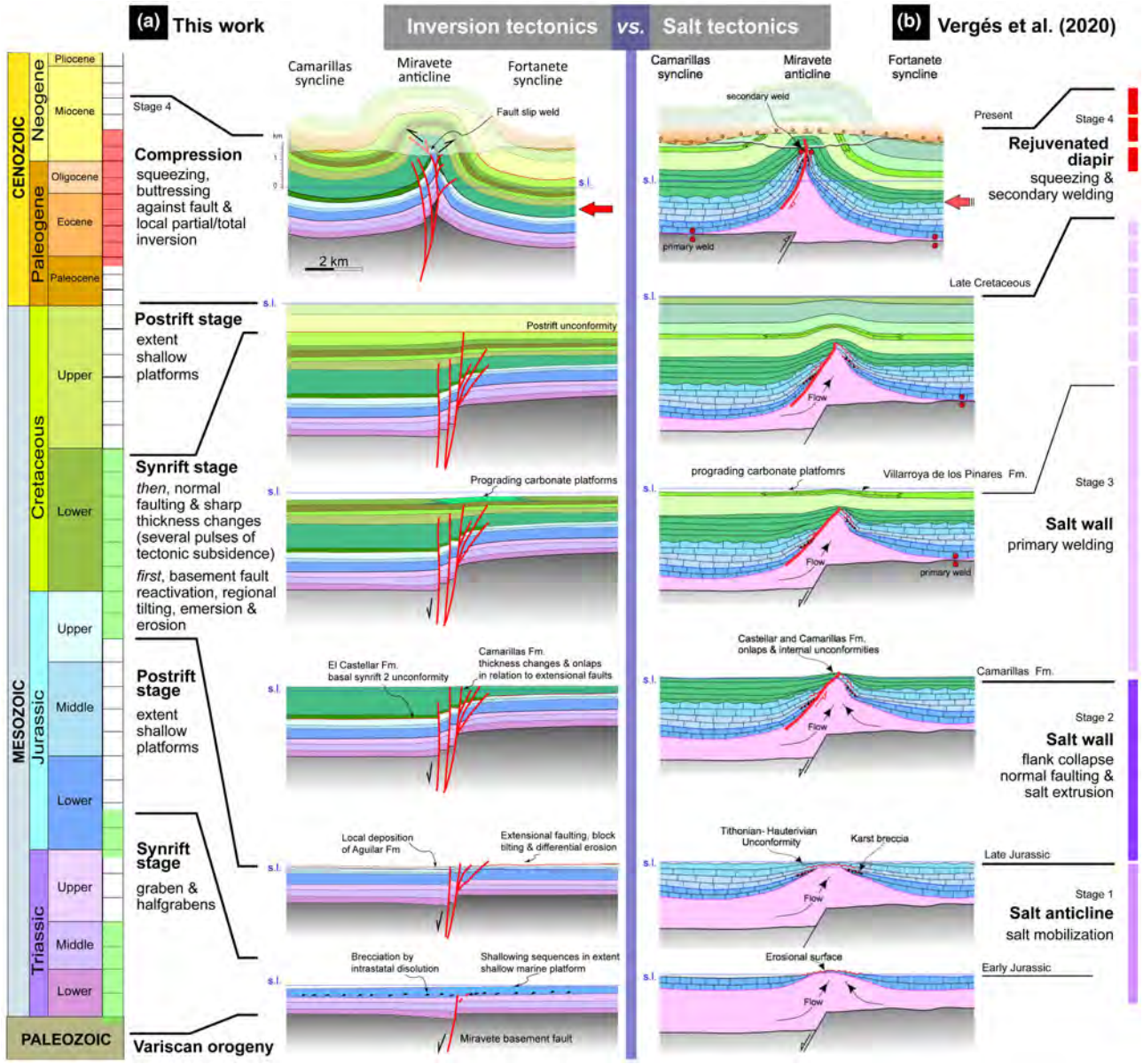

FIGURE 15 Confrontation of salt tectonics and extensional tectonics as the driving mechanism for the formation and evolution of the Maestrazgo basin exemplified in the structure of the Miravete anticline. (a) The extensional tectonic model and subsequent inversion proposed here, also applicable to the Cañada Vellida structure (the latter representing a more evolved compressional stage). (b) Diapiric model with salt remobilization building a salt anticline and salt wall during the Mesozoic, and a stage of rejuvenated diapir during the Cenozoic (after Vergés et al., 2020).

This arrangement involves a progressive but staggered pattern of thickness changes of the uppermost Jurassic–Lower Cretaceous synrift successions from one basement fault block to another. The folding of this arrangement was also responsible for the varied geometry and lateral change of the resulting inversion structure. The upward propagation of basement faults during the Mesozoic was probably controlled by incompetent layers within the cover such as the Upper Triassic mudstone and gypsum Keuper facies. Frequently, these ductile layers have hindered fault propagation and nucleated splay faults that widen upwards the fault zone.

The evolutionary model (Figure 15a) also takes into account regional information about the Mesozoic history of the region summarized in previous sections. The available information on the Triassic sequence, with a homogeneous distribution of facies and thickness on a regional scale, suggests that the first Mesozoic rifting stage was not very significant in this area (Capote et al., 2002). Also, the Jurassic and the Upper Cretaceous post-rift carbonate platform sequences show the uniform thickness and facies distribution, with no significant coeval synsedimentary tectonic structures (e.g. Alonso et al., 1993; Aurell et al., 2003).

6 | DISCUSSION

6.1 | Inversion tectonics vs salt tectonics for the western Maestrazgo anticlines

The model proposed to explain the evolution of the Cañada Vellida and Miravete anticlines is consistent with most structural and stratigraphic features of the Iberian Chain and other western Mediterranean chains, which can be explained by a Mesozoic extensional stage and a strong Cenozoic inversion, within the context of the kinematics of the Iberian, African and European plates (e.g. Álvaro et al., 1979; Capote et al., 2002; Guimerà, 2018; Liesa et al., 2018; Liesa, Soria, Casas, et al., 2019; Salas & Casas, 1993; among others). This model contrasts with the interpretation of these structures recently made by Vergés et al. (2020) using salt-tectonic concepts.

Based on their evolutionary model proposed for the Miravete anticline, Vergés et al. (2020) distinguish three salt tectonics stages in its Mesozoic evolution and a fourth stage during the Cenozoic (Figure 15b). During stage 1 (Jurassic), the mobilization of Triassic salt would have been responsible for the initial development of a salt anticline, involving the formation of an Early Jurassic erosional surface (surface A in Figure 12b), an Early Jurassic karst breccia (Cortes de Tajuña Fm) and a significant change in thickness of the Jurassic sequence. In stage 2 (latest Jurassic–earliest Barremian), an increase in salt mobility developed a salt wall, with flank collapse, normal faulting and salt extrusion, resulting in the development of the regional Tithonian-Hauterivian unconformity, and changes in thickness, onlaps and internal unconformities (surfaces B and C) in the El Castellar and Camarillas formations. During stage 3 (early Barremian–middle Aptian), the salt wall continued developing at lower rates due to primary welding reduced the salt flow feeding the salt structure and controlling the progradation of the carbonate platforms (Villarroya de Los Pinares Fm), producing a supposed Jurassic flap lapped onto by the Barremian-Aptian units, and a halokinetic hook structure in the Cañada Vellida anticline. These authors interpret a discontinuous diapiric activity until the Late Cretaceous, which would be responsible for changes in thickness associated with the salt wall. In Stage 4 (Cenozoic), regional shortening promoted squeezing and secondary welding (rejuvenated diapir).

Significant postulations in the model by Vergés et al. (2020) are (1) the great thickness of the Triassic salt sequence (thicker than the Jurassic sequence) and its sharp variations, cause and consequence, respectively, of salt tectonics; (2) the negligible contribution of extensional tectonics during the Jurassic-Cretaceous evolution, as indicated by the very small displacement of the basement faults, in contrast to its significant role during the shortening stage and (3) the disconnection between the infra- and supra-salt deformation structures. In the following sub-sections, some remarks are provided based on the available stratigraphic and structural data in order to make a critical review of the salt tectonics vs. inversion tectonics model for the investigated anticlines.

6.1.1 | The detachment level and salt volume

The evaporitic-rich units of the Middle and Upper Triassic (Middle Muschelkalk and Keuper facies, respectively) are considered the main source of salt flow during the Mesozoic. In previous works, these evaporite-rich units have been proposed to have significant control in the development of structures in the central-eastern part of the chain during the Mesozoic and the Cenozoic (e.g. Álvaro et al., 1979; Capote et al., 2002; Cortés-Gracia & Casas-Sainz, 1996; Guimerà & Álvaro, 1990; Izquierdo-Llavall et al., 2019).

The two alternative models presented in Figure 15 are based on different estimates of available salt volumes. As explained above, around the Cañada Vellida-Miravete area and the surrounding region, the Middle Muschelkalk and Keuper facies are relatively thin (<50 m and <150 m, respectively; Table 1). They also show a somewhat varied lithological composition, mainly mudstones with interbedded levels of gypsum, dolostones and sandstones, as also happens in most of the Iberian Chain. Evidence of the high thickness of the Middle and Upper Triassic units containing anhydrite and halite are found in subsurface data ca. 35–40 km eastwards of the study region (i.e. the Bovalar anticline, where up to 1200 m of Middle Muschelkalk materials have been drilled in the Bovalar 2 well, Lanaja, 1987). Nevertheless, the structure at depth is not yet well known because of chaotic seismic facies (Nebot & Guimerà, 2016b), and if the drilling actually cut its frontal limb (with dips up to 70° E at the surface) the real stratigraphic thickness could be much lower.

The salt tectonics model involves the idea of an almost flat and rigid pre-Late Triassic substratum, which only is cut and displaced by either normal or reverse basement faults in the Mesozoic and Cenozoic stages, respectively (Vergés et al., 2020; Figure 15b). Numerous examples along the Iberian Chain show, however, how the Palaeozoic basement and the Early–Middle Triassic cover are involved in major folds and thrusts (e.g. Casas et al., 2000; Guimerà et al., 2004; Liesa & Casas, 1994; Nebot & Guimerà, 2018; Simón & Liesa, 2011). This behaviour is also observed around the study area, in the Middle Triassic dolostones and marlstones (Muschelkalk

facies) cropping out in the upper block of the Cañada Vellida thrust (Corral del Zancado section; Ferreiro et al., 1991; Martín-Fernández et al., 1979) (Figures 3 and 4, and cross-section 4–4′ in Figure 5). In localities where the basement and the Triassic cover are exposed, as in the NW-SE-trending Montalbán anticline (ca. 15 km to the North; Figure 2), both units are involved in overturned limbs together with the Jurassic-Cretaceous cover, associated with thrusts also affecting Cenozoic strata (Aurell et al., 2017; Casas et al., 2000; Liesa et al., 2004).

In conclusion, although the role of Middle-Upper Triassic rich-evaporitic facies as an effective low-strength detachment is clear, given the thickness and lithology of the Keuper facies in the area around the Miravete and Cañada de Vellida anticlines, its capability as a possible source of diapiric salt ascent is debatable. In the case analysed here, the Triassic stratigraphy is well known from outcrop observation, and this provides a solid framework to control the local thickness variations of the mudstone-/evaporitic-rich units. The suggestion that the salt could have disappeared due to migration is not supported by the observed thickness distribution of salt-bearing and supra-salt units.

6.1.2 | Remarks on the Jurassic carbonate successions

In the salt tectonics model, it is assumed that there are significant thickness variations and segmentation of the Jurassic carbonate platforms related to synsedimentary salt migration (Vergés et al., 2020; see Figure 15b). However, review of the numerous studies dealing with the stratigraphy and sedimentary evolution of the Middle Triassic and Jurassic platforms around the study area indicates a relatively uniform distribution of thicknesses and facies on a regional scale (Table 1). In particular, the post-rift Jurassic sequences do not show significant thickness variation in the eastern and western limbs of the Miravete and Cañada Vellida anticlines. It is true that a significant thickness reduction of the Middle Jurassic carbonates occurs from west to east in the study area (70 m in Cañada Vellida vs. 30 m in Miravete), but it is satisfactorily explained by the progressive proximity to the Middle Jurassic Maestrazgo High (e.g. Aurell et al., 2003; Gómez & Fernández-López, 2006). This basin-scale thickness distribution pattern indicates subsidence processes related to the thermal cooling during a post-rift stage (e.g. Álvaro, 1987; Salas & Casas, 1993; Sánchez Moya et al., 1992; Van Wees et al., 1998).

To support the hypothesis of salt mobilization and extrusion during the Jurassic, Vergés et al. (2020) indicate the existence of thick Lower Jurassic breccia deposits with karstic overprint. However, this Hettangian breccia deposit, the Cortes de Tajuña Fm, is not exclusively found in this area but is rather recognized in a large part of the Iberian Chain (e.g. Gómez & Goy, 2005). Diagenetic dissolution of evaporite sequences (probably including anhydrite levels) provided ideal conditions for the formation of the widespread Hettangian collapse-breccia (e.g. Aurell et al., 2007; Bordonaba & Aurell, 2002; Gómez et al., 2007; Hernández et al., 1985; Ortí et al., 2017, 2020).

6.1.3 | Remarks on the 'Jurassic-Early Cretaceous unconformities related to diapiric uplift'

The interpretation of Mesozoic evolution of the salt-related structures provided by Vergés et al. (2020) is largely based on the inference of the absence of several sedimentary units towards the crest of the Miravete anticline (Figure 15b). These authors indicate the presence of three unconformities related to diapir uplift in the crest of the Miravete anticline (Peña de la Higuera outcrop; see dashed lines A, B, and C in Figure 12b).

The close view of the discontinuity A of Vergés et al. (2020) (see the spot indicated as 6d in Figure 12b) is reproduced here in Figure 12C. This discontinuity is located close to the transitional boundary between the massive carbonates of the Cortes de Tajuña Fm and the well-bedded peritidal carbonates of the Cuevas Labradas Fm (Figure 12a). This surface represents in fact a facies boundary between a micritic level with fenestral porosity (level A) and an intraformational breccia (flat-pebble conglomerates with clast imbrication, level B). These are typical features associated with the boundaries between the peritidal shallowing-upward carbonate sequences (e.g. James, 1984). Such shallowing-upward sequences and bounding surfaces are common in the Sinemurian Cuevas Labradas Fm (e.g. Bádenas et al., 2010), which is exposed elsewhere in the Iberian Chain and also in both the limb and the crest of the Miravete anticline, and they do not therefore represent a tectonic unconformity (see CL in Figure 12a).

Vergés et al. (2020) relate the presence of two unconformities (see dashed lines B and C in Figure 12b) with the uplift of the salt-related structure previous to the sedimentation of the uppermost Jurassic unit (i.e. former Villar del Arzobispo Fm or the new Cedrillas and Aguilar del Alfambra formations) and to the Barremian Camarillas Fm, respectively. However, in the mentioned work these unconformities have been misinterpreted because they correspond to fault planes indeed (Figures 12a, 13 and 14). Normal drag folds in the hanging-wall and footwall blocks and related unconformities (Figures 13a

and 14a) indicate that they developed during the Late Jurassic–Early Cretaceous rifting stage, and they actually were south-dipping, E-W to NE–SW striking normal faults (Figures 13d and 14b–d), as Liesa et al. (2004, 2006) also pointed out.

Another argument provided by Vergés et al. (2020) is the *unambiguous halokinetic geometry*, that is a hook geometry of two lower Barremian continental sequences, described in the Cañada Vellida thrust and anticline (see the interpretation by Vergés et al., 2020 in Figure 8e in this paper). However, detailed mapping (see Section 4.2) shows fault planes with different orientations (including planes parallel to the 'hook related unconformity'), not only in the previously figured outcrop (Figure 8e) but also in the exceptional road exposure that cuts the same structure 50 m to the South (Figure 8a–d). The relationship between the two sequences is clearly different to the unconformable relationship that would be expected for a hook structure. Instead, the sequences are separated by a narrow fault zone and are also affected by other minor faults synthetic with the main fault zone (Figure 8c). As explained above, the different dip of both sequences can be explained by normal dragging associated with the rift stage (Figure 8d).

The uppermost Jurassic-lower Cretaceous sequences are frequently bounded by synrift angular unconformities (e.g. Aurell et al., 2016, 2018, 2019; Liesa et al., 2004; Liesa, Soria, Casas, et al., 2019). However, these are not local unconformities associated with the crest of major anticlines but are rather widespread along the western Maestrazgo basin (i.e. the Galve sub-basin), indicating the existence of regional extensional tectonic processes. These synrift unconformities, as in other extensional basins and analogue models, are commonly associated with bed thinning and onlap geometries of the synrift series towards basin margins and other fault-controlled local structural highs, for example roll-over anticline crests (e.g. Aurell et al., 2016; Moore, 1992; Liesa et al., 2006; Soto et al., 2007; Tilmans et al., 2021; Williams, 1993; Withjack et al., 2002). In addition, normal dragging in hanging-wall and footwall blocks of Mesozoic normal faults, such as in the Barranco de las Suertes (Figure 10a), Peña de la Higuera (Figures 13a and 14a) or Cañada Vellida (Figures 5 and 8d), is a common process affecting both Jurassic and lower Cretaceous strata and synrift and intrarift unconformities. This feature, especially the downward drag of Jurassic strata in the footwall block, is difficult to reconcile with upward diapiric flow.

6.1.4 | Remarks on the 'variable thickness of units in relation to anticlines'

An additional set of arguments that have been invoked to underline the role of Mesozoic salt tectonics is the thinning of Cretaceous units towards the Miravete and Cañada Vellida anticline hinges and, especially, the change in thickness (sometimes twofold or threefold) from one limb to the other (Vergés et al., 2020). However, such thickness changes can be better explained by the Early Cretaceous synrift extensional faults. The Barranco de las Suertes outcrop in the anticline core clearly illustrates that the thickness changes of the El Castellar Fm occurred in relation to the evolving Miravete normal fault zone and not to a developing salt anticline (Figure 10a). The role of extensional tectonics as the driving mechanism is supported by the increase in thickness associated with each fault, the non–deposition of this unit to the east of the fault system (eastern limb), and the normal drag developed in both the underlying Jurassic layers and the unconformity located between them (Liesa et al., 2004, 2006). The Mesozoic normal faults, folded and partially inverted, shown in the northern sector (Campos-Aliaga) of the Miravete faulted anticline, as well as in the core of the central and southern parts of the Cañada Vellida anticline, reinforce the primary role of extensional tectonics in the changes in the thickness of the uppermost Jurassic–Lower Cretaceous sequences.

When considering the thickness changes between the limbs of a fold, the interpretation of their origin should be made with caution. When an anticline results from the positive inversion of a normal fault and there is no physical continuity between both limbs (such as the Miravete and Cañada Vellida anticlines), thinning in the uplifted fault block could be misinterpreted as associated with the current anticline hinge. Knowing which structure was active during sedimentation (normal fault or fold) is crucial to make a correct interpretation.

6.1.5 | Flaps vs. klippes

At the Cañada Vellida anticline, a particular controversial point is the claimed presence of an Upper Jurassic overturned flap, lapped onto by upper Barremian–Aptian units (Figure 11b of Vergés et al. 2020 vs. our Figure 7). However, this geological structure is better explained by coalescence of two klippes of Jurassic rocks, with a hanging-wall anticline and a footwall syncline sharing an overturned limb (Figures 6a and 7).

Symmetry or asymmetry of structures can provide a clue for distinguishing flaps and klippes because diapirs can be rather related to symmetric flaps (centrifugal in the case of rounded diapirs; symmetric in 2D view), whereas overturned beds (commonly found in recumbent synclines at the footwall block) can be ascribed to compressional, thrust structures. If none of the previous criteria is conclusive, the age criterion of synkinematic sediments can be used in those basins in which there is a clear separation between

the period of diapiric activity (usually coinciding with extensional activity) and the inversion stage. The structure of the Cañada Vellida anticline shows a marked asymmetry and NE-directed vergence (e.g. cross-section 4–4′; Figure 5), and the Jurassic-Cretaceous contact is a narrow fault zone. The upper Barremian-Aptian units are not lapping onto the overturned flap of Jurassic rocks, as indicated by Vergés et al. (2020), but are actually truncated by the thrust plane and dragged in its proximity, as indicated by the striated and brecciated blocks observed in the fault zone (Figure 7).

In the case of the Cañada Vellida anticline, syntectonic deposits are key to distinguish between Aptian diapiric (flap) and Cenozoic compressional (klippe) origins. Mass-wasting deposits (debris flow or lentils) and abrupt facies changes, common in halokinetic sequences and indicators of diapiric flow (e.g. Giles & Lawton, 2002; Giles & Rowan, 2012; Rowan et al., 2003, 2016), have not been observed in the Aptian sedimentary sequence that Vergés et al. (2020) assume to be onlapping the 'Jurassic overturned flap'. In contrast, the Aptian succession rather shows stacked shallow marine strata (Peropadre, 2012). Local abrupt thickness changes of the Aptian succession occur but are associated with normal growth faults, which in their turn are sealed by the upper Albian post-rift unconformity (base of the Utrillas Fm; Figure 6b). Furthermore, the Upper Cretaceous post-rift sequence is overturned in the limb of the Cañada Vellida anticline, and folding also affects the moderately E-dipping (45°) Cenozoic syn-inversion conglomerates (Figure 5).

6.1.6 | Remarks on the orientation of contractional structures

According to the salt tectonics interpretation, the last stage of diapiric growth would be related to Alpine N-S shortening during which the described salt-related structures were squeezed, welded and thrust (Figure 15b). In this context, the complex fold patterns of the area, consisting of sets of anticlines and synclines with different, sometimes orthogonal trends, are considered to provide additional support to the diapiric model. However, as explained in Section 2, multiple compression directions (and an inherited pattern of basement faults) explain the occurrence of multiple fold directions. The perpendicularity of the fold directions and the steep dip of many fold limbs result in a spectacular map pattern of buckling fold interference (Simón, 2004, 2005). Although diversely oriented folds can be found in diapiric areas, in this case, we interpret that the tectonic frame explains better most of the structures found, both at the map and at the outcrop scale (Liesa, 2000, 2011b; Simón, 1980, 2004, 2005). Fold interference is far from being unsystematic: each fold set results from a particular compression direction, active during a well-constrained time-lapse, which produced inversion of adequately oriented extensional faults.

The nearly N–S trending folds (such as the Miravete anticline) could be regarded as not consistent with the regional N-S to NNE–SSW shortening direction, orthogonal to the Pyrenean plate margin (e.g. Guimerà, 1988; Guimerà & Alvaro, 1990). Nevertheless, the earlier stages of intraplate deformation, characterized by ESE-WNW (Eocene) and NE–SW to ENE-WSW (Eocene–Late Oligocene) compressions, were suitable to form NNW–SSE to N-S folds (Liesa & Simón, 2009). The age of such folds strictly coincides with the time in which those paleostress directions were recorded in Cenozoic syn-inversion conglomeratic units (Simón, 2006). The hinge of the Miravete anticline is not observable in most parts of its trace, as in the Peña de la Higuera section, because the normal fault or its Cenozoic inversion juxtaposes different sedimentary units from the two-fold limbs (Figures 9 and 11c). In such a scenario, welding or *locking* in relation to normal fault slip or during inversion instead of the secondary (salt) welding proposed by Vergés et al. (2020) is the most reliable interpretation (Figure 12a vs. b) (see Section 5.3).

The most conspicuous interference structures found in the studied western Maestrazgo area (Aliaga, Camarillas-Jorcas, La Cañadilla, Los Olmos, and Sierra de El Pobo; Liesa, 2011b; Simón, 1980, 2004, 2005) result from superposition of E-W trending folds, Early Miocene in age, on NW-SE to NNW–SSE trending ones, Eocene–Oligocene in age (Figures 2, 3 and 9). Also, in this case, fold timing is robustly established in the Aliaga area on the basis of tectono–sedimentary relationships with synorogenic units of the Cenozoic Aliaga basin (Simón, 2004, 2005), while their contemporaneity with later, nearly N-S trending compressions has been evinced from paleostress analysis (Simón, 2006).

In summary, the NW-SE to NNW–SSE trending folds, as the Cañada Vellida and Aliaga-Miravete anticlines, developed during the main orogenic period in the Iberian Chain, under the *Pyrenean-Iberian* compressional stress field (compression trajectories roughly trending NE–SW, evolving or being locally deflected to ENE-WSW or E-W; Liesa, 2000; Liesa & Simón, 2007, 2009; Simón, 2006). Fold trend variations are mainly due to structural inheritance, since many folds nucleated on previous extensional faults during positive inversion of the Iberian basin. In particular, the nearly N-S trend of the Miravete anticline, belonging to this older fold set, is easily explained by its genetic relationship with the extensional Miravete fault, as explained above. The E-W trending folds developed during a much shorter late-orogenic stage under the *Late Betic* and *Late Pyrenean* stress fields (compression trajectories trending NNW–SSE and NNE–SSW, respectively; Liesa, 2000; Liesa

& Simón, 2007, 2009; Simón, 2006). Most of these fold interference structures are located within the Utrillas thrust sheet, and their sequential development is fully consistent with the displacement history of the thrust itself (Simón & Liesa, 2011).

6.2 | Mechanical stratigraphy: Dragging, welding and detachment levels

The Mesozoic of the Iberian Chain is a good example of the alternation of viscous and less viscous rock successions that conditioned the evolution of the basin during the extensional and inversion–contractional stages (Figure 4). In addition to the aforementioned main regional detachments (the Triassic mudstone and gypsum sequences of the Middle Muscheskalk and Keuper), two other thick incompetent mudstone and sandstone units stand out in the study region: the Barremian Camarillas Fm (~300 m thick, locally up to 900 m in the Galve sub-basin; Navarrete et al., 2013a; Navarrete, 2015), and the Aptian-Albian Escucha and Utrillas formations (300–500 m thick), both sandwiched between thick competent calcareous sequences (Table 1).

Drag folds are very common where rock sequences with significantly different mechanical properties are subjected to shear, the incompetent layers being stretched and smeared in the vicinity of faults (Aydin & Eyal, 2002; Schmatz et al., 2010). Drag folds develop by frictional sliding during faulting (e.g. Davis, 1984; Becker, 1995; Ramsay & Huber, 1987) or by folding at the tip of a propagating fault, conditioned by mechanical stratigraphy (e.g., Ferrill et al., 2012; Gross et al., 1997), regardless of their having normal, reverse or strike-slip component. Drag folds associated with salt mobilization strongly differ from those resulting from slip-on faults. As a general rule, the convexity of the drag folds will point in a different direction in each fault block, whereas they will point towards the same domain in diapir-drag folds (Figure 16).

Due to its particular mechanical stratigraphy, drag folds are very common in the Iberian Chain. They are associated with Mesozoic and Neogene-Quaternary normal faults (e.g. Casas-Sainz & Gil-Imaz, 1998; Cortés et al., 1999; Ezquerro et al., 2020; Rodríguez-López et al., 2007) as well as linked to Cenozoic high-angle reverse faults and thrusts (Casas et al., 2000; Simón & Liesa, 2011). Around the Miravete and Cañada Vellida anticlines, there are numerous drag folds associated with faults, favoured by the proximity of the incompetent Keuper facies. The kinematic indicators evidence that the drag folds have a tectonic origin and are mainly related to the displacement of normal faults (normal drag) during the Early Cretaceous basinal stage, as suggested by their relationship with local synrift and intrarift unconformities. At Peña de la Higuera locality, the Keuper facies has been strongly smeared during Cenozoic thrusting, practically locking the vertical to overturned, Lower Cretaceous limestone beds (El Castellar Fm) against the Hettangian breccia (Cortes de Tajuña Fm) (Figure 12a). Instead of the salt weld proposed by Vergés et al. (2020) (Figure 12b), the geometrical relationship between these units, which in turn represents the connection of the western and eastern limbs of the Miravete anticline, was produced during fault movement, that is it represents a case of fault slip locking during the tectonic inversion (Figures 11b and 12a).

On the other hand, both the particular mechanical stratigraphy of the Mesozoic cover and the deep detachment in the basement is primarily responsible for the regional and local deformation geometry. During the basin stage, different scales of extensional deformation may be related to the role of each ductile level and the size of the involved structures. Major faults or fault zones, more than 20 km long (e.g. the Miravete or Cañada Vellida high-angle normal faults), likely rooted at a deep basal detachment and controlled differential tectonic subsidence and sedimentation on a sub-basin scale during the latest Jurassic–Early Cretaceous (Capote et al., 2002; Liesa et al., 2006; Soria, 1997). Shallower detachments in the basement (e.g. the Silurian shales) and Mesozoic incompetent layers, especially the Keuper clays and gypsum, probably represented barriers to upward propagation of deformation, nucleating splay faults above the major faults that evolved forming complex fault zones. Ductile deformation on these upper layers gave rise to the formation of graben and half-graben systems at different scales depending on the detachment depth: structures developed above a shallower detachment level, that is in a thinner cover, were smaller. These intermediate- to minor-scale structures controlled differential subsidence on an intrabasinal to local scale. As examples of intermediate, kilometre-scale structures, the ENE-WSW striking Remenderuelas and Camarillas faults (Figures 9 and 11a) were likely rooted in the Silurian shales, whereas other associated faults with pronounced listric geometry (El Batán Fault) detached in the Upper Triassic (Liesa et al., 2006). Some ENE-WSW trending graben and half-grabens, 100 m to a few kilometres in size, developed in the younger Aptian units in Cañada Vellida (Figure 6) and the northern sector of the Miravete anticline (Figure 9), very likely detached in the mudstones of the Barremian Camarillas Fm.

6.3 | Overview and implications for the Maestrazgo basin

Review of the arguments supporting Mesozoic salt tectonics as the main mechanism responsible for the formation

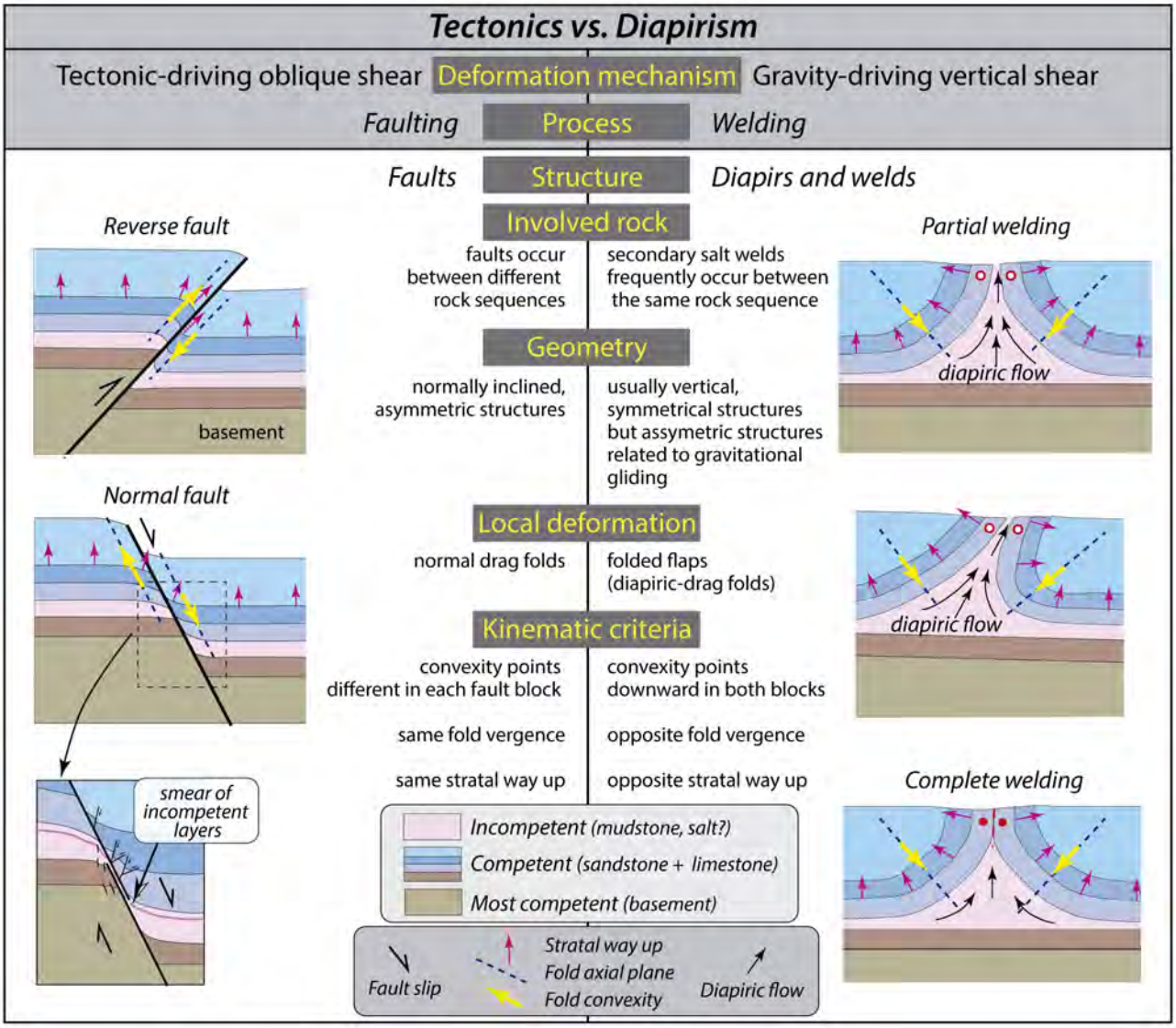

FIGURE 16 Drag folds as kinematic criteria to decipher processes (diapirism, tectonics) involved in the deformation. (a) Oblique shear (faulting). Drag folds associated with normal (A.1) and reverse (A.2) faults in layers of different competencies. Incompetent layers (mainly shales and mudstones, maybe including gypsum and a small amount of salt) are smeared on fault planes enabling dragging. In faults, regardless of having normal or reverse kinematics, the convexity of drag folds and the polarity of beds point to the same direction in both fault blocks. (b) Vertical shear (gravity). Kinematic criteria of drag folds and (secondary) salt welds formed by mobilization of large volumes of salt. In salt welds, regardless of whether the salt structure is symmetric or asymmetric, the convexity of drag folds and the polarity of beds point to opposite directions in both fault blocks.

of the Miravete and Cañada Vellida anticlines shows numerous inconsistencies, including the claimed Jurassic and Lowe Cretaceous salt-related unconformities and onlaps (Figures 12-14), the hook (Figure 8) and flap (Figure 7) structures or the change in thickness between the anticline limbs. Piercement has also not been observed or described in the region, which is the crucial observation to define a diapir (Jackson & Talbot, 1986). The arguments presented and discussed above show that the Cañada Vellida and the Miravete anticlines formed during the Cenozoic shortening stage by reactivation of extensional fault zones that developed during the Late Jurassic–Early Cretaceous rifting stage. The nucleation of these folds on previous faults is responsible for their anomalous trend (around NNW–SSE) in relation to the general NW-SE orientation of the folds and thrusts in the Iberian Chain. The nearby Ababuj and Cañada de Benatanduz anticlines (Figure 1b) have also been interpreted in the same way (Gautier, 1980; Simón-Porcar et al., 2019).

Middle Triassic to Early Jurassic evaporite-bearing successions shows limited thickness in the eastern Iberian realm. In most cases, Middle Muschelkak and Keuper facies are <150 m thick, and thin evaporitic beds (mostly <10–15 m thick gypsum beds) are intercalated between

thick peritidal red mudstones (Table 1; Marín, 1974; Ortí et al., 2017, 2020; Pérez-López et al., 2021). However, within the Maestrazgo basin, a vertical, apparent thickness of evaporites up to 1200 m has been drilled (i.e. Middle Muschelkalk in the Bovalar anticline; Figure 1b and Table 1). It should be noted, however, that this area only shows minor evidence of diapiric flow. From the study of seismic reflection profiles, Nebot & Guimerà (2016a, 2016b, 2018) identified very gentle 'domes' (NW-SE Mirambel and Monchén anticlines) or anticlines (NNW–SSE to N-S Bovalar anticline) that could partly be the result of salt migration. These authors state that Triassic extensional faults affect the Middle Triassic evaporite unit that fills the relief generated by the system of horsts, grabens and half-grabens and shows thickening and wedge geometries towards the normal faults and fan-shaped reflectors against them. The Middle Muschelkalk evaporitic unit is thinner upon the structural highs of the basement (Monchen and Iglesuela highs), which are also located in the upthrown blocks of NW-SE-trending Triassic normal faults (see Figure 7 of Nebot & Guimerà, 2016b). The supra-salt cover, from the Middle Triassic (Upper Muschelkalk) to the Lower Cretaceous, overlaps these structures lying nearly horizontal in most seismic profiles, indicating that there were no significant changes in the thickness of the salt units after deposition (Nebot & Guimerà, 2016b). Based on some examples of onlaps over the Upper Muschelkalk in gentle anticlines, these authors interpret a limited salt flow during deposition of the Upper Triassic (Keuper), triggered by the resumption of extensional tectonics.

Other lines of evidence also suggest either limited salt migration during the basinal stage or tectonics as a driving mechanism for the development of domes and anticlines in the Maestrazgo region. Due to the chaotic seismic facies appearing at depth (see figure 7c of Nebot & Guimerà, 2016b) and the 1200 m of Middle Muschelkalk evaporitic unit in its core, the origin of the N-S trending, 40 km long, Bovalar box anticline is open to discussion. It has been interpreted as (i) the result of salt migration (Bartrina & Hernández, 1990; ; Lanaja, 1987; Nebot & Guimerà, 2016a, 2016b; Vergés et al., 2020), (ii) a fold detached in the Triassic evaporites (Antolín-Tomás et al., 2007) or (iii) a propagation fold involving the basement (Nebot & Guimerà, 2016b, 2018). In our opinion, based on the geometrical parallelism and location with respect to the Cañada Vellida and Miravete box anticlines (Figure 1), a similar kinematic history for the Bovalar anticline cannot be ruled out. That is, the present-day structure can result from the Cenozoic positive inversion of a Mesozoic extensional fault involving the basement, in this case dipping to the east, which was probably active during the Permian-Middle Triassic and Late Jurassic-Early Cretaceous rifting stages.

Although thick salt levels have been locally detected in the Middle Muschelkalk evaporites, salt tectonics does not seem to have played a significant role in the eastern Iberian Chain during the Mesozoic basinal and Cenozoic compressional stages. The presence of successive detachment levels with significant thickness in the Iberian Chain influences many geometrical features of structures at basin borders, but their gravitational migration does not seem to be the primary driving factor controlling the tectonic evolution. The feasible figures for extension and compression in the central-eastern Iberian Chain (Guimerà et al., 1996; Seillé et al., 2015) do not leave much space for vertical movements. Crustal thinning and associated basement faulting can account for subsidence during the Mesozoic, while recovery of such thinning piling up an extra crustal thickness (Casas-Sainz & De Vicente, 2009) would correspond to the Cenozoic shortening stage.

Noticeably, the basal and intermediate detachment levels are of prime importance for the development of subsurface tectonic structures, but not less important is the geometry of structures in relation to the paleotopography, that is the ramps cutting the cover competent rocks during extension. In the central-eastern Iberian Chain, fault ramps, apart from the basement, are mainly linked to the thick limestone series of the Jurassic, Aptian and Upper Cretaceous. This competent cover exerted a major control during the subsequent compressive deformation, determining the location of anticlines that show the typical box-fold geometry related to fault-propagation folding (e.g. Casas et al., 1998b; Cortés et al., 1999; Cortés-Gracia & Casas-Sainz, 1996; Simón, Arenas, et al., 1998) or footwall shortcut thrusts (Casas et al., 2000; Liesa et al., 2000; Liesa & Simón, 2004; Simón & Liesa, 2011). In fact, the most representative and spectacular structures in the eastern Iberian Chain, which stand out in the present-day landscape due to the Quaternary differential river incision, are the La Olla vertical anticline (Figure 9) in Aliaga (Gibbons & Moreno, 2002; Simón, 2004; Simón, Arenas, et al., 1998), and the basement-involved Utrillas thrust (Figure 2) in Utrillas and Castel de Cabra (e.g. Casas et al., 2000; Simón & Liesa, 2011). Both are related to Cenozoic inversion of Mesozoic normal faults. These and many other structures, such as the Miravete and Cañada Vellida anticlines, are specifically linked to the deformation of the Mesozoic limestones related to fault ramps.

7 | CONCLUSIONS

The Cañada Vellida and Miravete anticlines in the eastern Iberian Chain (Maestrazgo basin, Spain), reinterpreted by Vergés et al. (2020) as examples of salt-tectonic features during Jurassic-Cretaceous basin formation and

evolution, are true folds resulting from positive inversion tectonics, in full coherence with the geologic history of the region indeed. Our careful 4D study of these structures has been crucial not only for their geometric characterization but also for the interpretation of processes driving their formation and evolution. According to our interpretation, the Mesozoic evolution of these structures, especially during the latest Jurassic–Early Cretaceous times, was characterized by the development of major extensional fault zones detached within the basement, which controlled subsidence and thickness distribution at local and regional scales. The Triassic clay and gypsum (Keuper) and other incompetent clay and marlstone sequences (mainly the Barremian Camarillas Fm) provide detachments for other minor scale fault systems controlling subsidence and deposition from intrabasinal to local scale. During the Cenozoic shortening, differential inversion along fault zones first nucleated and then developed major anticlines with complex box geometries, in which pre-existing normal faults were folded and inverted to a different degree.

Other pieces of evidence point to a negligible role of salt migration in the tectonic evolution of the central-eastern Iberian Chain (Maestrazgo): (i) the preferential accumulation of thick salt-bearing units in relation to Triassic graben and half-graben structures, lacking evidence of significant lateral migration and (ii) the relatively uniform thickness of Middle Triassic to Early Jurassic carbonate units covering the salt-bearing units. In summary, the notion of a Triassic diapiric province in the Maestrazgo basin is, in our view, not supported by the observation and interpretations summarized here.

ACKNOWLEDGEMENTS

The authors declare that they have no known competing financial interests or personal relationships that could have appeared to influence the work reported in this paper. We thank Laura Burrel, Alex Peace, Juan I. Soto and two anonymous reviewers and editor Craig Magee for constructive reviews of earlier versions of this manuscript. This research was supported by the Agencia Estatal de Investigación (AEI/10.13039/501100011033) of the Spanish Government (grant numbers PID2019-108705-GB-I00, PID2019-108753GB-C22 and CGL2017-85038-P) and the Aragon Regional Government (grant numbers LMP127_18 and E32_20R: Geotransfer research group).

PEER REVIEW

The peer review history for this article is available at https://publons.com/publon/10.1111/bre.12713.

DATA AVAILABILITY STATEMENT

The data that support the findings of this study are available from the corresponding author upon reasonable request.

ORCID

Carlos L. Liesa https://orcid.org/0000-0002-9130-117X
Antonio M. Casas-Sainz https://orcid.org/0000-0003-3652-3527
Marcos Aurell https://orcid.org/0000-0002-2430-7424
José L. Simón https://orcid.org/0000-0003-1412-5245
Ana R. Soria https://orcid.org/0000-0003-2963-8422

REFERENCES

Aldega, L., Viola, G., Casas-Sainz, A., Marcén, M., Román-Berdiel, T., & van der Lelij, R. (2019). Unraveling multiple thermotectonic events accommodated by crustal-scale faults in Northern Iberia, Spain: Insights from K-Ar dating of clay gouges. *Tectonics*, *38*(10), 3629–3651. https://doi.org/10.1029/2019TC005585

Allmendinger, R. W., Cardozo, N., & Fisher, D. (2012). *Structural geology algorithms: Vectors and tensors in structural geology*. Cambridge University Press.

Alonso, A., Floquet, M., Mas, R., & Meléndez, A. (1993). Late cretaceous carbonate platforms: origin and evolution, Iberian range, Spain: Chapter 24. *AAPG Special Volume*, *44*, 297–313.

Álvaro, M. (1987). La subsidencia tectónica en la Cordillera Ibérica durante el Mesozoico. *Geogaceta*, *3*, 34–37. https://sge.usal.es/archivos/geogacetas/Geo03/Art14.pdf

Álvaro, M., Capote, R., & Vegas, R. (1979). Un modelo de evolución geotectónica para la Cadena Celtibérica. *Acta Geológica Hispánica (Homenaje a Lluis Solé i Sabaris)*, *14*, 172–177.

Anadón, P., Ardevoll, L., Cabra, P., Clavet, F., Fernández, P., Giner, J., Guimerà, J., González, J., Julivert, M., Marzo, M., Salas, R., Simón, J. L., Simón, A., Ortí, F., López, F., & Barnolas, A. (1985). *Mapa geológico de España, escala 1:200.000, Vinaròs (hoja n° 48)* (p. 100). Instituto Geológico y Minero de España.

Antolín-Tomás, B., Liesa, C. L., Casas, A., & Gil-Peña, I. (2007). Geometry of fracturing linked to extension and basin formation in the Maestrazgo basin (Eastern Iberian Chain, Spain). *Revistade la Sociedad Geologica de España*, *20*, 351–365. https://sge.usal.es/archivos/REV/20(3-4)/Art16.pdf

Arche, A., Diez Ferrer, J. B., & López Gómez, J. (2007). Identification of the early Permian (Autunian) in the subsurface of the Ebro Basin, NE Spain, and its paleogeographic consequences. *Journal of Iberian Geology*, *33*, 125–133. https://eprints.ucm.es/id/eprint/17718/

Arthaud, F., & Matte, P. (1977). Late Paleozoic strike-slip faulting in southern Europe and northern Africa: Result of a right-lateral shear zone between the Appalachians and the Urals. *GSA Bulletin*, *88*(9), 1305–1320. https://doi.org/10.1130/0016-7606(1977)88<1305:LPSFIS>2.0.CO;2

Aurell, M., Bádenas, B., Canudo, J. I., & Casas, A. (2017). *Guía de Geología y Paleontología del Parque Cultural del río Martín* (p. 297). Asociación Parque Cultural del Río Martín.

Aurell, M., Bádenas, B., Canudo, J. I., Castanera, D., García-Penas, A., Gasca, J. M., Martín- Closas, C., Moliner, L., Moreno-Azanza, M., Rosales, I., Santas, L., Sequero, C., & Val, J. (2019). Kimmeridgian-Berriasian stratigraphy and sedimentary evolution of the central Iberian rift system (NE Spain). *Cretaceous Research*, *103*, 104153. https://doi.org/10.1016/j.cretres.2019.05.011

Aurell, M., Bádenas, B., Casas, A. M., & Salas, R. (2007). Peritidal carbonate–evaporite sedimentation coeval to normal fault

segmentation during the Triassic–Jurassic transition, Iberian Chain. In G. Nichols, E. Williams, & C. Paola (Eds.), *Sedimentary processes, environments and basins: A tribute to Peter Friend 38* (pp. 219–239). International Association of Sedimentologists. https://doi.org/10.1002/9781444304411.ch10

Aurell, M., Bádenas, B., Gasca, J. M., Canudo, J. I., Liesa, C., Soria, A. R., Moreno-Azanza, M., & Najes, L. (2016). Stratigraphy and evolution of the Galve sub-basin (Spain) in the middle Tithonian-early Barremian: Implications for the setting and age of some dinosaur fossil sites. *Cretaceous Research*, *65*, 138–162. https://doi.org/10.1016/j.cretres.2016.04.020

Aurell, M., Fregenal-Martínez, M., Bádenas, B., Muñoz-García, M. B., Élez, J., Meléndez, N., & de Santisteban, C. (2019). Middle Jurassic–Early Cretaceous tectono-sedimentary evolution of the southwestern Iberian Basin (central Spain): Major palaeogeographical changes in the tectonic framework of the Western Tethys. *Earth-Science Reviews*, *199*, 102983. https://doi.org/10.1016/j.earscirev.2019.102983

Aurell, M., Robles, S., Bádenas, B., Quesada, S., Rosales, I., Meléndez, G., & García-Ramos, J. C. (2003). Transgressive/regressive cycles and Jurassic palaeogeography of NE Iberia. *Sedimentary Geology*, *162*, 239–271. https://doi.org/10.1016/S0037-0738(03)00154-4

Aurell, M., Soria, A. R., Bádenas, B., Liesa, C. L., Canudo, J. I., Gasca, J. M., Moreno-Azanza, M., Medrano-Aguado, E., & Mélendez, A. (2018). Barremian synrift sedimentation in the Oliete subbasin (Iberian Basin, Spain): Palaeogeographical evolution and distribution of vertebrate remains. *Journal of Iberian Geology*, *44*, 285–308. https://doi.org/10.1007/s41513-018-0057-3

Aydin, A., & Eyal, Y. (2002). Anatomy of a normal fault with shale smear: Implications for fault seal. *AAPG Bulletin*, *86*, 1367–1381.

Bádenas, B., Aurell, M., & Bosence, B. (2010). Continuity and facies heterogeneities of shallow carbonate ramp cycles (Sinemurian, Lower Jurassic, northeast Spain). *Sedimentology*, *57*, 1021–1048. https://doi.org/10.1111/j.1365-3091.2009.01129.x

Bádenas, B., Aurell, M., & Gasca, J. M. (2018). Facies model of a mixed clastic-carbonate, wave-dominated open-coast tidal flat (Tithonian-Berriasian, north-east Spain). *Sedimentology*, *65*, 1631–1666.

Bartrina, T., & Hernández, E. (1990). Las unidades evaporíticas del Triásico del subsuelo del Maestrazgo. In F. Ortí & J. M. Salvany (Eds.), *Formaciones evaporíticas de la Cuenca del Ebro y cadenas periféricas, y de la zona de Levante. Nuevas aportaciones y guía de superficie* (pp. 34–38). ENRESA–Dep. Geoq. Prosp. Petrol. (UB).

Becker, A. (1995). Conical drag folds as kinematic indicators for strike-slip fault motion. *Journal of Structural Geology*, *17*, 1497–1506. https://doi.org/10.1016/0191-8141(95)00057-K

Bordonaba, A. P., & Aurell, M. (2002). Lateral facies variation in the lowermost Jurassic of the central Iberian Chain (NE Spain): Early diagenetic origin and synsedimentary tectonics. *Acta Geológica Hispánica*, *37*, 355–368.

Bover-Arnal, T. (2010). *The Aptian evolution of the Galve sub-basin (Maestrat Basin, E Iberia)* (p. 222) [PhD Thesis]). University of Bayreuth. http://opus.ub.uni-bayreuth.de/volltexte/2010/671/

Burrel, L., & Teixell, A. (2021). Contractional salt tectonics and role of pre-existing diapiric structures in the South Pyrenean foreland fold-and-thrust belt (Montsec and Serres Marginals). *Journal of the Geological Society, London*, *178*, jgs2020-085. https://doi.org/10.1144/jgs2020-085

Cámara, P., & Klimowitz, J. (1985). Interpretación geodinámica de la vertiente centro-occidental surpirenaica (cuencas de Jaca-Tremp). *Estudios Geológicos*, *41*(5–6), 391–404. https://doi.org/10.3989/egeol.85415-6720

Canérot, J., Cugny, P., Pardo, G., Salas, R., & Villena, J. (1982). Ibérica central-Maestrazgo. In *El Cretácico de España* (pp. 273–344). Universidad Complutense de Madrid.

Canérot, J., Fernández-Luanco, M. C., & Del Pan Arana, T. (1979). *Mapa Geológico de España 1: 50.000, hoja n° 519 (Aguaviva)* (p. 38). IGME.

Canérot, J., Pignatelli, R., Fernández-Luanco, M. C., Gautier, F., Mansilla, H., & Barnolas, A. (1979). *Mapa Geológico de España 1: 50.000, hoja n° 569 (Mosqueruela)* (p. 24). IGME.

Capote, R., Muñoz, J. A., Simón, J. L., Liesa, C. L., & Arlegui, L. E. (2002). Alpine tectonics I: The alpine system north of the betic Cordillera. In W. Gibbons & T. Moreno (Eds.), *The geology of Spain* (pp. 367–400). The Geological Society. https://doi.org/10.1144/GOSPP.15

Casas, A. M., Casas, A., Pérez, A., Tena, S., Barrier, L., Gapais, D., & Nalpas, T. (2000). Syn-tectonic sedimentation and thrust-and-fold kinematics at the intra-mountain Montalbán Basin (northern Iberian Chain, Spain). *Geodinamica Acta*, *13*, 1–17. https://doi.org/10.1016/S0985-3111(00)00105-4

Casas, A. M., Cortés, A. L., Gapais, D., Nalpas, T., & Román-Berdiel, T. (1998). Modelización analogica de estructuras asociadas a compresión oblicua y trasnpresión. Ejemplos del NE peninsular. *Revista. Sociedad Geologica de España*, *11*, 331–344. https://sge.usal.es/archivos/REV/11(3-4)/Art10.pdf

Casas, A. M., Cortés, A. L., Liesa, C., Soria, A. R., Terrinha, P., Kullberg, J. C., & Da Rocha, R. (1998). Estudio comparado de la evolución e inversión de distintas cuencas mesozoicas en la Placa Ibérica. *Geogaceta*, *24*, 67–70. https://sge.usal.es/archivos/geogacetas/Geo24/Art17.pdf

Casas-Sainz, A. M., & De Vicente, G. (2009). On the tectonic origin of Iberian topography. *Tectonophysics*, *474*, 214–235. https://doi.org/10.1016/j.tecto.2009.01.030

Casas-Sainz, A. M., & Gil-Imaz, A. (1998). Extensional subsidence, contractional folding and thrust inversion of the eastern Cameros Basin, northern Spain. *Geologische Rundschau*, *86*, 802–818. https://doi.org/10.1007/s005310050178

Cortés, A. L., Liesa, C. L., Soria, A. R., & Meléndez, A. (1999). Role of the extensional structures in the location of folds and thrusts during tectonic inversion (Northern Iberian Chain, Spain). *Geodinamica Acta*, *12*, 113–132. https://doi.org/10.1016/S0985-3111(99)80027-8

Cortés-Gracia, A. L., & Casas-Sainz, A. M. (1996). Deformación alpina de zócalo y cobertera en el borde norte de la Cordillera Ibérica (Cubeta de Azuara-Sierra de Herrera). *Revista. Sociedad Geologica de España*, *9*, 51–66. https://sge.usal.es/archivos/REV/9(1-2)/Art04.pdf

Crespo-Zamorano, A., Navarro-Vázquez, D., Canerot, J., Del Pan, T., Fernández-Luanco, M. C., & Leyva Cabello, F. (1979). *Mapa Geológico de España 1: 50.000, hoja n° 518 (Montalbán)* (p. 31). IGME.

Davis, G. H. (1984). *Structural geology of rocks and regions* (p. 492). Wiley.

De Vicente, G., Vegas, R., Muñoz-Martín, A., Van Wees, J. D., Casas-Sáinz, A., Sopeña, A., Sánchez-Moyae, Y., Arche, A., López-Gómez, J., Olaiz, A., & Fernández-Lozano, J. (2009). Oblique strain partitioning and transpression on an inverted rift: The

Castilian Branch of the Iberian Chain. *Tectonophysics*, *470*, 224–242. https://doi.org/10.1016/j.tecto.2008.11.003

Ezquerro, L., Simón, J. L., Luzón, A., & Liesa, C. L. (2020). Segmentation and increasing activity in the Neogene-Quaternary Teruel Basin rift (Spain) revealed by morphotectonic approach. *Journal of Structural Geology*, *135*, 104043. https://doi.org/10.1016/j.jsg.2020.104043

Ferreiro, E., Ruíz, V., López de Alda, F., Valverde, M., Lendínez, A., Lago San José, M., Meléndez, A., Pardo, G., Ardevol, L., Villena, J., Pérez, A., González, A., Hernández, A., Álvaro, M., Leal, M. C., Aguilar Tomás, M., Gómez, J. J., & Carls, P. (1991). *Mapa geológico de España, escala 1:200.000, de Daroca (hoja n° 40)* (p. 239). Instituto Tecnológico y Geominero de España.

Ferrill, D. A., Morris, A. P., & McGinnis, R. N. (2012). Extensional fault-propagation folding in mechanically layered rocks: The case against the frictional drag mechanism. *Tectonophysics*, *576–577*, 78–85. https://doi.org/10.1016/j.tecto.2012.05.023

Flinch, J., & Soto, J. I. (2017). Allochthonous triassic and salt tectonic processes in the betic-rif orogenic arc. In J. I. Soto, J. F. Flinch, & G. Tari (Eds.), *Permo-Triassic salt provinces of Europe, North Africa and the Atlantic margins: Tectonics and hydrocarbon potential* (pp. 417–446). Elsevier. https://doi.org/10.1016/B978-0-12-809417-4.00020-3

García-Lasanta, C., Oliva-Urcia, B., Román-Berdiel, T., Casas, A. M., Gil-Peña, I., Sánchez-Moya, Y., Sopeña, A., Hirt, A. M., & Mattei, M. (2015). Evidence for the Permo-Triassic transtensional rifting in the Iberian Range (NE Spain) according to magnetic fabrics results. *Tectonophysics*, *651*, 216–231. https://doi.org/10.1016/j.tecto.2015.03.023

García-Lasanta, C., Román-Berdiel, T., Oliva-Urcia, B., Casas, A. M., Gil-Peña, I., Speranza, F., & Mochales, T. (2016). Tethyan versus Iberian extension during the Cretaceous period in the eastern Iberian Peninsula: Insights from magnetic fabrics. *Journal of the Geological Society*, *173*, 127–141. https://doi.org/10.1144/jgs2015-068

Gautier, F. (1980). *Mapa y memoria explicativa de la Hoja núm. 543 (Villarluengo) del Mapa geológico de España 1:50.000. Segunda serie*. Instituto Geológico de España (IGME).

Gautier, F., & Barnolas, A. (1980). *Mapa Geológico de España 1:50.000, hoja n° 543 (Villarluengo)* (p. 45). IGME.

Gautier, F., & Barnolas, A. (1981). *Mapa Geológico de España 1:50.000, hoja n° 568 (Alcalá de la Selva)* (p. 32). IGME.

Gibbons, W., & Moreno, M. T. (2002). Introduction and overview. In W. Gibbons & M. T. Moreno (Eds.), *The geology of Spain* (pp. 1–6). The Geological Society.

Giles, K. A., & Lawton, T. F. (2002). Halokinetic sequence stratigraphy adjacent to the El Papalote diapir, northeastern Mexico. *AAPG Bulletin*, *86*(5), 823–840. http://aapgbull.geoscienceworld.org/cgi/content/abstract/86/5/823

Giles, K. A., & Rowan, M. G. (2012). Concepts in halokinetic-sequence deformation and stratigraphy. In G. I. Alsop, S. G. Archer, A. J. Hartley, N. T. Grant, & R. Hodgkinson (Eds.), *Salt tectonics, sediments and prospectivity* (Vol. *363*, pp. 7–31). Geological Society, London, Special Publications. https://doi.org/10.1144/SP363.2

Godoy, A., Moissenet, E., Ramírez, J. I., Olivé, A., Aznar, J. M., Jérez Mir, L., Aragonés, E., Aguilar, M. J., Ramírez del Pozo, J., Leal, M. C., Adrover, R., Alberdi, M. T., Giner, J., Gutiérrez Elorza, M., Portero, J. M., & Gabaldón, V. (1983). *Mapa Geológico de España 1:50.000, hoja n° 542 (Alfambra)*. IGME.

Godoy, A., Ramírez, J. I., Moissenet, E., Olivé, A., Aznar, J. M., Aragonés, E., Aguilar, M. J., Ramírez del Pozo, J., Leal, M. C., Adrover, R., Goy, A., Comas, M. J., Alberdi, M. T., Giner, J., Gutiérrez Elorza, M., Portero, J. M., & Gabaldón, V. (1983). *Mapa Geológico de España 1: 50.000, hoja n° 590 (La Puebla de Valverde)* (p. 68). IGME.

Godoy, A., Ramírez, J. I., Olivé, A., Moissenet, E., Aznar, J. M., Aragonés, E., Aguilar, M. J., Ramírez del Pozo, J., Leal, M. C., Jerez Mir, L., Adrover, R., Goy, A., Comas, M. J., Alberdi, M. T., Giner, J., Gutiérrez Elorza, M., Portero, J. M., & Gabaldón, V. (1983). *Mapa Geológico de España 1: 50.000, hoja n° 567 (Teruel)*. IGME.

Gómez, J. J., & Fernández-López, S. R. (2006). The Iberian Middle Jurassic carbonate-platform system: Synthesis of the palaeogeographic elements of its eastern margin (Spain). *Palaeogeography, Palaeoclimatology, Palaeoecology*, *236*, 190–205. https://doi.org/10.1016/j.palaeo.2005.11.008

Gómez, J. J., & Goy, A. (2005). Late Triassic and Early Jurassic palaeogeographic evolution and depositional cycles of the Western Tethys Iberian platform system (Eastern Spain). *Palaeogeography, Palaeoclimatology, Palaeoecology*, *222*, 77–94. https://doi.org/10.1016/j.palaeo.2005.03.010

Gómez, J. J., Goy, A., & Barrón, E. (2007). Events around the Triassic–Jurassic boundary in northern and eastern Spain: A review. *Palaeogeography, Palaeoclimatology, Palaeoecology*, *244*, 89–110. https://doi.org/10.1016/j.palaeo.2006.06.025

González, A., & Guimerà, J. (1993). Sedimentación sintectónica en una cuenca transportada sobre una lámina de cabalgamiento: La cubeta terciaria de Aliaga. *Revista. Sociedad Geologica de España*, *6*, 151–155. https://sge.usal.es/archivos/REV/6(1-2)/Art14.pdf

Granado, P., Roca, E., Strauss, P., Pelz, K., & Muñoz, J. A. (2018). Structural styles in fold-and-thrust belts involving early salt structures: The Northern Calcareous Alps (Austria). *Geology*, *47*(1), 51–54. https://doi.org/10.1130/G45281.1

Gross, M. R., Gutiérrez-Alonso, G., Bai, T., Wacker, M. A., Collinsworth, K. B., & Behl, R. J. (1997). Influence of mechanical stratigraphy and kinematics on fault scaling relations. *Journal of Structural Geology*, *19*(2), 171–183. https://doi.org/10.1016/S0191-8141(96)00085-5

Guimerà, J. (1984). Palaeogene evolution of deformation in the northeastern Iberian Peninsula. *Geological Magazine*, *121*(5), 413–420. https://doi.org/10.1017/S0016756800029940

Guimerà, J. (1988). *Estudi estructural de l'enllaç entre la Serralada Ibèrica i la Serralada Costanera Catalana* [PhD Thesis]. Universidad de Barcelona. http://diposit.ub.edu/dspace/handle/2445/34924

Guimerà, J. (2018). Structure of an intraplate fold-and-thrust belt: The Iberian Chain. A synthesis. *Geologica Acta*, *16*, 427–438. https://doi.org/10.1344/GeologicaActa2018.16.4.6

Guimerà, J., & Alvaro, M. (1990). Structure et évolution de la compression alpine dans la Chaîne Ibérique et la Chaîne côtière catalane (Espagne). *Bulletin de la Société Géologique de France*, *6*(2), 339–348. https://doi.org/10.2113/gssgfbull.VI.2.339

Guimerà, J., Mas, R., & Alonso, A. (2004). Intraplate deformation in the NW Iberian Chain: Mesozoic extension and Tertiary contractional inversion. *Journal of the Geological Society*, *161*, 291–303. https://doi.org/10.1144/0016-764903-055

Guimerà, J., & Salas, R. (1996). Inversión terciaria de la falla normal mesozoica que limitaba la subcuenca de Galve (Cuenca

del Maestrazgo). *Geogaceta*, *20*, 1701–1703. https://sge.usal.es/archivos/geogacetas/Geo20%20(7)/Art63.pdf

Guimerà, J., Salas, R., Vergés, J., & Casas, A. (1996). Extensión mesozoica e inversión compresiva terciaria en la Cadena Ibérica: Aportaciones a partir del análisis de un perfil gravimétrico. *Geogaceta*, *20*, 1691–1694. https://sge.usal.es/archivos/geogacetas/Geo20%20(7)/Art60.pdf

Hernández, A., Godoy, A., Álvaro, M., Ramírez, J. I., Leal, M. C., Aguilar, M., Anadón, P., Moissenet, E., Meléndez, A., Gómez, J. J., Martín, J. M., García, J. C., Aramburu, C., Ortí, F., Solé, N., & Gabaldón, V. (1985). *Mapa geológico de España, escala 1:200.000, de Teruel (hoja n° 47)* (p. 192). Instituto Geológico y Geominero de España.

Hudec, M. R., Dooley, T. P., Burrel, L., Teixell, A., & Fernández, N. (2021). An alternative model for the role of salt depositional configuration and preexisting salt structures in the evolution of the Southern Pyrenees, Spain. *Journal of Structural Geology*, *146*, 104325. https://doi.org/10.1016/j.jsg.2021.104325

Ibáñez, A. (2014). *Sedimentología y tectónica sinsedimentaria de la Fm. Artoles en Miravete (Teruel, Cordillera Ibérica)* (p. 50). Degree Project, Universidad de Zaragoza.

Ibañez, A. (2015). *Sedimentología y tectónica sinsedimentaria de la Fm. Artoles en el anticlinal de Miravete (Cordillera Ibérica, Teruel)* (p. 61) [Master Thesis). Univesidad de Zaragoza.

Ibáñez, A., Soria, A. R., & Liesa, C. L. (2015). Sedimentology and sedimentary evolution of the Artoles Fm in Miravete de la Sierra (Teruel, Iberian Chain). *Geogaceta*, *58*, 11–14.

Izquierdo-Llavall, E., Ayala, C., Pueyo, E. L., Casas-Sainz, A. M., Oliva-Urcia, B., Rubio, F., Rodríguez-Pintó, A., Rey-Moral, C., Mediato, J. F., & García-Crespo, J. (2019). Basement-cover relationships and their along-strike changes in the linking zone (Iberian Range, Spain): A combined structural and gravimetric study. *Tectonics*, *38*(8), 2934–2960. https://doi.org/10.1029/2018TC005422

Jackson, M. P. A., & Hudec, M. R. (2017). *Salt tectonics: Principles and practice*. Cambridge University Press.

Jackson, M. P. A., & Talbot, C. J. (1986). External shapes, strain rates, and dynamics of salt structures. *Geological Society of America Bulletin*, *97*(3), 305–323. https://doi.org/10.1130/0016-7606(1986)97<305:ESSRAD>2.0.CO;2

Jackson, M. P. A., & Vendeville, B. C. (1994). Regional extension as a geologic trigger for diapirism. *GSA Bulletin*, *106*, 57–73. https://doi.org/10.1130/0016-7606(1994)106<0057:REAAGT>2.3.CO;2

Jackson, M. P. A., Vendeville, B. C., & Schultz-Ela, D. D. (1994). Structural dynamics of salt systems. *Annual Review of Earth and Planetary Sciences*, *22*, 93–117. https://doi.org/10.1146/annurev.ea.22.050194.000521

James, N. P. (1984). Shallowing-upward sequences in carbonates. In R. G. Walker (Ed.), *Facies models* (pp. 213–228). Geological Associations of Canada 4, Geoscience Canada Reprint Series.

Julivert, M. (1978). The areas of alpine folding cover in the Iberian Meseta (Iberian Chain, Catalanides, etc.). In M. Lemoine (Ed.), *Geological atlas of alpine Europe and adjoining alpine areas* (pp. 93–112). Elsevier.

Koyi, H. (1996). Salt flow by aggrading and prograding overburdens. *Geological Society - Special Publications*, *100*, 243–258. https://doi.org/10.1144/GSL.SP.1996.100.01.15

Koyi, H., Jenyon, M. K., & Petersen, K. (1993). The effect of basement faulting on diapirism. *Journal of Petroleum Geology*, *16*, 285–312. https://doi.org/10.1111/j.1747-5457.1993.tb00339.x

Labaume, P., & Teixell, A. (2020). Evolution of salt structures of the Pyrenean rift (Chaînons Béarnais, France): From hyper-extension to tectonic inversion. *Tectonophysics*, *785*, 228451. https://doi.org/10.1016/j.tecto.2020.228451

Lanaja, J. M. (1987). *Contribución de la exploración petrolífera al conocimiento de la geología de España* (p. 465). IGME.

Liesa, C. L. (2000). *Fracturación y campos de esfuerzos compresivos alpinos en la Cordillera Ibérica y el NE peninsular* [PhD Thesis]. Universidad de Zaragoza.

Liesa, C. L. (2011a). Fracturación extensional cretácica en la Sierra del Pobo (Cordillera Ibérica, España). *Revista. Sociedad Geologica de España*, *24*, 31–48. https://sge.usal.es/archivos/REV/24(1-2)/art02.pdf

Liesa, C. L. (2011b). Evolución de campos de esfuerzos en la Sierra del Pobo (Cordillera Ibérica, España). *Revista. Sociedad Geologica de España*, *24*, 49–68. https://sge.usal.es/archivos/REV/24(1-2)/art03.pdf

Liesa, C. L., & Casas, A. M. (1994). Reactivación alpina de pliegues y fallas del zócalo hercínico de la Cordillera Ibérica: Ejemplos de las Sierra de la Demanda y la Serranía de Cuenca. *Cadernos do Laboratorio Xeolóxico de Laxe*, *19*, 119–135. http://hdl.handle.net/2183/6178

Liesa, C. L., Casas, A. M., & Simón, J. L. (2018). La tectónica de inversión en una región intraplaca: La Cordillera Ibérica. *Revista. Sociedad Geologica de España*, *31*, 23–50. https://sge.usal.es/archivos/REV/31(2)/RSGE31(2)_p_23_50.pdf

Liesa, C. L., Casas, A. M., Soria, A. R., Simón, J. L., & Meléndez, A. (2004). Estructura extensional cretácica e inversión terciaria en la región de Aliaga-Montalbán. In F. Colombo, C. L. Liesa, G. Meléndez, A. Pocoví, C. Sancho, & A. R. Soria (Eds.), *Itinerarios Geológicos por Aragón* (pp. 151–180). Geo-Guías 1, Sociedad Geológica de España, Zaragoza.

Liesa, C. L., & Simón, J. L. (2004). Modelos de inversión positiva en sistemas de fallas normales en graderío: Los márgenes de las cuencas extensionales cretácicas en la Cordillera Ibérica centro-oriental. *Geotemas*, *6*, 229–232.

Liesa, C. L., & Simón, J. L. (2007). A probabilistic approach for identifying independent remote compressions in an intraplate región: The Iberian Chain (Spain). *Mathematical Geology*, *39*, 337–348. https://doi.org/10.1007/s11004-007-9084-x

Liesa, C. L., & Simón, J. L. (2009). Evolution of intraplate stress fields under multiple rempote compressions: The case of the Iberian Chain (NE Spain). *Tectonophysics*, *474*, 144–159. https://doi.org/10.1016/j.tecto.2009.02.002

Liesa, C. L., Soria, A. R., Casas, A., Aurell, M., Meléndez, N., Bádenas, B., Fregenal-Martínez, M., Navarrete, R., Peropadre, C., & Rodríguez-López, J. P. (2019). The south-Iberian, central Iberian and Maestrazgo basins. In J. T. Oliveira & C. Quesada (Eds.), *The geology of Iberia: A geodynamic approach, Vol. 3 (the Alpine cycle), (Chapter 5) (Late Jurassic-Early Cretaceous rifting)* (pp. 214–228). Springer Nature. Regional Geology Reviews.

Liesa, C. L., Soria, A. R., & Meléndez, A. (2000). Estructura extensiva cretácica e inversión terciaria del margen noroccidental de la subcuenca de Las Parras (Cordillera Ibérica, España). *Geotemas*, *1*(2), 231–234.

Liesa, C. L., Soria, A. R., Meléndez, N., & Meléndez, A. (2006). Extensional fault control on the sedimentation patterns in a continental rift basin: El Castellar Formation, Galve sub-basin, Spain. *Journal of the Geological Society*, *163*, 487–498. https://doi.org/10.1144/0016-764904-169

Liesa, C. L., Soria, A. R., & Simón, J. L. (2019). Estructura extensional cretácica e inversion cenozoica en la region de Aliaga-Utrillas (Cordillera Ibérica). In M. Díaz, I. Expósito, S. Llana, & B. Bauluz (Eds.), *Rutas Geológicas por la Península Ibeérica, Canarias, Sicilia y Marruecos* (pp. 289–298). Geo-Guías 11, Sociedad Geológica de España, Sevilla.

López-Gómez, J., Alonso-Azcárate, J., Arche, A., Arribas, J., Barrenechea, J. F., Borruel-Abadía, V., Bourquin, S., Cadenas, P., Cuevas, J., De la Horra, R., Díez, J. B., Escudero-Mozo, M. J., Fernández-Viejo, G., Galán-Abellán, B., Galé, C., Gaspar-Escribano, J., Gisbert Aguilar, J., Gómez-Gras, D., Goy, A., … Viseras, C. (2019). Permian-Triassic rifting stage. In C. Quesada & J. Oliveira (Eds.), *The geology of Iberia: A geodynamic approach* (pp. 29–112). Regional Geology Reviews. Springer. https://doi.org/10.1007/978-3-030-11295-0_3

López-Gómez, J., Arche, A., Calvet, C., & Goy, A. (1998). Epicontinental marine carbonate sediments of the Middle and Upper Triassic in the westernmost part of the Tethys Sea, Iberian Peninsula. In G. H. Bachmann & I. Lerche (Eds.), *Epicontinental Triassic* (pp. 1033–1084). Zentralblatt für Geologie un Paläontologie.

López-Gómez, J., Arche, A., & Pérez-López, A. (2002). Permian and Triassic. In W. Gibbons & M. T. Moreno (Eds.), *The geology of Spain* (pp. 186–212). Geological Society. https://doi.org/10.1144/GOSPP.10

López-Mir, B., Muñoz, J. A., & García-Senz, J. (2015). Extensional salt tectonics in the partially inverted Cotiella post-rift basin (south-central Pyrenees): Structure and evolution. *International Journal of Earth Sciences*, *104*, 419–434. https://doi.org/10.1007/s00531-014-1091-9

Marcén, M., Casas-Sainz, A. M., Román-Berdiel, T., Oliva-Urcia, B., Soto, R., & Aldega, L. (2018). Kinematics and strain distribution in an orogen-scale shear zone: Insights from structural analyses and magnetic fabrics in the Gavarnie thrust, Pyrenees. *Journal of Structural Geology*, *117*, 105–123. https://doi.org/10.1016/j.jsg.2018.09.008

Marin, P. (1974). *Stratigraphie et évolution paléeogéographique post-Hercynienne de la Chaine Celtibérique oriental aux confins de l'Aragon et du Haut-Maestrazgo (prov. de Teruel et Castellón de la Plana, Espagne)* (Vol. *1*, p. 231). [PhD Thesis]). Universite Claude Bernand.

Martín-Fernández, M., Canerot, J., Pan Arana, T., & Leyva, F. (1979). *Mapa y Memoria explicativa de la Hoja núm. 517 (Argente). Del Mapa geológico de España 1:50.000*. Instituto Geológico de España (IGME).

Meléndez, A., Aurell, M., Bádenas, B., & Soria, A. R. (1995). Las rampas carbonatadas del Triásico Medio en el sector central de la Cordillera Ibérica. *Cuadernos de Geología Ibérica*, *19*, 173–199.

Meléndez, N., Liesa, C. L., Soria, A. R., & Melendez, A. (2009). Lacustrine system evolution during early rifting: El Castellar formation (Galve Sub-Basin, Central Iberian Chain). *Sedimentary Geology*, *222*, 64–77. https://doi.org/10.1016/j.sedgeo.2009.05.019

Moore, J. G. (1992). A syn-rift to post-rift transition sequence in the Main Porcupine Basin, offshore western Ireland. In J. Parnell (Ed.), *Basins on the Atlantic Seaboard: Petroleum sedimentology and basin evolution* (Vol. *62*, pp. 333–349). Geological Society, London, Special Publications. https://doi.org/10.1144/GSL.SP.1992.062.01.26

Nalpas, T., & Brun, J. P. (1993). Salt flow and diapirism related to extension at crustal scale. *Tectonophysics*, *228*, 349–362. https://doi.org/10.1016/0040-1951(93)90348-N

Navarrete, R. (2015). *Controles alocíclicos de la sedimentación barremiense en la Subcuenca de Galve (Fm. Camarillas, margen occidental de la Cuenca del Maestrazgo)* [PhD Thesis]. Universidad de Zaragoza.

Navarrete, R., Liesa, C. L., Castanera, D., Soria, A. R., Rodríguez-López, J. P., & Canudo, J. L. (2014). A thick Tethyan multibed tsunami deposit preserving a dinosaur megatracksite within a coastal lagoon (Barremian, eastern Spain). *Sedimentary Geology*, *313*, 105–127. https://doi.org/10.1016/j.sedgeo.2014.09.007

Navarrete, R., Liesa, C. L., Soria, A. R., & Rodríguez-López, J. P. (2013a). Actividad de fallas durante el depósito de la Formación Camarillas (Barremiense) en la subcuenca de Galve (E de España). *Geogaceta*, *53*, 61–64. https://sge.usal.es/archivos/geogacetas/geo53/G53art15.pdf

Navarrete, R., Rodríguez-López, J. P., Liesa, C. L., Soria, A. R., & Veloso, F. M. (2013b). Changing physiography of rift basins as a control on the evolution of mixed siliciclastic–carbonate back-barrier systems (Barremian Iberian Basin, Spain). *Sedimentary Geology*, *289*, 40–61. https://doi.org/10.1016/j.sedgeo.2013.02.003

Navarro-Vázquez, D., Crespo Zamorano, A., Pérez Castaño, A., Canérot, J., Martínez Díaz, C., Granados Granados, L., Del Pan Arana, T., Fernández Luanco, M. C., & Barnolas, A. (1981). *Mapa Geológico de España 1:50.000, hoja n° 544 (Forcall)* (pp. 26). IGME.

Nebot, M., & Guimerà, J. (2016a). La extension Triásica en el substrato de la Cuenca del Maestrat, y evidencias de tectónica salina en las evaporitas en facies Muschelkalk medio (Cadena Ibérica Oriental). *Geo-Temas*, *16*(1), 241–244.

Nebot, M., & Guimerà, J. (2016b). Structure of an inverted basin from subsurface and field data: The Late Jurassic-Early Cretaceous Maestrat basin (Iberian Chain). *Geologica Acta*, *14*, 155–177. https://doi.org/10.1344/GeologicaActa2016.14.2.5

Nebot, M., & Guimerà, J. (2018). Kinematic evolution of a fold-and-thrust belt developed during basin inversion: The Mesozoic Maestrat basin, E Iberian Chain. *Geological Magazine*, *155*, 630–640. https://doi.org/10.1017/S001675681600090X

Ortí, F. (1973). *El Keuper del Levante español. Litoestratigrafía, petrología y paleogeografía de la cuenca* [PhD Thesis. Universidad de Barcelona.

Ortí, F. (1974). El Keuper del Levante español. Litoestratigrafía, petrología y paleogeografía de la cuenca. *Estudios Geológicos*, *30*, 7–46.

Ortí, F., Guimerà, J., & Götz, A. E. (2020). Middle-upper Triassic stratigraphy and structure of the Alt Palància (eastern Iberian Chain): A multidisciplinary approach. *Geologica Acta*, *18*(4), 1–25. https://doi.org/10.1344/GeologicaActa2020.18.4

Ortí, F., Pérez-López, A., & Salvany, J. M. (2017). Triassic evaporites of Iberia: Sedimentological and palaeogeographical implications for the western Neotethys evolution during the Middle Triassic–Earliest Jurassic. *Palaeogeography, Palaeoclimatology, Palaeoecology*, *471*, 157–180. https://doi.org/10.1016/j.palaeo.2017.01.025

Peace, A. L., Welford, J. K., Ball, P. J., & Nirrengarten, M. (2019). Deformable plate tectonic models of the southern North

Atlantic. *Journal of Geodynamics*, *128*, 11–37. https://doi.org/10.1016/j.jog.2019.05.005

Pérez-López, A., Benedicto, C., & Orti, F. (2021). Middle Triassic carbonates of Eastern Iberia (Western Tethyan Realm): A shallow platform model. *Sedimentary Geology*, *420*, 105904. https://doi.org/10.1016/j.sedgeo.2021.105904

Peropadre, C. (2012). *El Aptiense del margen occidental de la cuenca del Maestrazgo: Controles tectónico, eustático y climático en la sedimentación* [PhD Thesis. Universidad Complutense de Madrid.

Quintà, A., Tavani, S., & Roca, E. (2012). Fracture pattern analysis as a tool for constraining the interaction between regional and diapir-related stress fields: Poza de la Sal Diapir (Basque Pyrenees, Spain). *Geological Society, London, Special Publications*, *363*, 521–532. https://doi.org/10.1144/SP363.25

Ramsay, J. G., & Huber, M. I. (1987). *The techniques of modern structural geology: Folds and fractures* (Vol. *2*). Academic Press.

Rodríguez-López, J. P., Liesa, C. L., Meléndez, N., & Soria, A. R. (2007). Normal fault development in a sedimentary succession with multiple detachment levels: The Lower Cretaceous Oliete sub-basin, Eastern Spain. *Basin Research*, *19*, 409–435. https://doi.org/10.1111/j.1365-2117.2007.00327.x

Rodríguez-López, J. P., Meléndez, N., Soria, A. R., & de Boer, P. L. (2009). Reinterpretación estratigráfica y sedimentológica de las formaciones Escucha y Utrillas de la Cordillera Ibérica. *Revista. Sociedad Geologica de España*, *22*(3–4), 163–219. https://eprints.ucm.es/id/eprint/27100/1/art04.pdf

Rowan, M. G., Giles, K. A., Hearon, T. E., & Fiduk, J. C. (2016). Megaflaps adjacent to salt diapirs. *AAPG Bulletin*, *100*(11), 1723–1747. https://doi.org/10.1306/05241616009

Rowan, M. G., Lawton, T. F., Giles, K. A., & Ratliff, R. A. (2003). Near-salt deformation in La Popa basin, Mexico, and the northern Gulf of Mexico: A general model for passive diapirism. *AAPG Bulletin*, *87*, 733–756. https://doi.org/10.1306/01150302012

Salas, R., & Casas, A. (1993). Mesozoic extensional tectonics, stratigraphy and crustal evolution during the Alpine cycle of the eastern Iberian basin. *Tectonophysics*, *228*, 33–55. https://doi.org/10.1016/0040-1951(93)90213-4

Salas, R., Guimerà, J., Mas, R., Martín-Closas, C., Meléndez, A., & Alonso, A. (2001). Evolution of the Mesozoic central Iberian rift system and its Cainozoic inversion (Iberian chain). In P. A. Ziegler, W. Cavazza, A. H. F. Robertson, & S. Crasquin-Soleau (Eds.), *Peri-tethys Memoir 6: Peri-tethyan rift/Wrench basins and passive margins* (Vol. *186*, pp. 145–186). Mémoires du Museum National d'Histoire Naturelle.

San Román, J., & Aurell, M. (1992). Palaeogeographical significance of the Triassic–Jurassic unconformity in the north Iberian basin (Sierra del Moncayo, Spain). *Palaeogeography, Palaeoclimatology, Palaeoecology*, *99*, 101–117. https://doi.org/10.1016/0031-0182(92)90009-T

Sánchez Moya, Y., Sopeña, A., Muñoz, A., & Ramos, A. (1992). Consideraciones teóricas sobre el análisis de la subsidencia: Aplicaciones a un caso real en el borde de la cuenca triásica ibérica. *Revista. Sociedad Geologica de España*, *5*(3–4), 1–40. https://sge.usal.es/archivos/REV/5(3-4)/Art02.pdf

Saura, E., Ardèvol i Oró, L., Teixell, A., & Vergés, J. (2016). Rising and falling diapirs, shifting depocenters, and flap overturning in the Cretaceous Sopeira and Sant Gervàs subbasins (Ribagorça Basin, southern Pyrenees). *Tectonics*, *35*, 638–662. https://doi.org/10.1002/2015TC004001

Saura, E., Vergés, J., Martín-Martín, J. D., Messager, G., Moragas, M., Razin, P., Grélaud, C., Joussiaume, R., Malaval, M., Homke, S., & Hunt, D. W. (2014). Syn-to post-rift diapirism and minibasins of the Central High Atlas (Morocco): The changing face of a mountain belt. *Journal of the Geological Society*, *171*, 97–105. https://doi.org/10.1144/jgs2013-079

Schmatz, J., Vrolijkb, P. J., & Urai, J. L. (2010). Clay smear in normal fault zones—The effect of multilayers and clay cementation in water-saturated model experiments. *Journal of Structural Geology*, *32*, 1834–1849. https://doi.org/10.1016/j.jsg.2009.12.006

Séguret, M. (1972). Étude tectonique des nappes et séries décollées de la partie centrale du versant sud des Pyrénées. PhD Thesis, Université des Scieces et Techniques du Languedoc, Montpellier, 1–155.

Seillé, H., Salas, R., Pous, J., Guimerà, J., Gallart, J., Torne, M., Romero-Ruiza, I., Diaz, J., Ruiz, M., Carbonell, R., & Mas, R. (2015). Crustal structure of an intraplate thrust belt: The Iberian Chain revealed by wide-angle seismic, magnetotelluric soundings and gravity data. *Tectonophysics*, *663*, 339–353. https://doi.org/10.1016/j.tecto.2015.08.027

Simón, J. L. (1980). Estructuras de superposición de plegamientos en el borde NE de la Cadena Ibérica. *Acta Geologica Hispanica*, *15*, 137–140. https://revistes.ub.edu/index.php/ActaGeologica/article/view/4193/5097

Simón, J. L. (2004). Superposed buckle folding in the Eastern Iberian chain, Spain. *Journal of Structural Geology*, *26*, 1447–1464. https://doi.org/10.1016/j.jsg.2003.11.026

Simón, J. L. (2005). Erosion-controlled geometry of buckle fold interference. *Geology*, *33*, 561–564. https://doi.org/10.1130/G21468.1

Simón, J. L. (2006). El registro de la compresión intraplaca en los conglomerados de la cuenca terciaria de Aliaga (Teruel, Cordillera Ibérica). *Revista. Sociedad Geologica de España*, *19*, 163–179. https://sge.usal.es/archivos/REV/19(3-4)/Art1.pdf

Simón, J. L., Arenas, C., Arlegui, L., Aurell, M., Gisbert, J., González, A., Liesa, C. L., Marín, C., Meléndez, A., Meléndez, G., Pardo, G., Soria, A. R., Soria, M., & Soriano, A. (1998). *Guía del Parque Geológico de Aliaga* (p. 155). Ayto. de Aliaga–CEDEMATE–Dpto. de Geología, Universidad de Zaragoza.

Simón, J. L., & Liesa, C. L. (2011). Incremental slip history of a thrust: Diverse transport directions and internal folding of the Utrillas thrust sheet (NE Iberian Chain, Spain). In J. Poblet & R. J. Lisle (Eds.), *Kinematic evolution and strucutral styles of fold-and-thrust belts* (Vol. *349*, pp. 77–97). Geological Society, London, Special Publications. https://doi.org/10.1144/SP349.5

Simón, J. L., Liesa, C. L., & Soria, A. R. (1998). Un sistema de fallas normales sinsedimentarias en las unidades de facies Urgon de Aliaga (Teruel, Cordillera Ibérica). *Geogaceta*, *24*, 291–294. https://sge.usal.es/archivos/geogacetas/Geo24/Art73.pdf

Simón-Porcar, G., Simón, J. L., & Liesa, C. L. (2019). La cuenca neógena extensional de El Pobo (Teruel, Cordillera Ibérica): Sedimentología, estructura y relación con la evolución del relieve. *Revista. Sociedad Geologica de España*, *32*(2), 17–42. https://sge.usal.es/archivos/REV/32(2)/RSGE32(2)_p_17_42.pdf

Sopeña, A., López, J., Arche, A., Pérez-Arlucea, M., Ramos, A., Virgili, C., & Hernando, S. (1988). Permian and Triassic rift basins of the Iberian Peninsula. In W. Manspeizer (Ed.), *Triassic-Jurassic rifting: Continental breakup and the origin of the Atlantic ocean*

and passive margins. Developments in geotectonics (Vol. *22*, pp. 757–786). Elsevier. https://doi.org/10.1016/B978-0-444-42903-2.50036-1

Soria, A. R. (1997). *La sedimentación en las cuencas marginales del surco ibérico durante el Cretácico inferior y su control structural* [PhD Tesis]. Universidad de Zaragoza.

Soria, A. R., Liesa, C. L., Rodríguez-López, J. P., Meléndez, N., de Boer, P. L., & Meléndez, A. (2011). First evidence of early Triassic erg system in Iberia. *Terra Nova*, *23*, 76–84. https://doi.org/10.1111/j.1365-3121.2011.00986.x

Soto, J. I., Flinch, J. F., & Tari, G. (2017). *Permo-triassic salt provinces of Europe, North Africa and the Atlantic margins, tectonics and hydrocarbon potential*. Elsevier.

Soto, R., Casas-Sainz, A. M., & Del Río, P. (2007). Geometry of half-grabens containing a mid-level viscous décollement. *Basin Research*, *19*, 437–450. https://doi.org/10.1111/j.1365-2117.2007.00328.x

Soto, R., Casas-Sainz, A. M., Oliva-Urcía, B., & García-Lasanta, C. (2019). Triassic stretching directions in Iberia and North Africa inferred from magnetic fabrics. *Terra Nova*, *31*(5), 465–478. https://doi.org/10.1111/ter.12416

Teixell, A., Barnolas, A., Rosales, I., & Arboleya, M. (2017). Structural and facies architecture of a diapir-related carbonate minibasin (lower and middle Jurassic, High Atlas, Morocco). *Marine and Petroleum Geology*, *81*, 334–360. https://doi.org/10.1016/j.marpetgeo.2017.01.003

Tillmans, F., Gawthorpe, R. L., Jackson, C. A.-L., & Rotevatn, A. (2021). Syn-rift sediment gravity flow deposition on a Late Jurassic fault-terraced slope, northern North Sea. *Basin Research*, *33*, 1844–1879. https://doi.org/10.1111/bre.12538

Val, J., Aurell, M., Bádenas, B., Castanera, D., & Subias, S. (2019). Cyclic carbonare-siliciclastic sedimentation in a shallow marine to coastal environment (latest Kimmeridgian-early Tithonian, Galve sub-basin, Spain). *Journal of Iberian Geology*, *45*(1), 195–222.

Van Wees, J. D., Arche, A., Beijdorff, C. G., López-Gómez, J., & Cloetingh, S. A. P. L. (1998). Temporal and spatial variations in tectonic subsidence in the Iberian Basin (eastern Spain): Inferences from automated forward modelling of high-resolution stratigraphy (Permian-Mesozoic). *Tectonophysics*, *300*(1–4), 285–310. https://doi.org/10.1016/S0040-1951(98)00244-3

Vennin, E., & Aurell, M. (2001). Stratigraphie sequentielle de l'Aptien du sous-basin de Galvé (Province de Teruel, NE de l'Espagne). *Bulletin de la Société Géologique de France*, *172*, 397–410.

Vergés, J., Moragas, M., Martín-Martín, J. D., Saura, E., Casciello, E., Razin, P., Grélaud, C., Malaval, M., Joussiaume, G., Sharp, I., & Hunt, D. W. (2017). Salt tectonics in the Atlas mountains of Morocco. In J. I. Soto, J. Flinch, & G. Tari (Eds.), *Permo-Triassic salt provinces of Europe, North Africa and the Atlantic margins* (pp. 563–579). Elsevier. https://doi.org/10.1016/B978-0-12-809417-4.00027-6

Vergés, J., Poprawski, Y., Almar, Y., Drzewiecki, P. A., Moragas, M., Bover-Arnal, T., Macciavelli, C., Wright, W., Messager, G., Embry, J. C., & Hunt, D. (2020). Tectono-sedimentary evolution of Jurassic-Cretaceous diapiric structures, Maestrat Basin, Spain. *Basin Research*, *32*, 1653–1684. https://doi.org/10.1111/bre.12447

Williams, G. D. (1993). Tectonics and seismic sequence stratigraphy: An introduction. In G. D. Williams & A. Dobb (Eds.), *Tectonics and seismic sequence stratigraphy* (Vol. *71*, pp. 1–13). Geological Society, London, Special Publication. https://doi.org/10.1144/GSL.SP.1993.071.01.01

Withjack, M. O., Schlische, R. W., & Olsen, P. E. (2002). Rift-basin structure and its influence on sedimentary systems. *Sedimentation in Continental Rifts*, *73*, 57–81.

Ziegler, P. A. (1987). Late Cretaceous and Cenozoic intra-plate compressional deformations in the Alpine foreland—A geodynamic model. *Tectonophysics*, *137*, 389–420. https://doi.org/10.1016/0040-1951(87)90330-1

Ziegler, P. A. (1990). *Geological atlas of western and central Europe* (2nd ed., p. 239). Shell Internationale Petroleum Mij. B.V. and Geological Society.

How to cite this article: Liesa, C. L., Casas-Sainz, A. M., Aurell, M., Simón, J. L., & Soria, A. R. (2022). Salt tectonics vs. inversion tectonics: The anticlines of the western Maestrazgo revisited (eastern Iberian Chain, Spain). *Basin Research*, *00*, 1–41. https://doi.org/10.1111/bre.12713